8003277

BEICHMAN, CHARLES ARNOLD

THE FORMATION OF LATE O AND EARLY B STARS WITHIN DENSE MOLECULAR CLOUDS

University of Hawaii PH.D. 1979

University Microfilms International 300 N. Zeeb Road, Ann Arbor, MI 48106 18 Bedford Row, London WC1R 4EJ, England

THE FORMATION OF LATE O AND EARLY B STARS WITHIN DENSE MOLECULAR CLOUDS

A Dissertation Submitted to the Graduate Division of the
University of Hawaii in Partial Fulfillment
of the Requirements for the Degree of
DOCTOR of PHILOSOPHY
In ASTRONOMY

AUGUST 1979

By
Charles Arnold Beichman

Dissertation Committee:
Eric E. Becklin, Chairman
H. Melvin Dyck
Frank Q. Orrall
David E. Yount
George Andermann

ACKNOWLEDGEMENTS

In a project of this duration and magnitude one incurs debts for assistance with various scientific and practical matters. I have benefitted greatly from discussions about the material presented in this dissertation with Drs. C. G. Wynn-Williams, N. J. Evans, II, A. I. Sargent, J. N. Heasley, T. D. Kunkle, and Ms. S. Edwards. Drs. M. Kutner, R. L. Dickman, R. Loren and A. Wooten kindly made CO data available in advance of publication. Drs. C. J. Lada, L. Blitz, J. Moran and M. Reid communicated to me the results of their VLBI experiment on the Cep A H_2O maser shortly after the data were first reduced.

Drs. R. W. Capps and H. M. Duck were responsible for the photometer and sensitive detector systems used to make these observations. Dr. T. D. Kunkle's astrometry program was used to determine the positions of field stars on the Palomar prints. Night assistants Harrison Ward and Frank Cheigh skillfully manned the controls of the 224-cm telescope while the Mauna Kea Observatory support staff, including Tom Kreiger, Curt Nakayama and Gail Forbes, usually kept the telescope alive, the astronomers fed and the helium flowing.

The NASA Infrared Telescope Facility provided much of the financial support that made this research possible.

I am most grateful to Dr. J. T. Jefferies, director of the Institute for Astronomy, for the generous hospitality of the Institute during the past six years. The vision and scientific enthusiasm of its director has led to the creation of an observatory that is second to none for infrared astronomy, and of an Institute that is

a most congenial place for work.

Mrs. Mary Missbach, Ms. Jeanne Koch, Mrs. Diane and Mrs. Mary Patricio cheerfully turned innumerable revisions of manuscript and figures into a polished work. Permission to use their talents for parts of this dissertation is gratefully acknowledged.

I must also thank Jameson's and Dickens' Pubs which provided many a midnight Irish coffee when neither Tom Kunkle nor I could face a beckoning typewriter or computer terminal.

My last and largest debts are to my parents, to whom I owe an ideal of intellectual excellence and a love of the English language; and to Susie Burke, who survived it all, laughing---most of the time.

The Star System

While you're a white-hot youth, emit the rays
Which, now unmarked, shall dazzle future days.
Burn for the joy of it, and waste no juice
On hopes of prompt discovery. Produce!

Then, white with years, live wisely and survive.
Thus you may be on hand when you arrive,
And, like Antares, rosily dilate,
And for a time be gaseous and great.

Richard Wilbur
in The Mind Reader, 1955 .

ABSTRACT

The dense, hot cores of 24 molecular clouds were examined at infrared wavelengths between 2.2 and 25 μm in search of embedded, luminous objects thought to massive O and B stars at an early stage of their evolution. 19 of the clouds were examined at 20 μm for high sensitivity to sources of low color temperature between 80 and 200 K. The clouds IC 1848 A, S 235, S 255, S 269, IR 12.4 + 0.5, S 140 and Cepheus A contain a total of 12 embedded sources of radiation more luminous than 6×10^3 $L_\odot$ of which 7 were discovered during the course of this research. The 20 μm searches were particularly fruitful, yielding discoveries of 4 objects too red to be discovered in previous searches at 2.2 and 10 μm. In all cases the infrared sources are found projected against the densest part of the molecular cloud where the ^{13}CO column density exceeds 2×10^{16} cm^{-2}. On the other hand, no compact infrared sources were found in clouds such as Cepheus B which has high gas temperature, about 30 K, but low gas density less than 3×10^3 cm^{-3}. The absence of embedded sources in some cases suggests that heating by stars external to the cloud can result in elevated temperatures in rarified clouds.

The success of the 20 μm searches points out two biases inherent in studies made at shorter wavelengths. First, the effect of intra-cloud extinction is to obscure deeply embedded objects at wavelengths shorter than 20 μm. A reliance on counts of sources discovered at 2.2 and 10 μm will result in a serious underestimate of the rate of formation of massive stars. Second, short wavelength studies favor the discovery of objects which lie close to the front of a cloud where the intra-cloud extinction is low, thereby creating an artificial need to

explain the preferential location of these objects close to the cloud boundaries. The importance of these prejudices to theories of star formation is discussed.

This work has led to the realization that infrared sources in molecular clouds tend to form in clusters whose characteristic size is very similar to that found in trapezium-like groups of O and B stars. It seems likely that molecular clouds fragment as their densities reach 10^4 cm^{-3} into independently collapsing nuclei separated by about 0.1 pc and each capable of producing one (or more) star(s).

Some embedded infrared sources are surrounded by a small amount of ionized material. The strength of the radio emission seen toward objects brighter than 10^4 $L_\odot$ such as Cepheus A and S 140 is consistent with these objects being pre-main sequence O and B stars.

TABLE OF CONTENTS

LIST OF TABLES

LIST OF ILLUSTRATIONS

CHAPTER I

INTRODUCTION

Astronomers have long suspected that the stars are formed by the gravitational collapse of interstellar material, for it is an observational fact that the bright and dark gaseous nebulae are found together, close to stars whose properties indicate their extreme youth (Spitzer 1968). The luminous O and B stars whose UV radiation ionizes large volumes of interstellar hydrogen,called H II regions,cannot be very old, for they consume their nuclear material at such a prodigal rate that they must run out in less than $\simeq 10^7$ years. In this short time, far less than the galactic rotation period of 2×10^8 years, the stars cannot have moved far from their birthplaces. Less luminous stars found at the periphery of interstellar material are also inferred to be young on the basis of their spectroscopic properties (Herbig 1960; Cohen and Kuhi 1979). It is reasonable to look in the vicinity of these stars for the sites of their formation. Until recently astronomers could only conjecture about the process of star formation, for even the most powerful optical telescopes were unable to peer through the dust that veils the interiors. In the past decade, however, observations at infrared and radio wavelengths have made it possible to look deep within these clouds and witness the birth of stars directly.

Millimeter wavelength radio astronomy has contributed the crucial concept that much of the interstellar medium exists in dense, cold clouds 5 to 50 parsecs across (1 pc = 3.086×10^{18} cm = 3.26 light years) containing as much as 10^5 $M_\odot$ (1 $M_\odot$ = 1.989×10^{33} g). The bulk of the material is molecular, not atomic, hydrogen (Thaddeus 1977). Such clouds form when enough matter is gathered together so that the

visual extinction exceeds a magnitude or so and the outer boundary of the volume of gas becomes opaque to the ambient interstallar UV and X-ray radiation fields. Acting like the terrestrial ozone layer, the outer rim protects the interior gas from dissociating photons, providing a benign environment wherein molecular hydrogen and a pharmacoepia of other organic and inorganic molecules can form (Hollenbach, Werner and Salpeter 1971).

Unfortunately the H_2 within these "molecular clouds" is difficult to observe in its quiescent state due to its lack of either an intrinsic dipole moment or fine or hyperfine structure (Field, Somerfield, and Dressler 1966). However, the distribution of the molecular component of the gas can be traced using less abundant, but more easily detected molecules such as carbon monoxide. Due to similar conditions for formation and destruction, CO and H_2 are spatially coextensive and surveys in the rotational transition lines of CO, particularly in the $J = 1 \rightarrow 0$ line at 2.6 mm, have been used to map H_2 in the galaxy (Burton et al. 1975). These maps show that the H_2 has a clumpy distribution which follows closely the distribution of extremely young Population I objects such as OB stars and H II regions. Detailed maps of molecular line emission show that regions of recent or ongoing star formation are associated with dense molecular clouds (Israel 1979, and references therein). Infrared measurements show that the newest generation of stars is being formed within the densest, hottest parts of those clouds (Werner, Becklin, and Neugebauer 1977).

If OB stars (5 to 50 $M_\odot$) form within molecular clouds, it is reasonable that they should be observable while still embedded within the cloud, because the time scale for the formation of such stars is

less than the time scale for the dissipation of the cloud (Larson and Starrfield 1971). For stars of roughly solar mass or less, the time scales reverse and one expects to observe pre-main sequence objects outside of clouds. The observations of T Tauri stars and other young, low mass objects confirm this conjecture (Cohen and Kuhi 1979).

In a prescient paper Davidson and Harwit (1967) described the characteristics of a massive OB star embedded in the placental material of an interstellar cloud. The "cocoon star," as they called it, has all of its optical and UV radiation absorbed by the surrounding gas and dust, leaving nothing for optical astronomers to observe. The dust grains, they calculated, would be heated to ~100 K, producing a strong source of 10- and 20-μm radiation detectable by ground-based infrared astronomers.

What made the prediction remarkable was the fact that such an object had just been found in the Orion Nebula, a young H II region associated with a great mass of interstellar material (Figure 1). Becklin and Neugebauer (1967) discovered an intense source of 10-m radiation with an energy distribution suggestive of thermal emission from 600 K grains and a luminosity in excess of 10^3 solar luminosities ($1\ L_\odot = 3.826 \times 10^{33}$ erg s^{-1}). The object has no optical counterpart. Just south of the so-called BN object, Kleinmann and Low (1967) found an extended source of infrared emission, now named the KL nebula, with a color temperature of only 80 K. Studies of molecular lines show that BN and KL are located within a dense portion of the giant Orion Molecular Cloud (designated OMC 1) that lies behind the visible H II region (Wilson, Jefferts, and Penzias 1970; Kutner, Evans, and Tucker 1976).

Nowhere is the association between interstellar matter and star formation more apparent than in the Orion region. Figure 1 (Kutner et al. 1977) is a schematic representation of the molecular clouds and the plethora of young objects--the dark clouds (Lynds 1962), H II regions, reflection nebulae, T Tauri stars and Herbig-Haro objects and the infrared sources in OMC 1 (BN and KL), OMC 2 (Gatley et al. 1974), and NGC 2024 (Grasdalen 1974). It is apparent that stars are forming over a region 15° in size, or tens of parsecs across (Blaauw 1964).

In the twelve years since the discovery of BN and KL many other infrared objects have been found in regions for star formation throughout the galaxy (Werner et al. 1977; Habing and Israel 1979). Most of these objects are "cocoon stars" (Kahn 1974) or, less poetically, compact ($\leq$0.5 pc) H II regions embedded within a molecular cloud. These sources are identified as H II regions by radio continuum observations at centrimetric wavelengths of the thermal bremsstrahlung radiation from the hot, dense plasma (10^4 K, 10^3 cm^{-3}) swaddling the newborn stars. The small size of the H II regions usually requires that interferometric techniques be used for detailed observations. For example, the molecular cloud abutting onto the W3-W4-W5 H II region complex (Westerhout 1958) is studded with embedded, compact H II regions such as W3-IRS 1, 2, 3 (IRS stands for infrared source) and W3(OH) (Wynn-Williams, Becklin, and Neugebauer 1972).

Radio observations also show that infrared sources are often associated with maser emission from the OH, H_2O, and SiO molecules. The excitation of these masers is not understood, but may be due to shocks in the ionized gas surrounding developing OB stars. Masers are good,

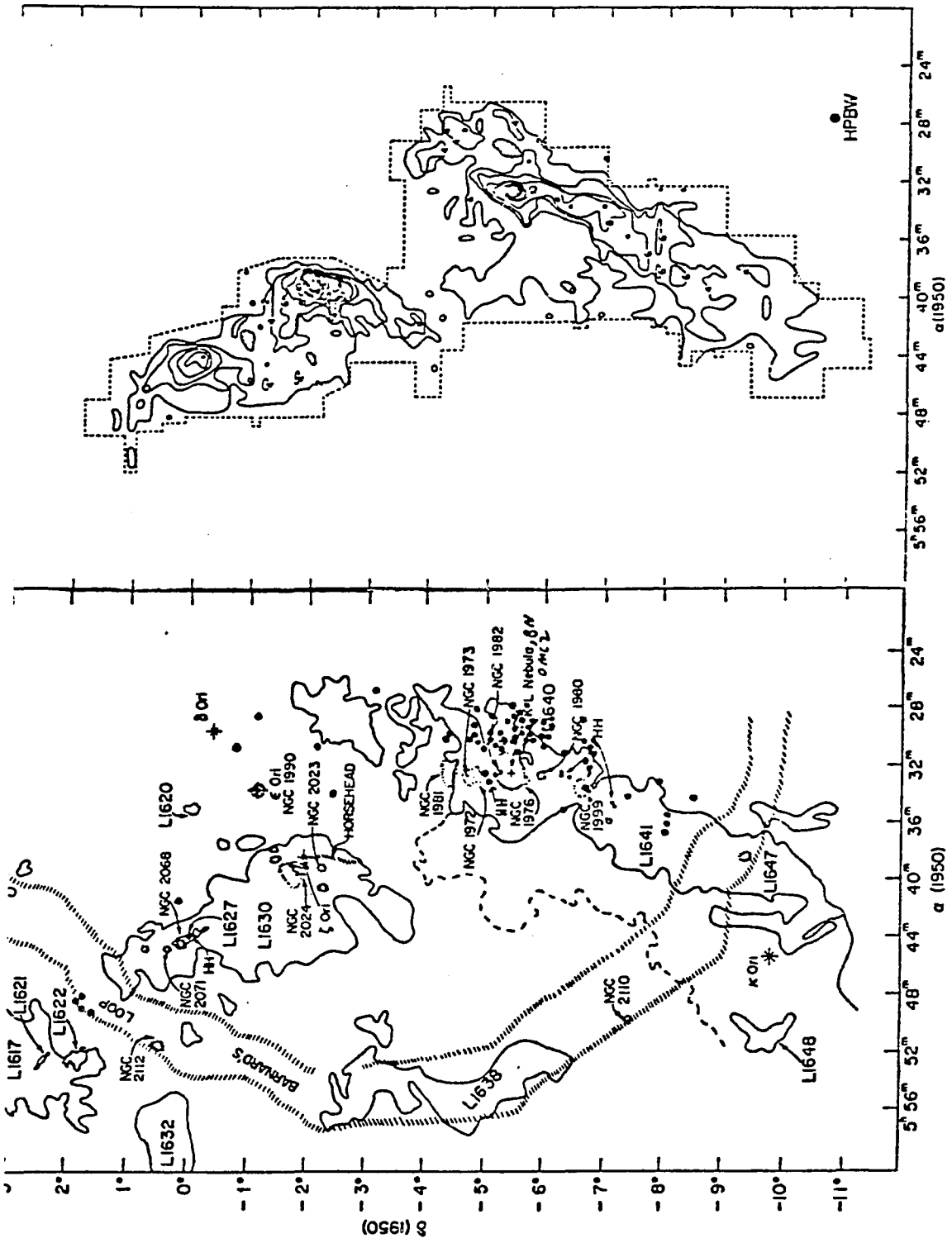

Figure I.1 A region 15° across in Orion contains every kind of young stellar object. Marked on the left hand figure are conspicuous optical features: HII regions (NGC), dark clouds (Lynds 1962), infrared objects BN and KL, Herbig-Haro objects (HH) and T Tauri stars (filled circles; Herbig and Rao 1972). To the right is a CO map showing the extensive molecular cloud that covers the whole region. Figure from Kutner et al.(1977).

but not infallible signposts for the presence of infrared objects and compact H II regions (Genzel and Downes 1977).

As shown in Table I.1, there are some infrared objects located within molecular clouds that emit little or no radio continuum radiation. While a typical compact HII region such as W3(OH) has a 6 cm flux density of ~1 Jy (Harten 1976; 1 Jansky = 10^{-26} Wm^{-2} Hz^{-1}), the radio weak sources have fluxes that are a factor of 100 smaller. The total luminosities of the compact H II regions and the radio weak sources are comparable, 10^4 to 10^5 $L_\odot$. Recently, Beichman, Becklin, and Wynn-Williams (1979, hereafter B^2W^2) have made sensitive radio observations with the Very Large Array telescope and found that some of the objects thought to be radio-quiet actually emit a small amount of radio continuum radiation, 1 to 2 mJy. Possible explanations for the weakness of the radio emission from these objects include:

(1) Theoretical calculations show that massive stars may approach the main sequence along tracks of roughly constant luminosity and ever increasing temperature (Iben 1965; Bodenheimer 1972). At an early stage in its evolution, such a star would appear as a cool luminous source emitting far fewer ionizing UV photons than appropriate to a main sequence of the same luminosity. A low level of radio continuum emission would result.

(2) A newly formed main sequence star might still be accreting so much material that dust would absorb all of the ultraviolet radiation in successful competition with the gas (Bedejin, Habing, and deJong 1978).

(3) A young cocoon star might be surrounded by an ultra-compact H II region so small as to be undetectable with present-day techniques. At a distance of 1 kpc a flux limit of 1 mJy corresponds to a size of

Table I.1

Radio Weak Infrared Sources

Name	d(kpc)*	$L(L_\odot)$	S_ν(6cm, mJy)	Notes
W3-IRS 5	3.0	$\sim 10^5$	<12	1,2
AFGL 490	0.9	1.4×10^3	<30	3,4
IC 1848A	2.0	$>10^3$	<8	5,6
BN/KL	0.5	$>10^4$:	<30	1,7
OMC 2-IRS 3	0.5	10^3	<250	8
S235-IRS 4	1.8	6×10^3	<5	5,9
Mon R2-IRS 3	2.5	5×10^4	-	10
S255-IRS 1,2	2.5	8×10^4	<6	5,11
IR 12.4+0.5	2.1:	2×10^4	<10	5,12,13
M17-KW	2.1	$\sim 10^4$	<25	14, 15
W33 A	4.6	$>3 \times 10^4$	<15	16, 17
AFGL 2591	3:	10^5:	<5	1
S140-IRS 1-3	0.9	1.4×10^4	10	5, 11,18
Cep A	0.7	4.9×10^4	25	5, 11, 19

*Colon denotes uncertain distance.

Notes:

1) Werner et al., 1977 and refs. therein.
2) Harris and Wynn-Williams, 1976.
3) Harvey et al.1979.
4) Shows Bγ emission. Simon et al. 1979, Thompson and Tokunaga 1979.
5) This dissertation. Shows Bγ, Tokunaga and Thompson 1979b
6) 11 cm flux limit from Wynn-Williams 1978, private communication.
7) Martin and Gull 1976.
8) Gatley et al, 1974.
9) Israel and Felli 1977; Harris 1976.
10) Beckwith et al. 1976.
11) B^2W^2
12) unpublished VLA observation, 1979.
13) Wright et al.1979.
14) Gatley et al. 1979; shows Bγ, Tokunaga and Thompson 1979a.
15) Matthews, Harten and Goss 1979.
16) Habing et al. 1974.
17) Dyck and Simon 1977.
18) Harvey et al. 1978.
19) Koppenaal et al. 1979

$\leq 10^{15}$ cm for an optically thick H II region at 10^4 K (Habing et al. 1974).

(4) The infrared luminosity might arise in a group of embedded cool stars. The extremely non-linear dependence of UV production on photospheric temperature (Panagia 1973) makes it possible for a group of, say, ten B3 stars to provide 10^4 $L_\odot$ without violating the stringent radio limits.

The first three of the above alternatives suggest that the radio quiet infrared sources are at an earlier evolutionary stage than the compact H II regions. As a result they have been called "protostars" in contradistinction to the "cocoon stars" or compact H II regions (Werner et al. 1977).

The infrared properties of the protostars and ultra-compact H II regions are very similar and include: (1) an energy distribution characteristic of emission from grains with temperatures of 100 to 600 K; (2) absorption in some or all of the silicate and "ice" bands at 3, 10, and 20 μm, implying extinction by cold, foreground grains (Gillett et al. 1975; Knacke 1978; for a controversial, alternative identification of these bands see Hoyle and Wickramsinghe 1978); (3) strong 30 to 200 μm emission from 30 to 50 K grains in a surrounding molecular cloud; (4) bolometric luminosities of 10^4 to 10^5 $L_\odot$; (5a) point-like sources smaller than 1" and warm, 200 to 500 K, color temperatures; or (5b) extended sources, 5 to 10" across at 20 μm, with cooler, 80 to 200 K, color temperatures. The spectrum of a typical BN-like, radio weak infrared source, S140-IRS 1, is shown in Figure I.2, along with the 30 to 200 μm spectrum of the surrounding molecular cloud.

Relatively few of the radio weak sources are known because of an important selection effect--namely that most infrared searches have been

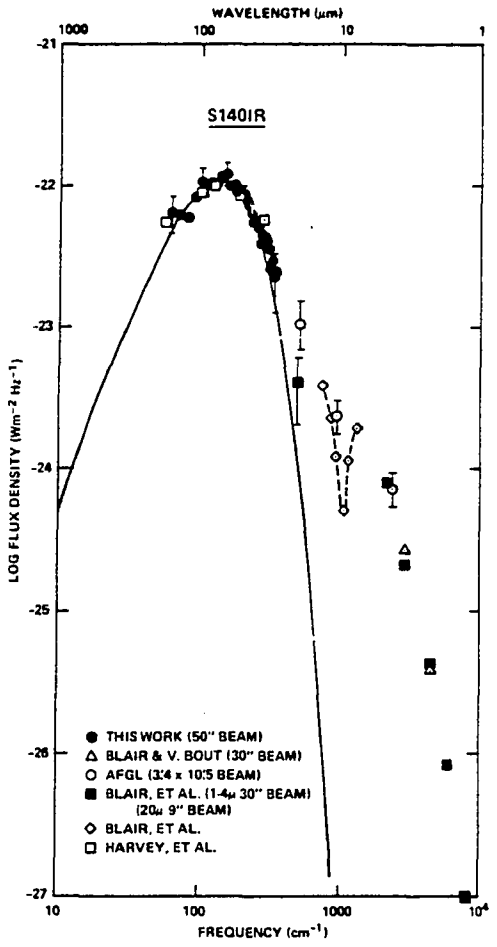

Figure I.2 The total infrared spectrum of S 140 (from Tokunaga et al. 1978, and refs. therein). Below 20 μm the energy comes from the point source S 140-IRS 1. The silicate absorption at 10 μm indicates that the object is embedded within a large amount of dust. Longward of 30 μm the dust in the molecular cloud itself, heated by the bright point source, radiates strongly.

conducted around the positions of known radio continuum sources. As a result of this bias, the intrinsic frequency of the "protostellar" objects is unknown. The small sample of objects makes it impossible to draw conclusions about intrinsic properties with any statistical significance. The primary aim of this dissertation is to examine molecular clouds for infrared sources without strong radio emission.

Another reason to examine closely the interiors of molecular clouds is to look for the development of multiple stellar systems. It is well known that O and B stars often form in groups of 3 to 10 stars with typical separations of 0.1 pc (Sharpless 1954). Studying the early stages of such systems can give information about the fragmentation of collapsing clouds. To investigate this problem clouds with one already known infrared source were searched for others.

This dissertation presents the results of searches conducted at infrared wavelengths of selected molecular clouds. Seven new infrared objects were discovered, four of which resemble BN and three of which resemble KL. No radio emission stronger than 25 mJy was seen from any of these sources, despite bolometric luminosities greater than 6×10^3 $L_\odot$.

Chapter II describes the selection of clouds and the method of observation. Chapter III presents the results. Chapter IV is a discussion of the observations. A summary and conclusions are given in Chapter V.

CHAPTER II
OBSERVATIONS

II.1 Design of a Search Program

Theoretical considerations and the properties of already-known objects within molecular clouds suggested that these sources would appear as emitters of infrared radiation with apparent color temperatures of 80 to 500 K. The Wein displacement law, which relates the wavelength of peak emission to the temperature of a radiating blackbody, $\lambda T=5100$ K μm, dictated searches in the 10 to 60 μm range. The fact that at ground level the atmosphere transmits infrared radiation only in discrete windows between 1 and 34 μm and becomes opaque between 34 and 350 μm placed important constraints on the wavelength coverage of the search. Because only ground-based observations were considered, searches at wavelengths longward of 34 μm were excluded and the detection of sources with color temperatures colder than about 200 K was compromised, particularly because the radiation observable at the ground from very cold sources falls on the steep exponential side of the Planck curve. All clouds were observed at 20 μm for maximum sensitivity to very red sources.

A second observational consideration led to the selection of 2.2 μm as an additional search wavelength. Longward of 3 μm the dominant source of noise is fluctuations in the thermal background radiation emitted by the telescope and atmosphere. This radiation can be considered as arising from a 270 to 300 K blackbody with an emissivity of 0.01 to 0.5 depending on wavelength (Traub and Stier 1976). For maximum sensitivity it is necessary to limit the amount of background reaching the detector by using small focal-plane apertures. Such

a constraint is at odds with the desire to search as much of a molecular cloud as possible. The 10 to 20 μm photometer at MKO has been optimized for observations of point sources by using a 2.5-mm aperture (7" at 224-cm telescope), thereby making searches of areas of sky much larger than 2 × 2' probibitively time consuming. To complement the long wavelength work, searches of large areas, around 5'x5', were undertaken at 2.2 μm with a 40" aperture.

Consider the upper limit to the total luminosity of a source of blackbody radiation that would escape detection in a search of a wavelength λ, down to a limiting flux density $F_{\nu o}$. For an object of temperature T, a distance d away, the limiting luminosity is

$$L < 4\pi d^2 \int F_\nu d\nu = 4\pi d^2 F_{\nu o}/B_{\nu o} \int B_\nu d\nu = 4\pi d^2 T^4 \sigma F_{\nu o}/B_{\nu o}$$

or

$$L(L_\odot) < 2.76(T/500)^4(\lambda/10\ \mu)^3(e^{14388/\lambda T} - 1)F_\nu(Jy)d^2_{kpc} \qquad \text{II.1}$$

where B_ν is the Planck function, $F_{\nu o}$ is measured in Jansky, d in kpc, λ is in microns, and the luminosity is in solar units, $L_\odot$.

Figure II.1 is a plot of limiting luminosities as a function of source temperature based on Equation II.1 using typical wavelengths and flux limits. The positions of a number of protostellar sources, normalized to 1 kpc, are indicated for reference.

The fact that the observed spectra of most infrared objects is distinctly not that of a blackbody makes Equation II.1 of heuristic value only. Radiative transfer effects due to the existence of strong temperature gradients and to scattering conspire to produce spectra much broader than that of a single temperature blackbody making astronomical

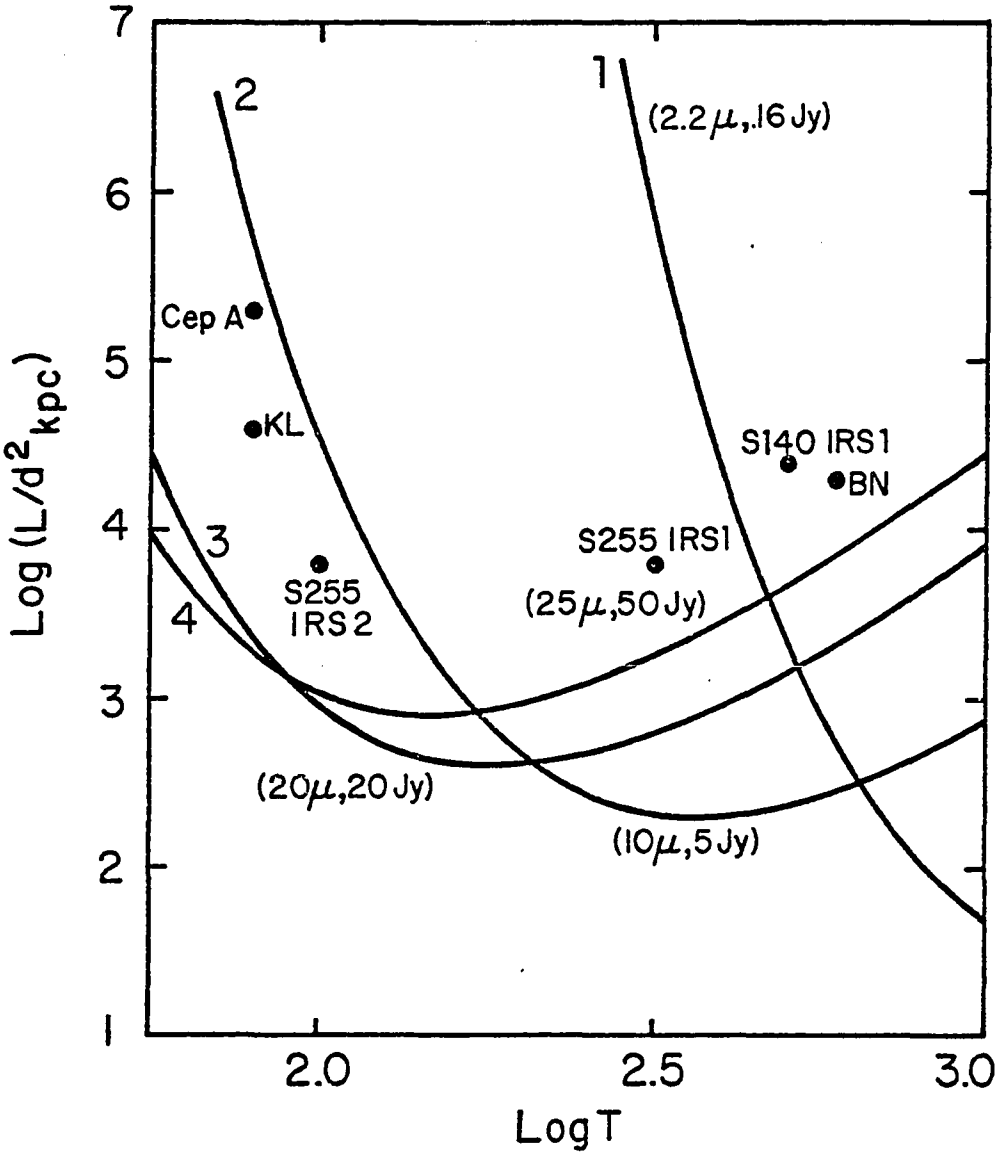

Figure II.1 Sensitivity limit as a function of temperature based on equation II.1. A blackbody of temperature T and luminosity $L(L_{\odot})$ a distance d(kpc) away is detectable at a certain wavelength if it lies above the appropriate solid line. Sensitivities typical of the searches conducted for this dissertation are shown: 1) 2.2 μm and 0.16 Jy; 2) 10 μm and 5 Jy; 3) 20 μm and 20 Jy; 4) 25 μm and 50 Jy.

objects easier to detect than Equation II.1 would indicate. The discovery of a source of 2.2-μm radiation can lead to finding a source of much lower color temperature, as happened in the clouds S235 and S269 (see Chapter III).

On the other hand, the effects of foreground extinction by cold grains within the surrounding molecular cloud can degrade the limits of Equation II.1. Standard interstellar extinction curves (Becklin et al. 1978) suggest that the limits of Equation II.1 should be raised, very approximately, by amounts of $e^{0.1A_V}$, $e^{0.08A_V}$ and $e^{0.05A_V}$ at wavelengths of 2.2, 10 and 20 μm, where A_V is the amount of visual extinction to the object in magnitudes. The effect can be significant in very dense clouds were A_V's exceed 100.

In summary, searches of molecular clouds can be made practically over in a small area at 10 and 20 μm with good sensitivity to sources of color temperatures in excess of 70 K. Searches at 2.2 μm provide good spatial coverage at the expense of sensitivity to very red objects.

II.2 Selection of Molecular Clouds

Molecular clouds were selected for observation on the basis of a number of radio, infrared and optical criteria. First of all, the 2.6-mm line of CO ($J = 1 \rightarrow 0$) was used to define the extent of a molecular cloud and to locate the central position for a search (Blair, Peters, and Van den Bout 1975; Knapp et al. 1977; Sargent 1977; Kutner and Dickman 1978). A subtlety of CO observations is that measurements in the optically thick line of the most abundant $^{12}C^{16}O$ isotope (called simply CO) are a probe of gas temperature, and that measurements in the optically thin $^{13}C^{16}O$ line (called ^{13}CO) are a probe of gas density (Thaddeus 1977). It has been found that molecular clouds contain

"hotspots" where the CO temperature exceeds 20 K and where infrared sources are often found (Evans 1978). These hotspots are also usually found to be regions of high density. Because the 10 and 20 μm searches had to be restricted to relatively small areas, it was decided to examine the immediate vicinity of either "hotspots" or regions of high density. The justification for this choice is simply that on a pitch dark night it is best to start searching under the available street lamps.

H_2O and Type 1 OH masers are good "street lamps" of the conditions required for star formation and often accompany infrared objects and compact H II regions (Genzel and Downes 1977). Priority was given those clouds known to contain masers.

As one of the avowed purposes of this dissertation was to study infrared objects that do not have strong H II regions surrounding them, a conscious effort was made to select molecular clouds without strong radio continuum emission (Felli and Churchwell 1977; Felli et al. 1978a). However, because CO observers, like infrared observers, tend to look in regions where the probability of success is high, molecular line studies have a built-in bias that places the observed clouds in proximity to known H II regions. The survey by Blair et al. (1975) of the Sharpless (1959) H II regions is one example. As a result of these competing effects, the clouds searched do not have strong H II regions within them, but are often found close to well-developed radio or optical H II regions.

Two infrared criteria were used to choose between otherwise suitable molecular clouds. Some clouds containing at least one well-studied infrared source, such as Sharpless 140 (designated simply S140) or S255,

were examined in the hope of uncovering new objects. In other cases, clouds were selected on the basis of being close to an infrared object listed in the AFGL rocket survey (Price and Walker 1976). This nearly full sky survey lists over three thousand sources of 4, 11, 20, or 27 μm radiation. Those clouds in the vicinity of an AFGL object were given high priority. Search centers were taken from CO data whose positional accuracy is much greater than that of the AFGL survey.

Although there were no conscious optical selection criteria, the reliance on CO data does bring with it certain biases. The Sharpless H II regions were themselves discovered by their appearance on the Palomar Observatory Sky Survey (POSS) plates. Other CO surveys have concentrated on regions with peculiar optical properties such as reflection nebulae (Knapp et al. 1977; Kutner and Dickman 1978) and OB Associations (Sargent 1977). Thus, the use of existing CO data tends to bias the infrared searches toward relatively nearby clouds (<3 kpc) suffering from little interstellar extinction. The resulting optical selection effects bias the results toward centers of activity located at the edges and on the near sides of molecular clouds. The importance of these effects will be assessed in the discussion (Chapter IV).

II.3 Observational Method

A. Photometry

The observations for this dissertation were made using the 60- and 224-cm telescopes of the Mauna Kea Observatory. A variable aperture, photovoltaic InSb detector system, similar to that described by Hall et al. (1975) was used for observations in the five near-infrared photometric bands (Johnson 196). A helium cooled bolometer (Low and Hoffman 1963) with a fixed 2.5-mm focal plane aperture and twelve

intermediate and broadband filters was used for observations between 7.8 and 33 μm. The bandpasses of the filters are given in Table II.1. Also presented are the flux densities corresponding to $0^{m}.0$ and typical telluric extinction corrections (in magnitudes/airmass).

The two telescopes were used with f/35 chopping secondaries which alternately placed the source and an adjacent piece of sky into the detector field of view. The resulting AC signal was synchronously demodulated with a lock-in amplifier tuned to the 10 or 20 Hz chopping frequency. At the 224-cm telescope the amplifier output was sent to the IBM 1800 data acquisition system for processing using standard programs. At the 60-cm telescope the amplifier output was either recorded directly on a strip chart recorder, converted to a frequency using a voltage-frequency converter and summed in a high-speed counter, or sent into an LSI-11 data system and processed using standard programs.

Photometric observations made using standard beam switching techniques (Low and Rieke 1974) were reduced to unit airmass and calibrated with respect to the standard stars of Table II.2 (Neugebauer 1978, private communication; Morrison and Simon 1973). The calibration of the physical flux corresponding to $0^{m}.0$ (Table II.1) is from Beckwith _et al_. (1976) and has an uncertainty of ten percent. A Rayleigh-Jeans interpolation was used to calibrate intermediate wavelengths.

Apart from calibration errors the main sources of error are random, being due to guiding, seeing, variations in atmospheric transmission through the night and simply low signal-to-noise ratios on faint sources. Whenever possible the photometric observations were repeated on different nights to minimize these effects. The photometric data

Table II.1

Filters and Calibration of 0 mag.

Filters	λ_o	λ_ℓ^1	λ_u^1	$F_\nu(J_y)$	Ext. (mag/AM)
J	1.25	1.1	1.4	1520	0.05
H	1.65	1.52	1.80	980	0.06
K	2.20	1.99	2.41	620	0.10
L	3.80	3.51	4.18	280	0.15
M	4.80	4.48	5.05	153	0.30
N	10.8	8.16	13.35	37	0.10
Q[2]	~20	~17	~25	10	0.30
	7.8	6.01	8.14	62	0.50
	8.4	7.7	9.3	53	0.20
	8.9	8.4	9.33	50	0.15
	10.5	10.21	10.77	37	0.10
	11.1	10.1	12.1	31	0.05
	12.8	11.28	13.83	23	0.15
	18.1	17.28	18.92	12	0.30
	19.7	16.69	22.64	10	0.35
	25[3]	22.8	33	6.6	0.50
	33[3]	27	(43)	3.4	-

Notes:

1) Unless otherwise noted the upper and lower wavelengths are for the half-power points of the filter transmission excluding the effect of the atmosphere.

2) The true filter passband extends from 15.5 to 25 μm so that the passband is defined exclusively by the properties of the atmosphere.

3) Convolved with atmospheric transmission.

TABLE II.2

Standard Stars

Star	J	H	K	L	M	8.7	9.5	10	11.2	12.8	20[1]	25[2]
α Tau	1.86	-2.64	-2.80	-2.98	-2.77	-2.98	-3.01	-2.99	-3.08	-3.14	-3.23	-3.2
α Ori				-4.48	-4.24	-4.86	-5.14	-5.13	-5.39	-5.40	-5.74	-5.7
α Boo	-2.21	-2.90	-2.99	-3.10	-2.95	-3.17	-3.22	-3.15	-3.23	-3.33	-3.32	-3.3
α Sco				-4.17	-3.84	-4.55	-4.60	-4.54	-4.77	-4.76	-4.86	-4.9
α Her	-2.29	-3.14	-3.37	-3.71	-3.44	-3.84	-3.91	-3.87	-4.05	-4.16	-4.26	-4.3
β Peg	-1.19	-2.05	-2.22	-2.39	-2.21	-2.45	-2.56	-2.55	-2.59	-2.70	-2.74	-2.7
Vega	0.0	0.0	0.0	0.0	0.0	0.0	0.0	0.0	0.0	0.0	0.0	0.0
α Ari	-0.10	-0.24	-0.64	-0.74	-0.82							
β Boo	9.93	1.44	1.35	1.40	1.56							

[1]From Morrison and Simon 1973

[2]Assumed to be same as 20 μm magnitude

presented in Chapter III have random errors (exclusive of calibration errors) of 1σ or ten percent, whichever is larger.

A systematic error may affect the photometry because the energy distributions of cool sources ($T \lesssim 500$ K) differ strongly from those of the stars ($T \gtrsim 3000$ K) used for calibration. As a result of the way that the incident energy fills the filter passband there may be a color-temperature dependent shift in effective wavelength and in the inferred flux density (Morrison 1973). The effect on the flux can be as large as 30 percent in the extreme case of a source of extremely low color temperature observed with a very broadband filter (such as the 20-μm, Q, filter). More typical values are less than ten percent. Due to uncertainties in the amount of water vapor present on a given night, on which the effect depends critically, no correction was applied to the data. To minimize the problem narrowband measurements were made in preference to using the very broad N and Q filters, except for mapping purposes when the maximum amount of signal was required.

B. Search Technique and Sensitivity

The technique for searching a region was the same at both telescopes. A rectangular area was examined in a series of declination scans separated by one-half the beamwidth in right ascension. As the scanning and chopping directions were both North-South, sources passed through both the positive and negative beams, giving rise to a readily-identifiable S-curve response (Figure II.2). The distinctive signature was useful in rejecting spurious sources. The sensitivity of a scan depended on the detector response and noise, on the quality of the night, and on the scan rate. All scans at the 60-cm telescope were made at a rate of 0.75 or 1.0"/sec, in the 2.2-μ filter with a 40" beam. The

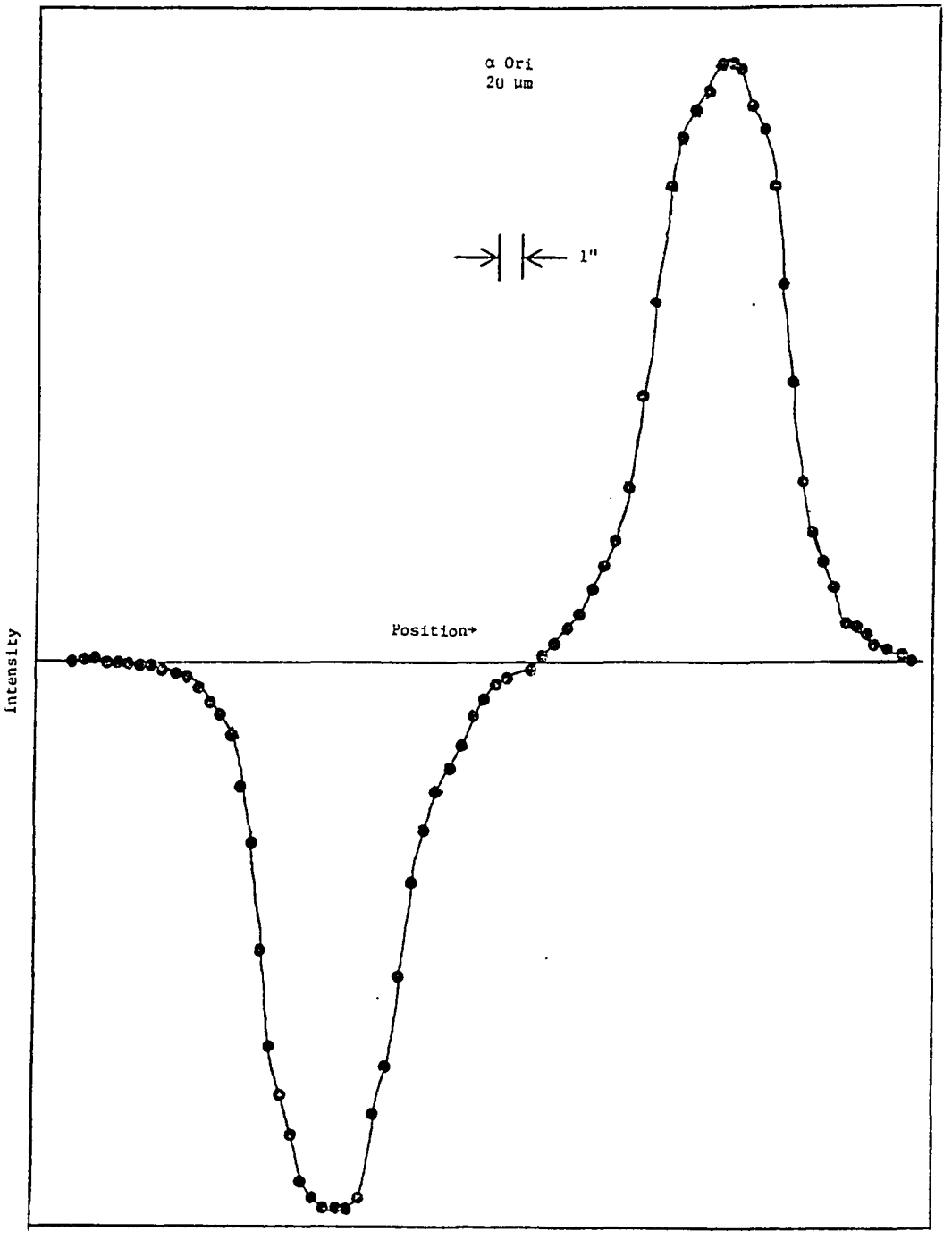

Figure II.2 A scan across the star Ori made at 20 μm using the 224 cm telescope with the chopping secondary. The distinctive S-curve response is the result of the star passing through the two beams produced by the chopping secondary.

3-σ limit for detection was approximately 9^m. Most of the scans at the 224-cm telescope used a rate of 1"/sec with average sensitivities to point sources of 5 Jy at 10 μ, 20 Jy at 20 μ, and 50 Jy at 25 μ. A few scans were made at the faster rate of 3"/sec resulting in detection limits a factor of two worse. All scans at the 224-cm telescope were made under computer control using the RASTER program.

C. Positions

The positions of sources observed for this dissertation were measured with respect to nearby field stars in two ways. At the 224-cm telescope, encoder readouts were used to give differences in position repeatable to within 1 to 2". At the 60-cm telescope and on occasion at the 224-cm telescope position differences were measured using a micrometer offset stage in the focal plane. The plate scale of the 224-cm telescope with the f/35 secondary has been measured to be 2.76 ± 0.04"/mm (Kunkle, private communication 1978). The plate scale at the 60-cm telescope is 9.8"/mm.

The positions of the reference field stars were either taken from the SAO catalog (1966) or measured on POSS prints with respect to at least seven SAO stars with a repeatability of 1". Corrections to the observed positional differences were applied for the effects of stellar proper motion, differential precession, and nutation at the epoch of observation to reduce the observations to epoch 1950.0. (Nautical Almanac, 1978 p. 508). These effects were typically less than 1". No corrections were applied for differential refraction or for possible motions of the infrared sources themselves.

The major uncertainty in obtaining positions at the 224-cm telescope was found to be the error inherent in centering the infrared

source in the 7" aperture. The repeatability of the observations indicates that this procedure is accurate to 1 to 4" depending on the brightness and size of the object. The combined errors indicate that absolute positional errors are on the order of 3 to 4". Relative positions of sources within a cluster are accurate to 1 to 2".

The positional accuracy of the observations at the 60-cm telescope is poor because of the large beam size (40") used. The 2.2-μm positions have an estimated uncertainty of 20".

D. Luminosity

An important characteristic of each infrared source is its energy output between 1.25 and 25 μm. This luminosity, denoted, L_{25}, is obtained by integrating the energy distribution over wavelength and in the case of extended sources over an area of the sky as well. The amount of energy radiated in a wavelength band is obtained from the observations from

$$L = 4\pi d^2 \int_{\nu_1}^{\nu_2} F_\nu d\nu \ .$$

With a trapezoidal approximation to this integral, the observed fluxes can be combined to give L_{25} (in $L_\odot$):

$$L = 4\pi d^2 \frac{c}{2} \sum (F_i + F_{i+1}) \left(\frac{1}{\lambda_i} - \frac{1}{\lambda_{i+1}}\right)$$

$$= 46.9 \ d_{kpc}^2 \sum F_i \left(\frac{1}{\lambda_{i-1}} - \frac{1}{\lambda_{i+1}}\right) L_\odot \qquad \text{II.2}$$

where F_i is measured in Jy at a λ_i in microns. In calculating L_{25} a straight line interpolation was made over the 10-μm absorption band, but

no other correction was made to account for the effects of intervening absorption.

Errors in the derived luminosity are due to statistical uncertainies in the photometry and to uncertainties in the absolute calibration. The use of a small aperture and a small chopper throw makes the observations insensitive to regions of low surface brightness and may result in a systematic underestimate of the total luminosity. Finally,the distances to many infrared objects, particularly those without optical counterparts, are not well known. As a result of all of these uncertainties, luminosities cannot be considered as being more accurate than 20 to 30 percent (and possibly far worse if the distance is ambiguous).

E. Restoration of Line Scans

A side effect of using spatial chopping to eliminate the thermal background is that a scan over an extended source of radiation gives the derivative of the true surface brightness distribution and not the brightness itself. The scan of Figure II.2 shows what happens when a simple point source passes through both the positive and negative beams. Scans across sources of more complicated structure must be integrated to give the brightness distribution. The line scans obtained at the 224-cm telescope were sampled at 1" intervals and the resulting derivative curves restored using the algorithm of Simon (1976).

F. Sizes of Extended Sources

A first-order correction for the effects of instrumental broadening on the size of an extended source can be made by noting that the result of convolving two gaussians of full-width-at-maxima (FWHM), w, is a third gaussian with a FWHM given by (Bracewell 1966, p. 173)

$$\underline{w}_o = (\underline{w}_b^{\,2} + \underline{w}_s^{\,2})^{1/2} \ . \qquad \text{II.3}$$

From the observed FWHM, $\underline{w}_o$, and the known beam size, $\underline{w}_b$, it is possible to estimate the true source size, $\underline{w}_s$.

The accuracy of the correction rapidly deteriorates for sources smaller than one-half the beam width. In practice this means that a source is considered unresolved in a 6" aperture if it is smaller than about 2".

G. 10-μm Optical Depth

The depth of the absorption feature at 10 μm is obtained solely from the observations. A straight line continuum is drawn between the 7.8 and 12.8 μm data. The deficit between the observed 10.5-μm datum and the 10.5-μm "continuum" is used to define the 10-μm optical depth, $\tau(10.5)$. The deepest part of the absorption band, however, comes at 9.7 μm. To obtain values of $\tau(9.7)$ for comparison with others in the literature, the observed $\tau(10.5)$ is multiplied by the ratio of 9.7 to 10.5 μm opacities, $Q(9.7)/Q(10.5) = 1.25$ (Gillett *et al*. 1975). It should be noted that $\tau(9.7)$ may be only very loosely related to the actual amount of material in the line of sight due to radiative transfer effects (Kwan and Scoville 1976).

CHAPTER III

RESULTS

III.1 The Data

The tables and figures of this section present all of the data obtained from the searching and mapping of molecular clouds as well as the photometry of objects discovered in the course of the searches. The format of presentation is as follows:

Table III.1 summarizes all of the searches at all wavelengths of the selected molecular clouds. In the table, Columns 1-3 identify the cloud, the wavelength and date of search. The existence of an AFGL rocket survey source is noted in Column 1. Columns 4 and 5 give the 1950 positions for the center of the search raster pattern. Columns 6 and 7 give the size of the raster box in the east-west and north-south directions (in minutes of arc). When only one number is given in Column 6 (or 7), then that number is the total width of the box around the central position given in column 4 (or 5). When two numbers are given, then these give the size of the box to either side of the central coordinate. For example, the entry in Column 6 for the object S184 is 2!6-3!3, meaning that a region from 2!6 east to 3!3 west of the central position of $00^h49^m27^s.6$ was examined. The single entry, 5!0, in Column 7 indicates the north-south extent of the search was 5', symmetric about the declination 56°17'31" given in Column 5. Column 8 gives the 3σ limiting flux density of the search. Column 9 gives the distance to the cloud in kpc. Columns 10 and 11 are upper limits to the luminosity of 100 K and 500 K sources of blackbody radiation that could have escaped detection, based on Equation II.1, the flux limit and the distance. Column 12 gives the peak CO temperature in the surrounding molecular cloud.

TABLE III.1 SEARCHES OF MOLECULAR CLOUDS AT 2.2, 10 and 20μm

Source	Date (UT)	λ(μm)	α(1950)	δ(1950)	$\alpha_E-\alpha_W$	$\delta_N-\delta_S$	F_{max}(Jy)	d(kpc)	$L_{100}(10^3L_o)$	$L_{500}(10^3L_o)$	T_{CO}(K)
S 184	01/18/78	2.2	$00^h49^m27^s.6$	56°17'31"	216-313	510	0.2	2.1[1]	-	10	15[1]
	01/24/78	20			018	112	40		8	10	
	12/30/77	20			110	110	40		8	10	
S 187	12/06/77	2.2	01 20 13	61 37 58	319-116	510	0.2	1.2[2]	-	4	27[2]
(GL 205)	12/07/77	2.2	01 19 40	61 35 24	210-116	510	0.2		-	4	
W3(OH)[3]	10/31/77	20	02 23 16.5	61 38 57	018	115	20	3.0	8	13	24[4]
IC 1848A	01/23/78	10	02 57 34.8	60 17 28	015-018	115	5	2.0[5]	150	1	20[6]
(GL 4029)	09/18/78	20			116	115	20		4	6	
VdB 19	12/09/77	2.2	03 41 22	31 59 23	213-216	510	0.2	0.3[7]	-	0.3	20[8]
NGC 1579 (LkHα101)	11/03/77	20	04 26 59	35 10 42	115	115	20	0.8[9]			17[9]
OMC 2	11/03/77	20	05 32 59	-05 12 10	110	115	20	0.5	0.3	0.3	49[25]
VdB 45	12/07/77	2.2	05 33 14	31 48 30	210-016	510	0.2	0.9[7]	-	2	20[8]
	01/22/78	10	05 33 16	31 47 51	115	115	7		44	0.3	
	09/18/78	20	05 33 16	31 47 51	115	115	25		1	1	
S 235 B	11/02/77	20	05 37 31.5	35 40 24	018	115	20	1.8[10]	3	5	26[11]
S 255	10/30/77	10	06 09 58.6	18 00 12	018	115	5	2.5[12]	240	1	30[12]
(GL 896)	10/29/77	20			018	115	20		6	9	
S 269 (GL 902)	11/01/77	20	06 11 47.1	13 50 34	018	115	20	2.0[14]	4	6	20[13]
VdB 92	12/08/77	2.2	07 01 33	-11 30 00	010-113	510	0.2	0.7[7]	-	1	20[8]
ρ Oph #29[15]	07/01/78	20	16 24 07.7	-24 30 40	115	115	30	0.2[15]	0.06	0.1	28[16]
IR 12.4+0.5	07/01/78	20	18 07 53.8	-17 57 10	114	115	20	2.1[18]	4	6	18[17]

TABLE III.1 SEARCHES OF MOLECULAR CLOUDS AT 2.2, 10 and 20 m (continued)

Source	Date (UT)	$\lambda(\mu m)$	$\delta(1950)$	$\delta(1950)$	$\alpha_E-\alpha_W$	$\delta_N-\delta_S$	F_{max}(Jy)	d(kpc)	$L_{100}(10^3 L_o)$	$L_{500}(10^3 L_o)$	T_{CO}(K)
MC 12.8+0.5	07/05/78	20	18 08 29.6	-17 32 04	115	115	20	2.1[16]	4	6	24[17]
VdB 130	07/04/78	10	20 16 01.8	39 12 23	410	210	20	1.0[7]	150	1	21[6]
	07/04/78	20	20 15 56.7	39 12 20	410	210	40		2	3	
VdB 132	06/24/78	20	20 22 56	42 13 17	310	310	30	1.0[7]	1	2	31[c]
GL 2591[19]	10/31/77	10	20 27 35.9	40 01 16	018	115	5	1.5[19]	90	0.5	-
	10/31/77	20			018	115	20		2	3	
VdB 136	06/13/78	2.2	20 36 29.8	41 53 50	213-017	510	0.2	0.4[7]	-	0.5	27[8]
(GL 2620)	06/20/78	20	20 36 29.8	41 53 50	113-317	117-313	60		0.5	0.7	
	06/23/78	20	20 36 26.2	41 56 58	110	115	20		0.2	0.2	
	06/23/78	10	20 36 26.2	41 56 58	110	115	5		6	0.04	
S 140	10/29/77	10	22 17 41.3	63 03 39	018	115	5	0.9[23]	30	0.2	24[21]
(GL 2884)	10/29/77	20			018	115	20		0.8	1	
VdB 155	12/09/77	2.2	22 51 02.3	61 52 46	310-213	510	0.2	0.6[7]	-	1	25[8]
Cep A	09/16/78	20	22 54 20.3	61 46 01	110	110	30	0.7[22]	0.7	1	18[23]
	09/18/78	20	22 54 19.5	61 45 51	115	115	30		0.7	1	
	09/18/78	20	22 54 20.0	61 44 42	110-015	115	30		0.7	1	
	09/19/78	20	22 54 19.5	61 45 51	012-112	115-015	30		0.7	1	
Cep B	07/01/78	20	22 55 31	62 21 30	210	310	30	0.7[22]	0.7	1	30[23]
(GL 3000)	07/02/78	20	22 55 31[24]	62 19 30	118	310	60		1	2	
	07/04/78	10	22 55 31	62 19 30	118	310	10		40	0.2	

Notes to Table III.1

1. Elmegreen and Lada 1978. Search centers on H_2O maser
2. Blair *et al*. 1975.
3. Wynn-Williams 1971.
4. T_b from Lada *et al*. 1978.
5. Estimates range from 1.7 to 2.3 kpc (Becker and Fenkart 1971).
6. Loren and Wooten 1978
7. Racine 1968.
8. Kutner and Dickman 1978, private communication.
9. Knapp *et al*. 1977.
10. Georgelin, Y. M. 1978, private communication.
11. Evans, 1978, private communication.
12. Evans *et al*. 1977. See note added in proof.
13. Blair *et al*. 1975.
14. Israel 1976.
15. Elias 1978.
16. Encrenaz 1975.
17. Wright *et al* 1979
18. Distance is that to M17, Reifenstein *et al*. 1970.
19. Wynn-Williams *et al*. 1977.
20. Crampton and Fisher 1974.
21. Blair *et al*. 1978.
22. Garmany 1973.
23. Sargent 1977.
24. Position center for Figure III.1h.
25. Gatley *et al*. 1974.

Figures III.1a-h are sketches of those regions for which CO maps are available (from the references given in Table III.1). Each map is 10' on a side with North to the top and East to the left and is centered on the position given in Table III.1. Contours of CO antenna temperature are drawn in to delineate the extent of molecular cloud. The areas searched at 2.2 μm and 10 or 20 μm (whichever is larger) are shown within dashed and solid lines. The positions of infrared objects detected at 10 to 25 μm are marked (+).

Table III.2 lists the positions of all sources found during the 2.2-μm searches at the 60-cm telescope. Also given is the 1.25 to 3.4-μm photometry taken with both telescopes.

Table III.3 lists the positions of sources uncovered during 10 and 20-μm searches at the 224-cm telescope. Also tabulated are the depth of the silicate band, the ratio of the 25-μm to 12.8-μm fluxes, the 20-μm size, the observed luminosity out to 25 μm, L_{25}, and, for future reference, the total luminosity, L_{tot}, when available from airborne observations. The depth of the 10-μm band follows the definition given in Section II.3.G. Table III.4 (also Figures III.2a,b) gives the 7.8 to 25-μm photometry of the sources listed in Table III.3. In the case of extended objects the photometry is for the central 6".5 of the object. The values of L_{25} given in Table III.3 do, however, take into account the extended nature of some of the objects.

Table III.5 lists unpublished far-infrared observations for two molecular clouds, S235 and S255, used to derive the total luminosities given in Table III.3. The data were taken from Kuiper Airborne Observatory (KAO) using a 1' beam and the photometer described by Gatley et al. (1977).

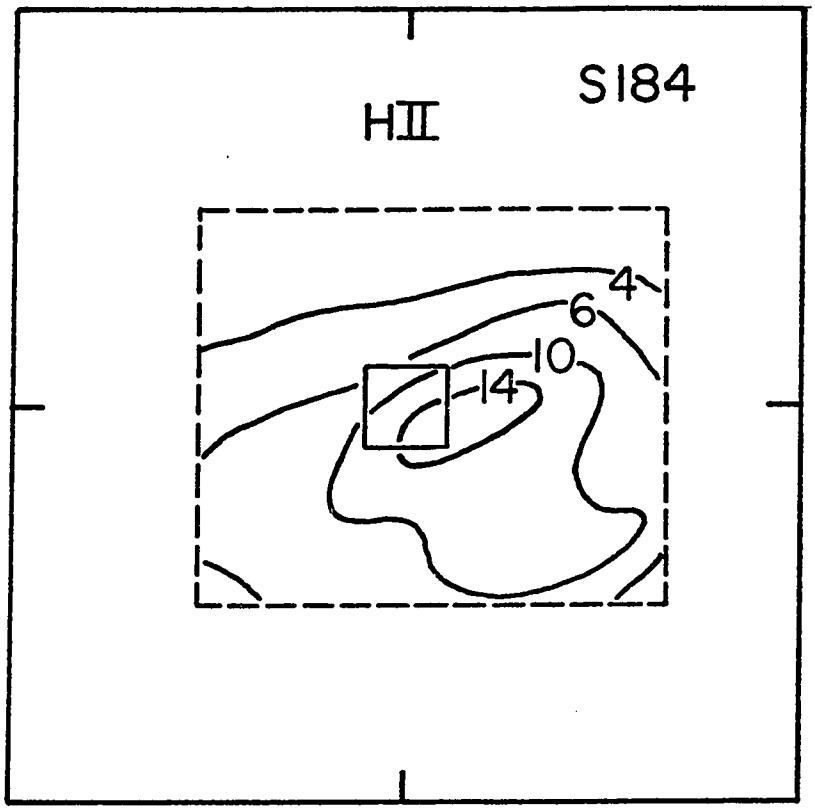

Figure III.1a Sketch of the molecular cloud near S184. The dashed line demarcates the region searched at 2.2μm. The smaller solid box shows the region examined at 20 μm. Numerals give CO temperatures.

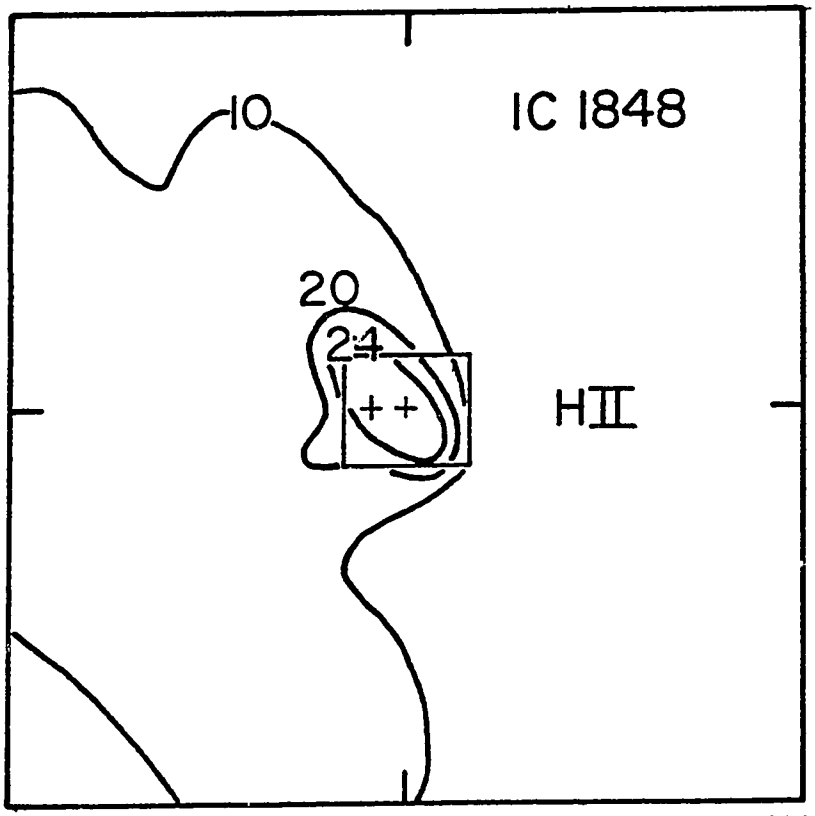

Figure III.1b. Similar to figure 1a, but for the cloud IC1848A. Crosses denote the positions of infrared objects.

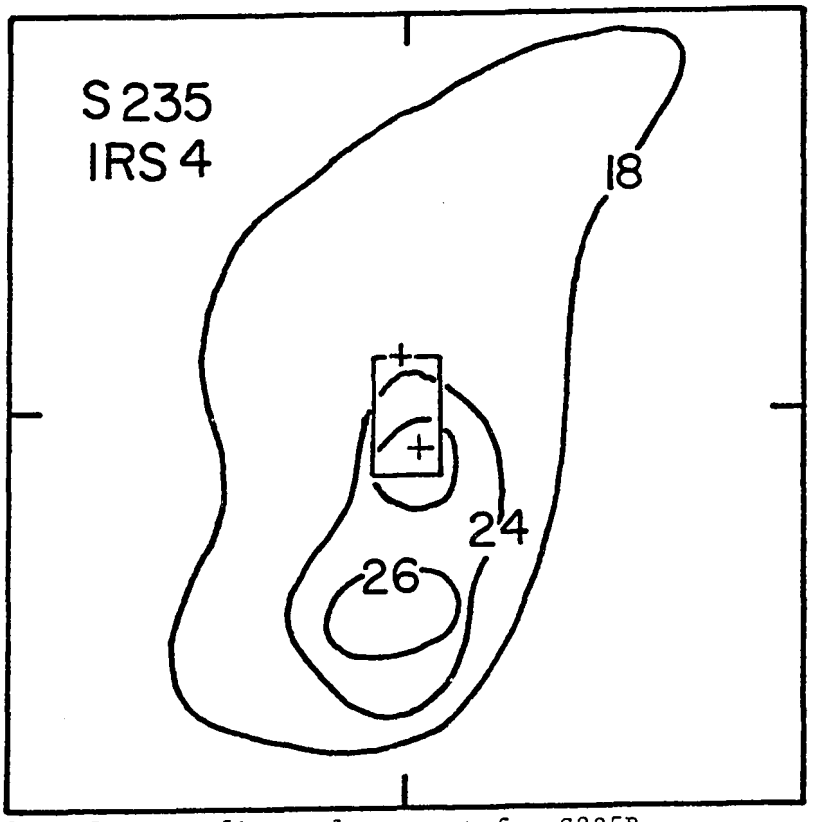

Figure III.1c. Same as figure 1a except for S235B.

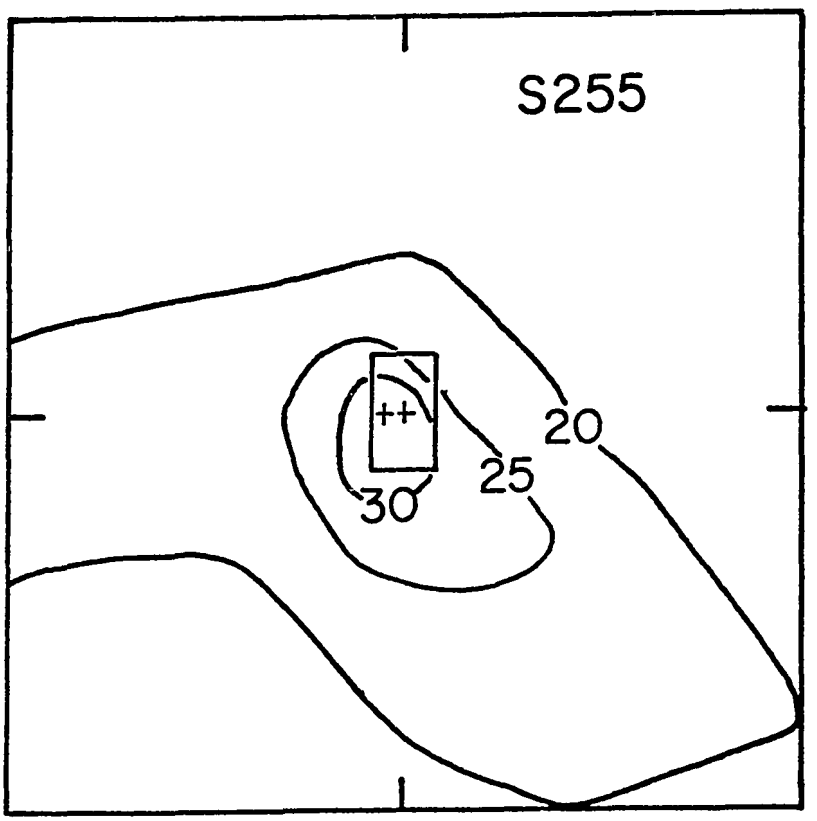

Figure III.1d. Same as figure 1a except for S255.

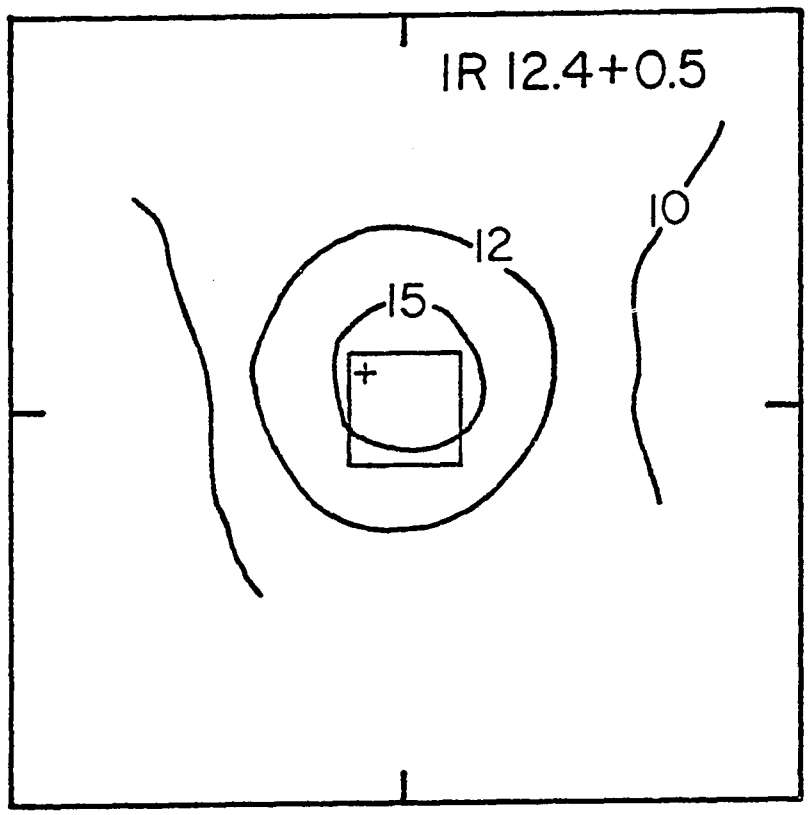

Figure III.e. Same as figure III.1a, except for IR 12.4+0.5.

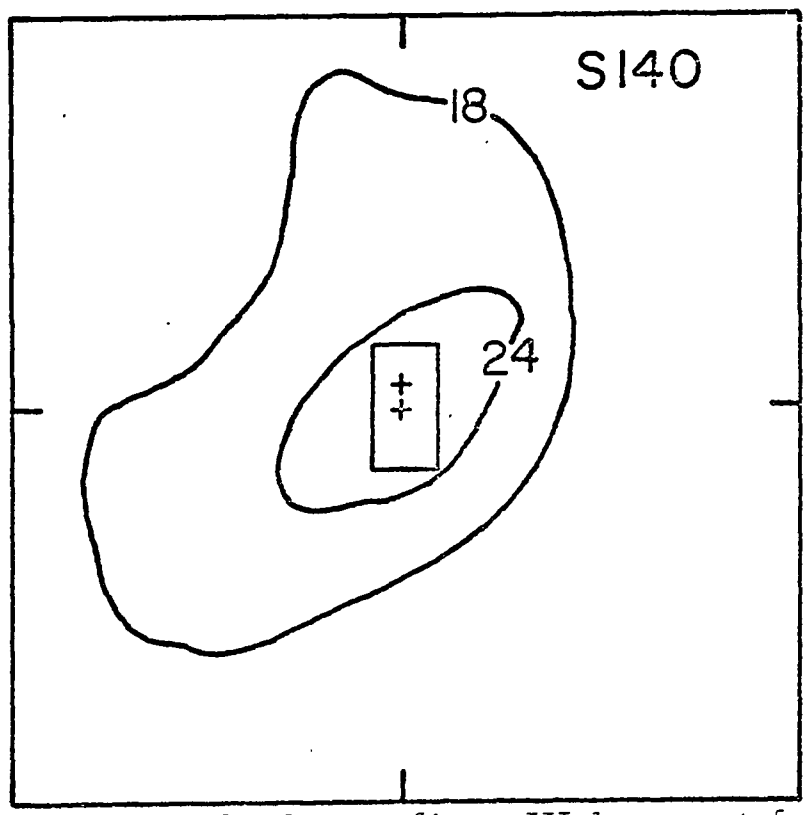

Figure III.1f. Same as figure III.1a, except for S 140.

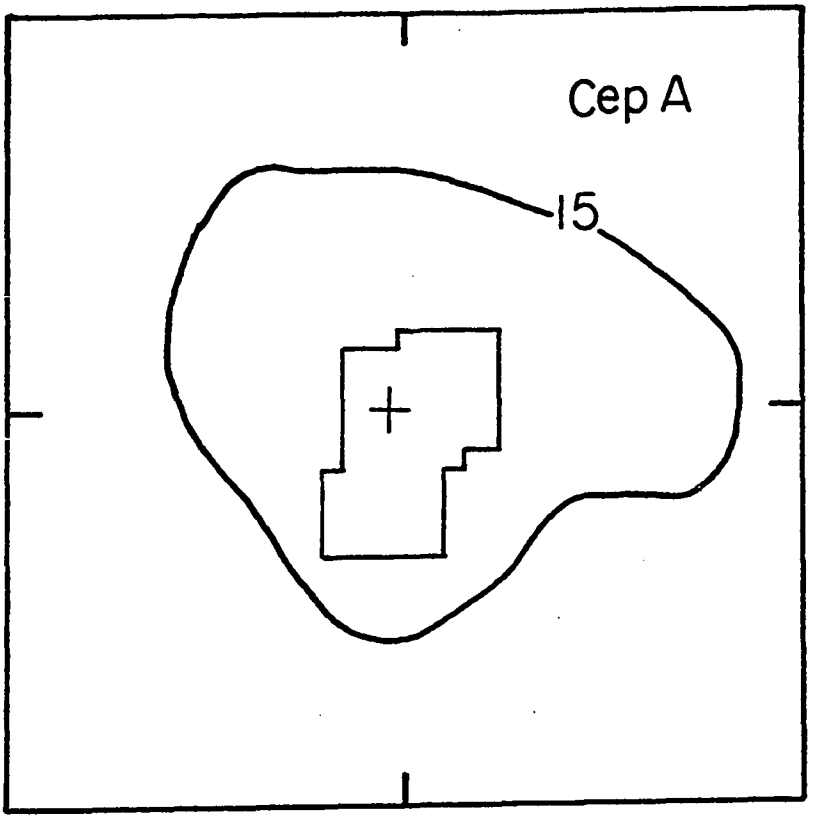

Figure III.1g. Same as 1a except for Cep A.

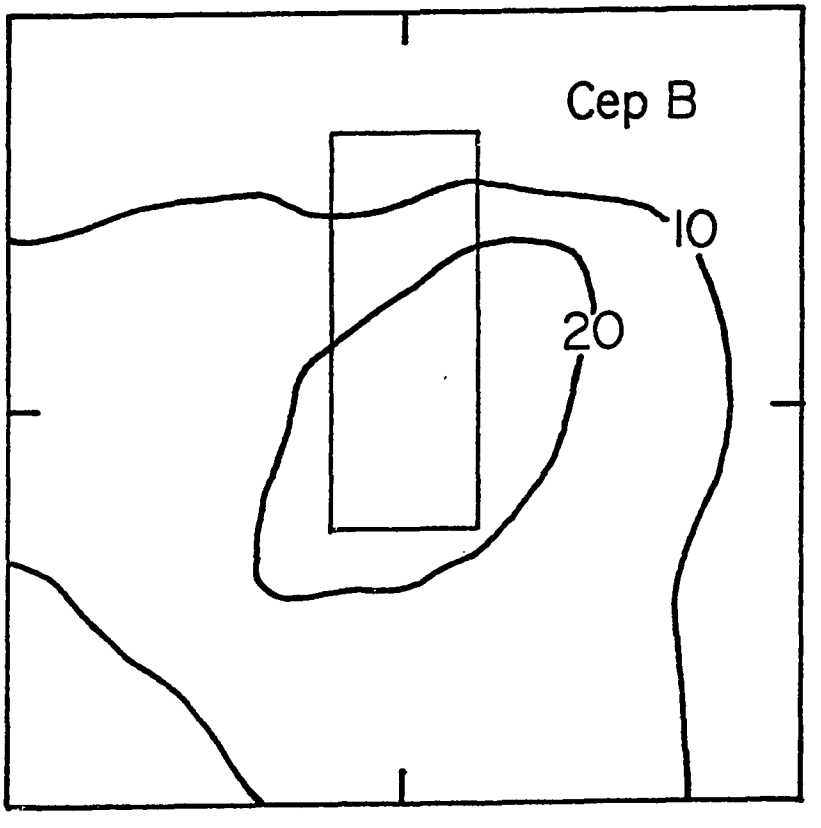

Figure III.1h. Same as 1a except for Cep B.

TABLE III.2

Results of 2.2 μm Searches

Object	α (1950)	δ (1950)	J	H	K	L
S 184/1	$00^h49^m17^s.3$	56°18'12"	10.7 ±0.4	10.7 ±0.5	10.0 ±0.2	-
S 187/1	01 20 13.7	61 35 34	10.3 ±0.2	-	8.0 ±0.2	-
S 187/2	01 20 01.8	61 34 16	8.60±0.05	-	8.8 ±0.2	<6.9
S 187/3	01 21 13	61 37 58	7.60±0.03	7.32±0.05	5.72±0.05	-
S 187/4	01 19 37	61 38 39	10.8 ±0.2	9.4 ±0.1	8.5 ±0.1	-
VdB 19	03 41 25.8	32 00 23	7.15±0.05	7.50±0.05	6.96±0.07	-
VdB 19/1	03 41 26.7	32 00 43	8.2 ±0.1	8.2 ±0.1	7.4± 0.1	-
VdB 19/2	03 41 22.7	32 00 16	10.1 ±0.3	-	-	-
VdB 19/3	03 41 18	32 00 52	9.0 ±0.1	-	8.4 ±0.2	-
VdB 19/4	03 41 22	31 55 19	8.1 ±0.1	-	7.6 ±0.1	-
VdB 19/5	03 41 23.5	31 57 34	9.3 ±0.1	-	8.4 ±0.1	-
VdB 19/6	03 41 24	31 59 06	9.9 ±0.1	-	9.9 ±0.04	-
VdB 19/8	03 41 31	31 59 23	10.1 ±0.3	-	8.5 ±0.2	-
VdB 19/9	03 41 28	31 56 48	9.3 ±0.1	-	8.2 ±0.1	-
VdB 19/11	03 41 11	31 57 45	9.9 ±0.2	-	9.6 ±0.4	-
Vdb 19/12	03 41 10	32 00 12	9.4 ±0.2	-	8.4 ±0.2	-
VdB 45	05 33 26	31 49 54	9.2 ±0.1	9.0 ±0.1	8.7 ±0.1	-
VdB 45/1	05 33 16	31 47 51	12.1 ±0.1	10.6 ±0.1	9.5 ±0.1	7.3±0.3
VdB 45/2	05 33 28	31 46 40	-	8.3 ±0.1	8.3 ±0.1	-
S 269/3	06 11 46	13 50 30	11.5 ±0.2	10.1 ±0.03	8.8 ±0.2	6.2±0.2

TABLE III.2 continued

Object	α (1950)	δ (1950)	J	H	K	L
VdB 92/1	$07^h01^m33^s$	-11°30'00"	8.5 ±0.1	-	8.6 ±0.1	-
VdB 92/2	07 01 30.7	-11 30 20	8.7 ±0.1	-	8.7 ±0.1	-
VdB 92/3	07 01 33	-11 29 10	9.5 ±0.2	-	9.1 ±0.1	-
VdB 92/4	07 01 22.6	-11 28 36	11.4 ±0.4	9.6 ±0.2	9.3 ±0.2	-
Z CMA	07 01 27.7	-11 29 54	5.85±0.05	4.61±0.06	3.51±0.03	4.3±0.1
IR 12.4 0.45*	18 07 55.8	-17 56 32	13.8 ±0.1	11.22±0.03	9.28±0.04	7.0±0.1
VdB 136/1	20 36 40.7	41 55 44	10.4 ±0.3	-	8.6 ±0.1	-
VdB 136/2	20 36 37.9	41 52 10	< 10	-	7.4 ±0.1	-
VdB 155	22 51 18	61 52 46	7.1 ±0.1	6.62±0.05	6.40±0.05	<5.4
VdB 155/1	22 51 13	61 53 25	11.4 ±0.2	10.0 ±0.1	9.6 ±0.3	<4.4

* From 224 cm telescope

Table III.3

Characteristics of Infrared Sources

Source Name	α (1950)	α (1950)	$\tau_{9.7}$	$F_{25}/F_{12.8}$	$L_{25}(10^3 L_o)$	$L_{tot}(10^3 L_o)$	20μm size	Notes
IC 1848A-IRS 1	$02^h57^m34^s.7\pm0^s.3$	60°17'28"±3"	1.4±0.2	8 ±1	1.3± 0.1	-	<3"	-
IC 1848A-IRS 2	02 57 37.7±0.3	60 17 31 ±3	1.6±0.5	33 ±8	0.8± 0.1	-	7"±2"	-
S235-IRS 4	05 37 30.6±0.2	35 39 59 ±3	1.4±0.2	14 ±2	0.4± 0.05	6	<3"	1
S255-IRS 1	06 09 58.6±0.2	18 00 12± 3	2.5±0.3	1.9±0.1	9.4± 0.2	80	<3"	2
S255-IRS 2	06 09 59.7±0.2	18 00 09± 3	>2	23 ± 5	2.8± 0.2	-	6"±2"	3
S269-IRS 2	06 11 47.4±0.2	13 50 32± 3	-	-	-	-	5"±2"	4
S269-IRS 3	06 11 47.1±0.2	13 50 34± 3	1.5±0.8	17 ±4	0.5 ±0.1	-	3"	-
IR 12.4±0.5	18 07 55.8±0.2	-17 56 32± 3	<0.3	22 ±7	2.1 ±0.2	20	4"±2"	5
S 140-IRS 1	22 17 41.3±0.2	63 03 39± 2	1.4±0.1	2.7±0.1	4.2± 0.2	20	<3"	6
S 140-IRS 2	22 17 41.2±0.2	63 03 56± 3	1.3±0.3	12 ± 2	0.20±0.02	-	<3"	-
S 140-IRS 3	22 17 42.7±0.2	63 03 42± 3	1.7±0.1	3.8±0.3	0.40±0.1	-	<3"	-
Cep A	22 54 19.3±0.3	61 45 52± 3	-	70 ± 10	0.27±0.03	100	7"±1"	7

Table III.4

7.8 μ - 25 μm Photometry F_ν (Jy)

	7.8	8.4	8.9	N	10.5	11.5	12.8	18	19.8	Q	25
IC1848A-IRS 1	9±2	6.5±0.5	5.3±0.5	-	3.0±0.5	5 ±1	9 ± 1	36±8	29±7	40±4	70±10
IC1848A-IRS 2	2.0±0.5	1.2±0.5	-	-	0.7±0.2	-	2.1± 0.3	26±3	32±3	33±9	70±15
S 235-IRS 4	3.3±0.3	-	3.4±0.3	3.3±0.4	1.4±0.2	-	3.2±0.3	27±2	22±2	24±2	44±5
S 255-IRS 1	84±4	-	34±3	40±2	13±1	-	110±5	100±5	100±5	120±10	210±10
S 255-IRS 2	1.6±0.7	1.5±0.2	1.5±0.2	1.1±0.1	<1.0	-	2.1±0.3	16±2	22±2	23±2	49±9
S 269-IRS 3	2.0±0.2	-	1.5±0.2	1.6±0.2	1.0±0.3	-	6.0±0.8	22±3	22±2	31±3	100±20
IR 12.4+0.5	-	-	3.0±0.5	-	3.9±0.5	4.4±0.3	9±2	110±20	90±20	-	200±50
S 140-IRS 1	150±30	130±5	93±5	145±5	83±5	-	345±10	570±30	540±30	690±40	920±40
S 140-IRS 2	<5	3.8±0.4	-	4.0±0.8	3.2±0.8	-	12±1	52±5	68±5	100±8	140±10
S 140-IRS 3	26±2	21±2	12±1	15±1	7 ±1	-	42±4	76±5	77±6	105±8	160±10
Cep A	<5	-	<0.8	0.8±0.1	<15	<2.1	3.3±0.3	32±5	35±5	48±5	220±30

Table IV.5

Far Infrared Fluxes (Jy)

Source	30μm	50μm	100μm	200μm
S255 peak	1350±100	2250±50	2970±50	1140±100
1'N*	-50±125	420±10	1740±25	820±195
2'N	150±175	15±30	205±45	330±195
1'E	190±210	275±40	580±45	430±330
1'W	450±160	380±30	825±35	270±250
1'S	75±125	100±25	525±40	860±330
S235-IRS 4	440±100	450±70	710 ±50	530±170

*Directions are inclined by 20° to true north.

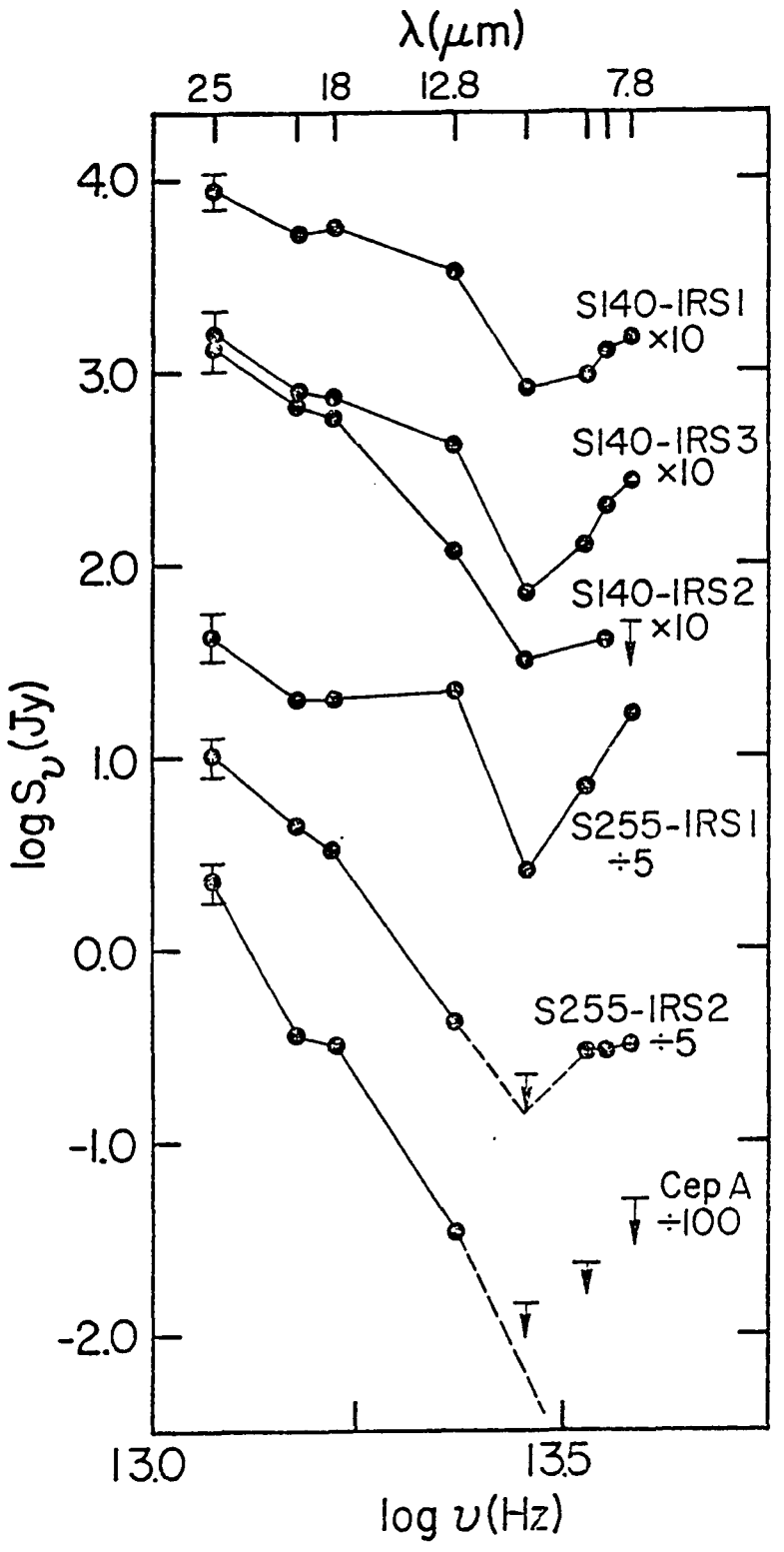

Figure III.2a. Energy distributions from 7.8-25 μm photometry for central 6".5 of all sources. Limits are 2σ . Errors are as given in the error bars, or nσ larger than the filled circles.

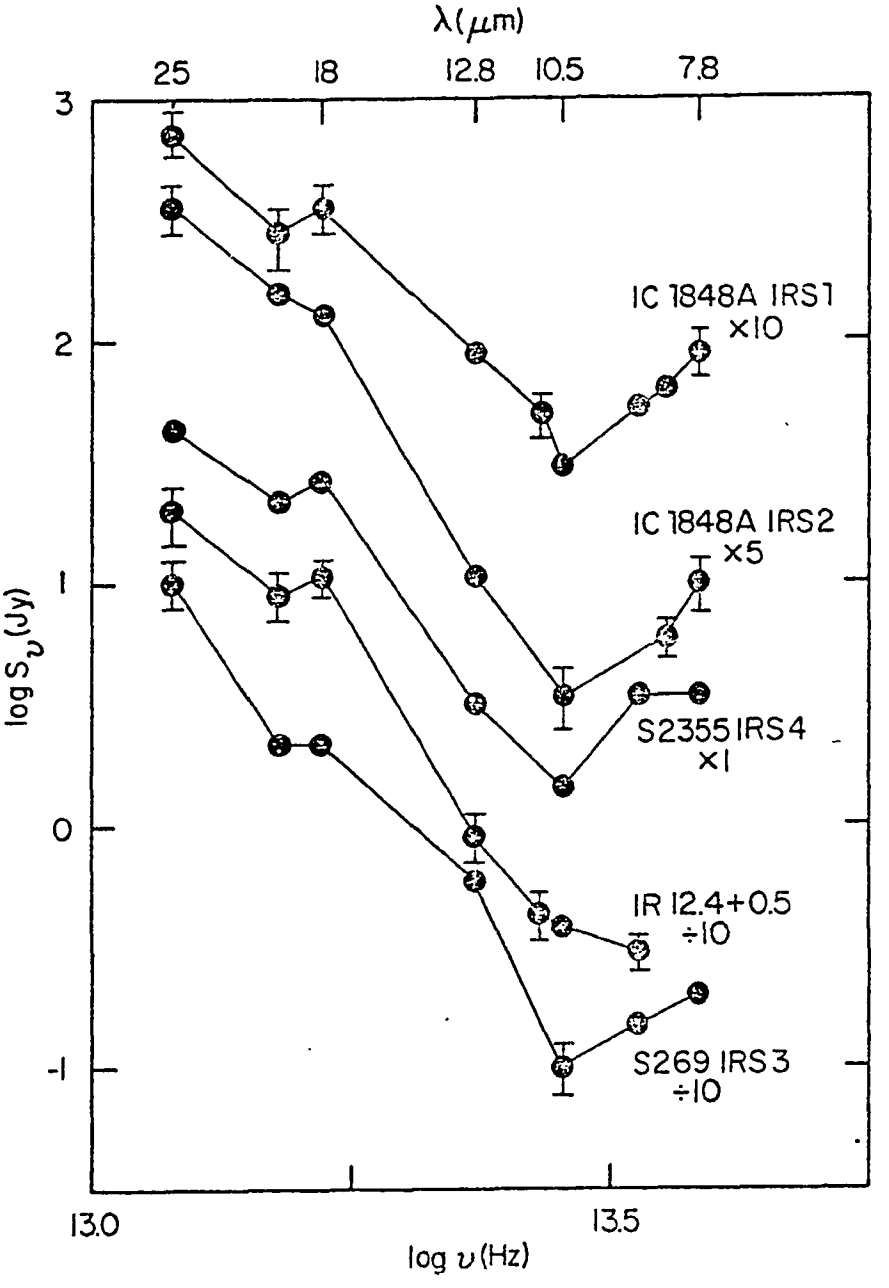

Figure III.2b. Energy distributions from 7.8 μm to 25 μm photometry.

Following the tabular data, the observations are discussed on region-by-region basis. Additional data such as 10, 20 and 25-μm maps and line scans are presented for those regions with either a group of objects or an extended source of emission.

1. Sharpless 184 (NGC 281)

Elmegreen and Lada (1978) mapped the CO emission in the vicinity of the optical H II region and also discovered an H_2O maser close to the edge of the 15 K cloud. The maser position was taken for the 20-μm search center, but no sources were discovered.

2. Sharpless 187

Blair *et al*. (1975) discovered strong CO emission near the H II region and the AFGL survey lists the presence of source #205 in the vicinity. Searches were made over a large area at 2.2 μm without finding any objects which could not be identified as stars (see below for a discussion of the criteria for separating normal stars from the more interesting embedded molecular cloud sources).

3. W3 (OH)

The vicinity of this ultra-compact H II region (Wynn-Williams *et al*. 1972) was examined in the hope of finding new objects. No additional sources were discovered.

4. IC 1848-A (W5)

The emission nebula IC 1848-A is a large region some 35 pc in diameter. Observations of molecular lines by Loren and Wooten (1978) showed that the bright rim of emission at the eastern end of the nebula (Pottasch 1956) is due to an ionization front impinging on the surface of an adjacent molecular cloud. Inside the cloud Loren and Wooten found a bright source of 2.2 μm to 5 μm radiation.

Observations from MKO show that there are two sources of 10 to 20 μm radiation within the cloud. IC 1848A-IRS 1 is an unresolved object similar in many respects to BN. For reasons to be enumerated shortly, IRS 1 probably corresponds to the object discovered by Loren and Wooten, despite a positional discrepancy of some 40". To the east of IRS 1 is a cooler, extended source and with a 20-μm size of 7" ± 2", designated IC 1848A-IRS 2. Figure III.3 shows north-south scans at 20 μm across the two infrared objects as well as a comparison scan across the star α Ori, taken immediately after the IC 1848 data. The extended nature of IRS 2 is evident.

Four arguments suggest that IRS 1 is identical to the object discovered by Loren and Wooten. (1) Scans over their quoted position revealed no 10 to 20-μm sources despite the fact that an extrapolation of their 2 to 5-μm photometry would lead one to expect a strong 10-μm emitter. (2) The 8 to 25-μm photometry on IRS 1 from Mauna Kea matches up well with the 2 to 5-μm data, indicating a single source. (3) The uncertainty in the 2-μm position is "somewhat larger" than their 30" beam size, so that the positional discrepancy is within the errors. (4) The MKO location of IRS 1 and IRS 2 places them within the cloud rather than at the edge--a position consistent with their presumed role as the main energy sources for the molecular cloud.

5. <u>VdB 19 (IC 348)</u>

This is one of seven Van den Bergh (1966) reflection nebulae for which the CO data of Kutner and Dickman (1978, private communication) indicate the presence of a warm molecular cloud. The 2.2-μm searches around the CO peak revealed eleven objects, most of which could be identified with visible stars (Harris, Morgan and Roman 1954).

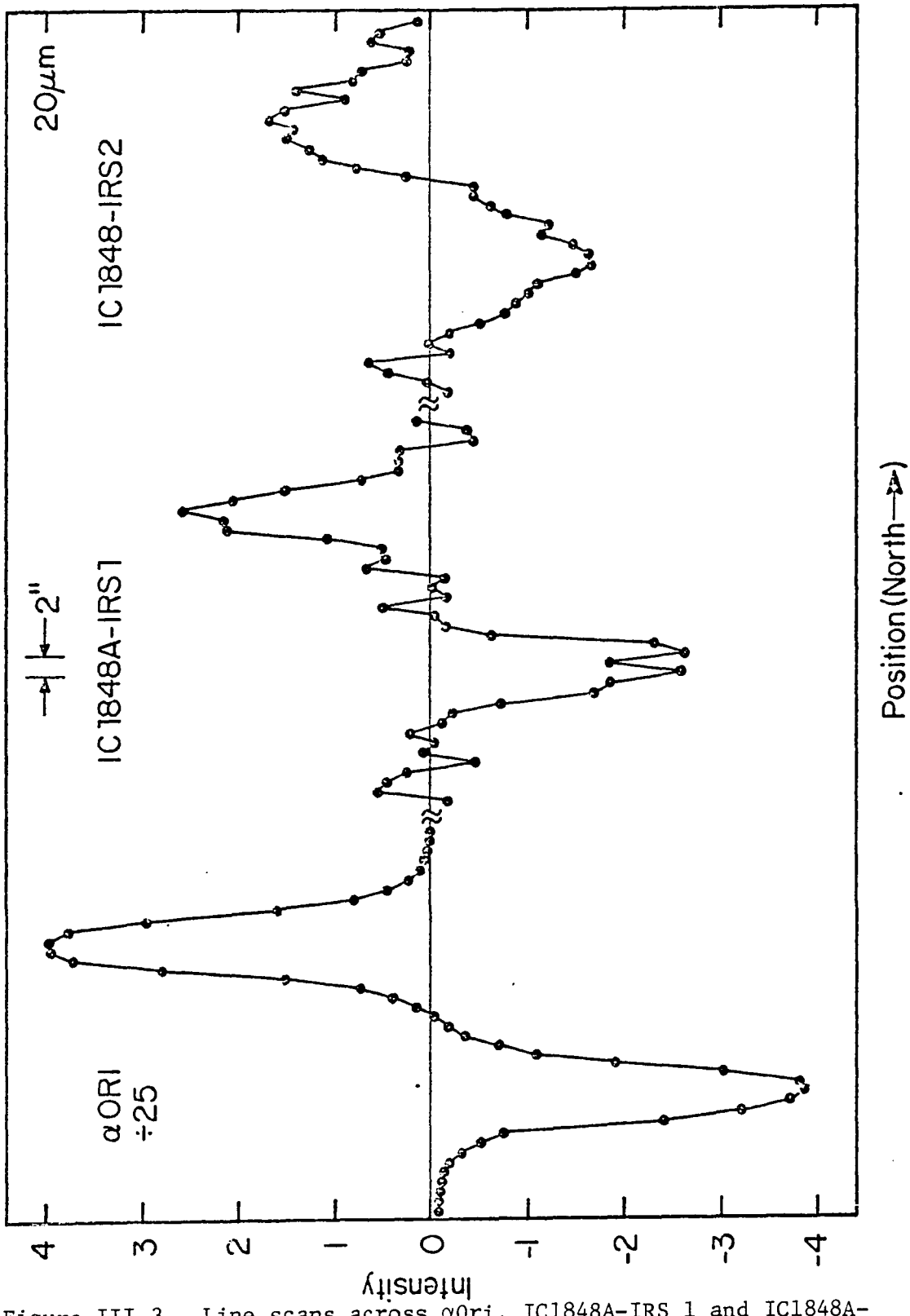

Figure III.3. Line scans across αOri, IC1848A-IRS 1 and IC1848A-IRS 2 at 20 μm. IRS 1 is unresolved while IRS 2 is clearly extended. The scan of α Ori was taken immediately after those in IC 1848A. .

Table III.6 lists those stars which showed up in the infrared search (Table III.2). Only two objects VdB 19/5 and VdB 19/6 do not appear in the plate of Harris et al., but these have colors similar to the other stars.

6. NGC 1579 (LkHα101)

The molecular cloud surrounding the peculiar emission star (Herbig 1971; Cohen and Woolf 1971) has been studied by Knapp et al. (1975). No infrared object other than LkHα101 itself was found in a 20-μm search.

7. OMC 2

The vicinity around OMC 2-IRS 3 (Gatley et al. 1974) was examined at 20 μm but no new objects were found.

8. VdB 45

One 2.2-μm object was found at the location of peak CO emission. The 1.2 to 3.4-μm spectrum of the source resembles that of the BN or S140-IRS 1 (Figure III.4) in its sharp rise to long wavelengths; but searches with the 224-cm telescope at 10 and 20 μm did not lead to the discovery of any emission. This failure could be due to the intrinsic faintness of the source (an extrapolation of the 2 to 3.4-μm spectrum out to 10 μm leads to a predicted 10-μm flux less than 1 Jy, below the search limit), or to a turnover in the spectrum between 5 and 10 μm.

9. Sharpless 235B

Near the CO peak (Evans, private communication, 1978) is a point-like infrared source, discovered at 20 μm and designated S235-IRS 4. Three other infrared objects in S235 all show radio emission making them compact H II regions and are thus not of interest to the present study (Israel 1976; Israel and Felli 1978). The observations place IRS 4 within 3" ± 3" of the peculiar emission line object M1-82-1 which

Table III.6

Stars in VdB 19

Number from Harris *et al.*	Number from Table III.2	Spectral Type[1]
12	1	A2III
10	2	A2V
9	3	F2IV-V
6	12	F0III-V
11	4	F0
*	8	-
13	9	B9
7	11	-

*Visible on plate of Harris *et al.* 1954.

[1] Spectral types from Harris *et al.* except for star #13 which is from its colors and an inferred reddening of $A_V = 5^m.3$.

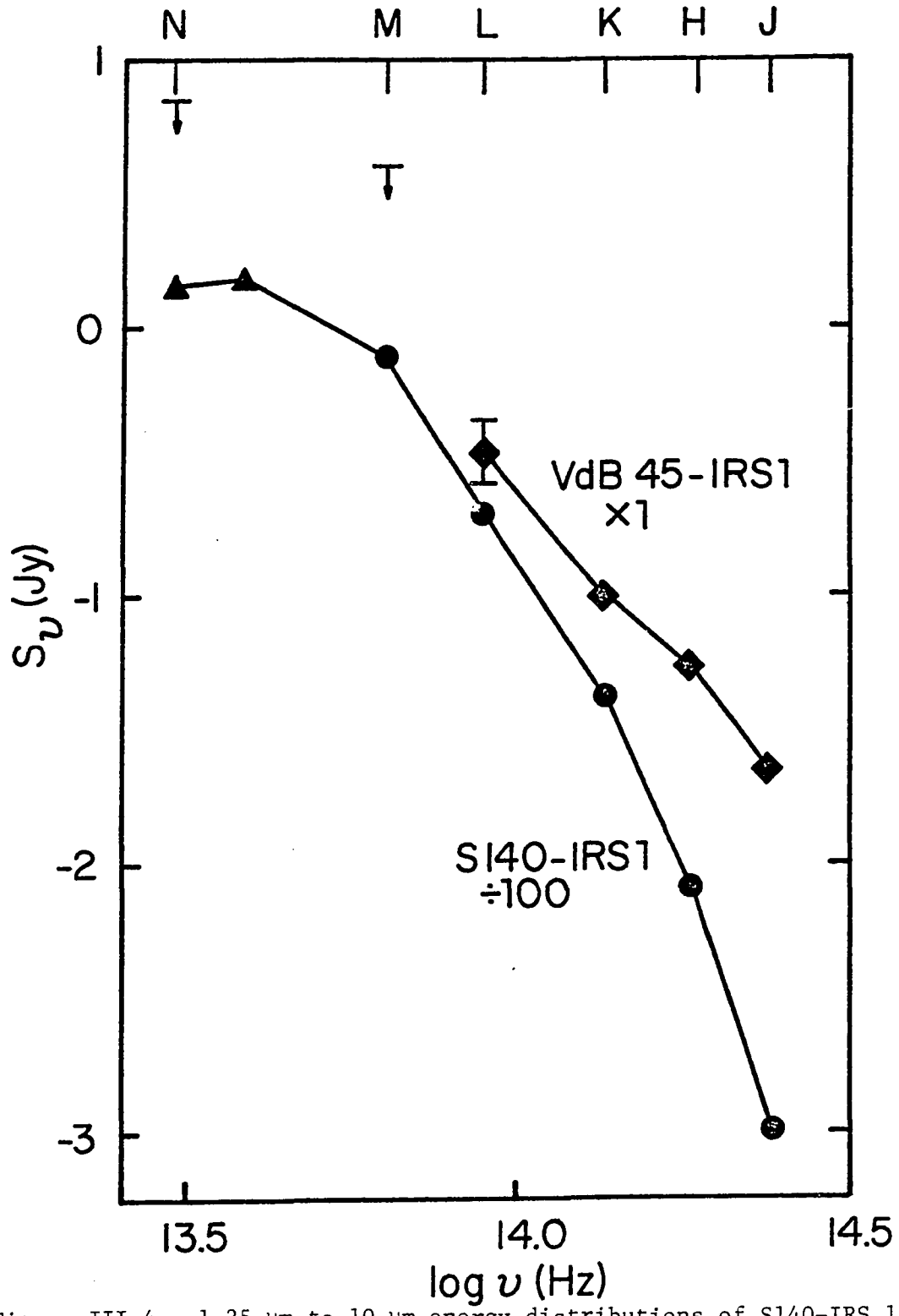

Figure III.4. 1.25 μm to 10 μm energy distributions of S140-IRS 1 and an unidentified object in the relfection nebula VdB 45 (IRS 1).

has been studied by a number of authors (Allen 1972; Glushokov et al. 1975; Krassner et al. 1978. The possible association of the optical/near infrared emission with the 10 to 20-μm source will be discussed later.

A 1' area centered on S235-IRS 4 was observed with the KAO between 30 and 200 μm. The total luminosity is 6×10^3 $L_\odot$ at an assumed distance of 1.8 kpc (Georgelin 197 , private communication).

10. Sharpless 225

Pipher and Soifer (1976) and Evans, Blair and Beckwith (1977) discovered an unresolved infrared object (here designated S255-IRS 1), similar to BN, in the S255 molecular cloud. The 10, 20 and 25-μm maps presented in Figures III.5a show, in addition, the presence of a cold, extended source, 18" east of IRS 1 and designated IRS 2. IRS 2 has a very red spectrum and increases dramatically in brightness at longer wavelengths until by 25 μm it outshines S255-IRS 1.

The KAO data given in Table III.5 yield a total luminosity of 8×10^4 $L_\odot$ for a 3' region around S255-IRS 1 and S255-IRS 2. The 100-μm source is extended with a corrected FWHM of 1!1.

11. Sharpless 269

At the edge of the radio and optical H II region is a 20 K hotspot (Blair et al. 1975), near which Wynn-Williams, Becklin and Neugebauer (1974) found a weak, extended 2.2-μm nebula, but no source of long wavelength emission. (They also found IRS 1 at the center of the nebula, but IRS 1 has the colors of a reddened star and will not be considered further). The present study revealed S269-IRS 3, a point-like source of 10 to 20-μm radiation 4" ± 1" east and 2" ± 1" north of IRS 2. No infrared data longward of 25 μm are available.

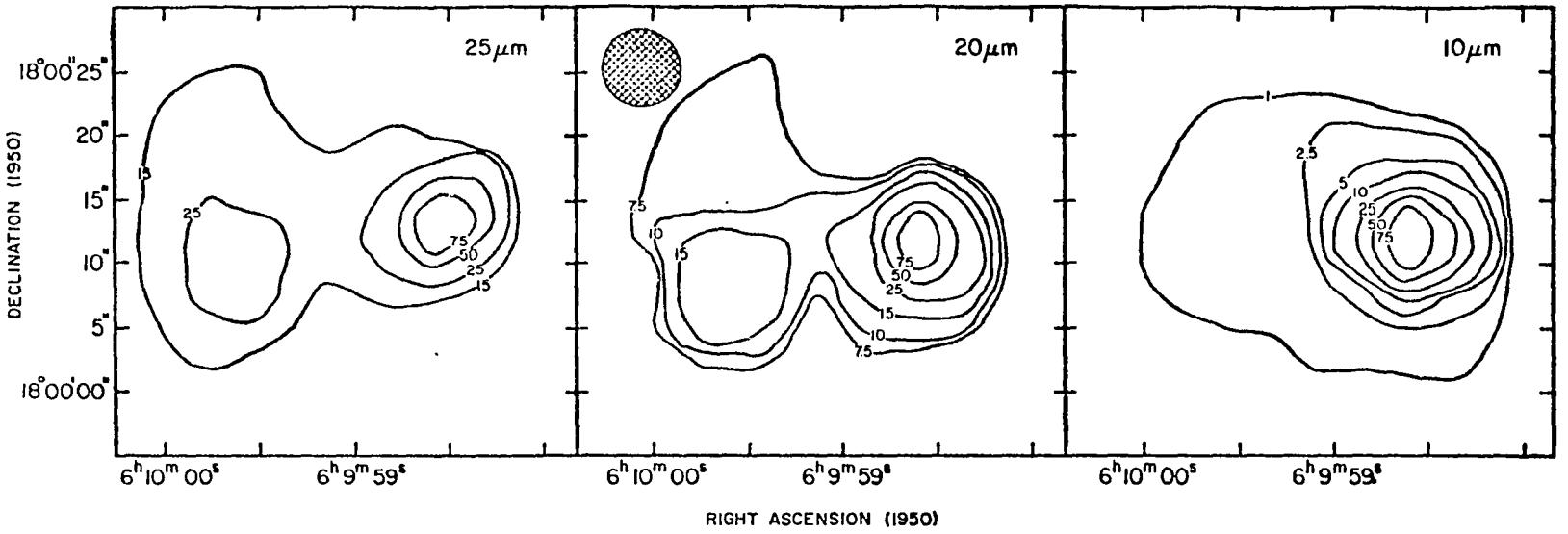

Figure III.5a. 10, 20 and 25 μm contour maps of the S255 region. S255-IRS 1 is to the West and S255-IRS 2 is the extended source in the East. Contours are in percent of the peak fluxes in a 6".5 (FWHM) beam: 10 μm, 40 Jy; 20 μm, 120 Jy; 25 μm, 210 Jy.

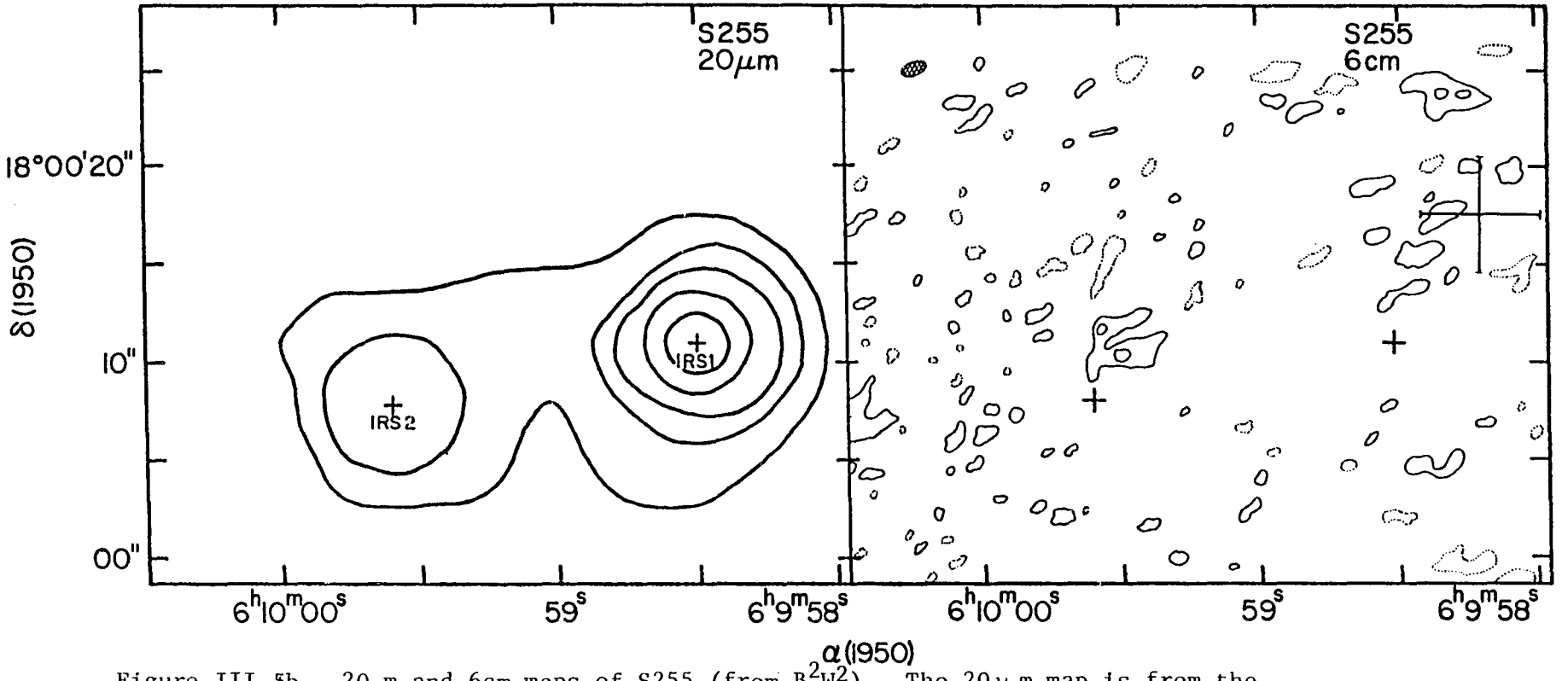

Figure III.5b. 20 m and 6cm maps of S255 (from B^2W^2). The 20μm map is from the same data as figure III.7a and shows contours at 10,20,40,60,80 percent of the flux in a 6.5" beam of 120Jy. Contours in the 6 cm map are at 50 and 90 percent of the peak flux of 1.6 mJy in a 1".2 by 1".0 beam. Dotted contours are at -90 percent. The large cross in the Northwest marks an H_2O maser (Lo and Burke 1973; Genzel and Downes 1977).

12. VdB 92 (Z Cma)

The reflection nebula around the peculiar star Z Cma has been shown to result from the illumination of a hot molecular cloud (Kutner and Dickman 1978; Loren 1976). A partial search of the cloud was made at 2.2 μm, but the only objects found in the survey could be identified with stars (Herbig 1960).

13. ρ Oph #29

The ρ Oph dark cloud has been studied in detail at infrared wavelengths by Elias (1978). The vicinity of source #29 was examined, but no new sources were found.

14. IR 12.4 + 0.5 and MC 12.8 + 0.5

These two objects lie in a molecular cloud that is probably part of the giant M17 molecular cloud (Elmegreen 1977) 2.1 kpc away (Reifenstein *et al*. 1970). IR 12.4 was found at 69 μm using the CFA/UA balloon telescope in a 18 K "warmspot" (Wright *et al*. 197). Searches at 20 μm showed one source that probably corresponds to the 69-μm object as the discrepancy of the 69-μm and 20-μm positions is less than the 1 × 1.5' beamwidth of the balloon telescope. Nothing, however, could be found at the position of the hotter, 24 K, molecular cloud peak, MC 12.8 + 0.5.

Four north-south line scans were co-added to give the composite scan shown in Figure III.6. A cross-correlation algorithm was used to register the scans to an accuracy of 0".5 (Barnea and Silverman 1972). The observed halfwidth of 7".5 corresponds to a deconvolved source size of 4" ± 2".

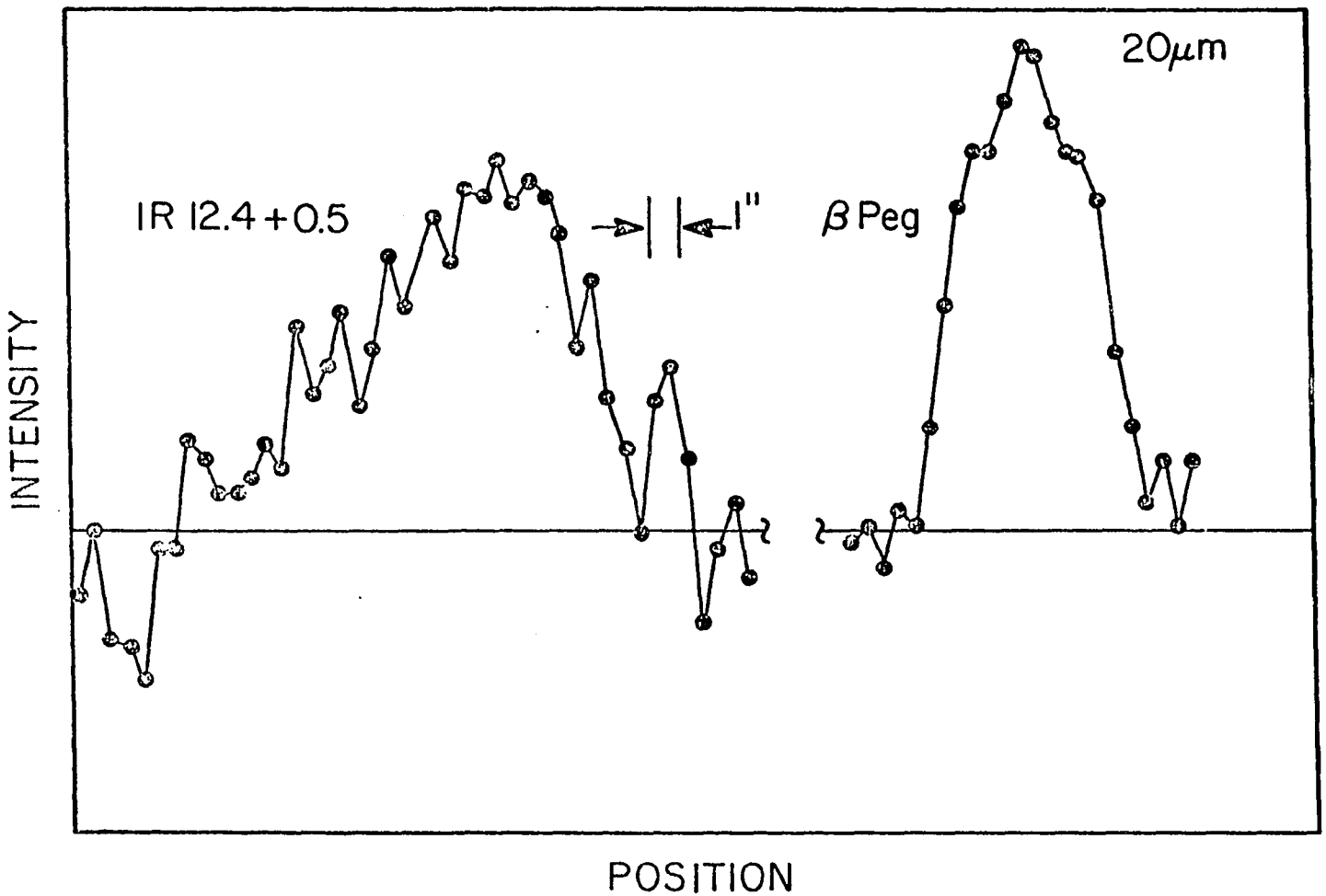

Figure III.6 Four north-south line scans at 20 μm were co-added to show the extended nature of IR 12.4 + 0.5. A scan across the star β Peg was taken immediately after and is shown for reference.

15. VdB 130 and 132

These reflection nebulae have hot CO clouds (20 to 30 K), but apparently no bright non-stellar infrared sources.

16. AFGL 2591

This well-known BN-like object is located close to, but not coincident with, a compact H II region (Wynn-Williams *et al*. 1977). No new sources of 10 or 20-μm radiation were found during searches around the infrared position.

17. VdB 136

Strong CO emission and the presence of an AFGL source, #2620, both led to the selection of this region. However, searches over a relatively large area (for a 10 to 20-μm investigation) revealed no sources.

18. Sharpless 140

Blair *et al*. (1978) discovered a bright infrared object, designated S140-IRS 1, in the densest portion of the S140 molecular cloud. The maps of Figure III.7a show two new point sources of radiation: IRS 2, north of IRS 1, and IRS 3, east of IRS 1. Blair *et al*. examined a large 10' × 10' area in the cloud at 2.2 μm and could find no other non-stellar sources. B^2W^2 have found evidence for weak (~2 mJy) radio emission from S140 IRS 1 and 2 (Figure III.7b)

19. VdB 155

This reflection nebula shows a strong CO cloud, but only apparently stellar infrared sources.

20. Cep A

The molecular cloud associated with the Cepheus OB3 Association was studied extensively by Sargent (1977), who found several parsec-sized regions of enhanced density and temperature in a cloud extending over

Figure III.7a. 10, 20, and 25 μm contour maps of the S140 region. The brightest point source is S140-IRS 1. S140-IRS 2 is north of IRS 1 while S140-IRS 3 is east of IRS 1. Contours are in percentages of the following fluxes in a 6".5 beam: 10 μm, 145 Jy; 20 μm, 690 Jy; 25 μm, 920 Jy. The beam FWHM is shown as a dashed circle.

Figure III.7b. 20 μm and 6 cm maps of the S140 region. 20 μm contours are drawn at 20, 40, 60 and 80 percent of the peak flux of 690 Jy in a 6".5 beam. Contours on the 6 cm map are shown at 20, 40, 60 and 80 percent of the peak flux of 2.6 mJy in a 1".4 by 1".0 beam. Dotted contours are at the -20 percent level. The dashed areas correspond to the 0.9 μm nebulosity observed by Dinerstein et al (1979). The large cross denotes the position of an H_2O maser (Genzel and Downes 1979).

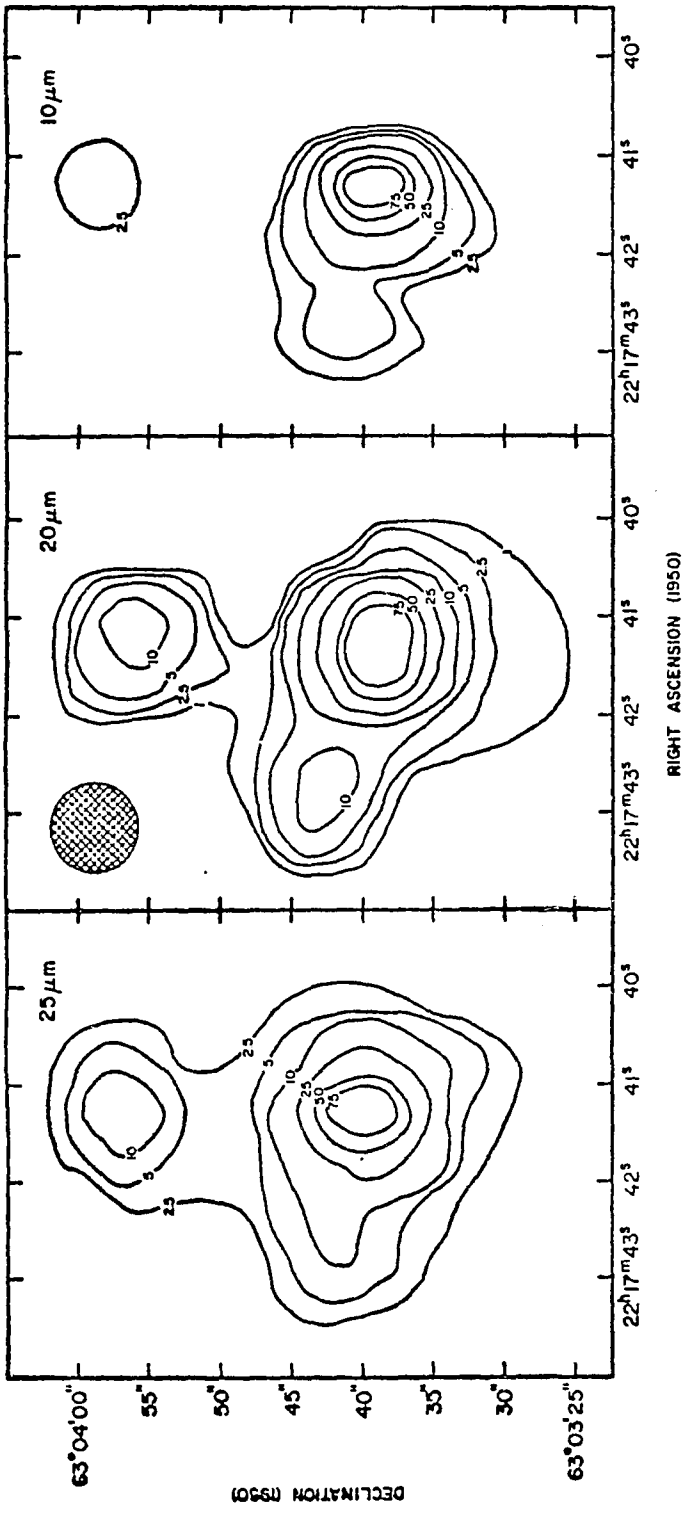

Figure III.7a

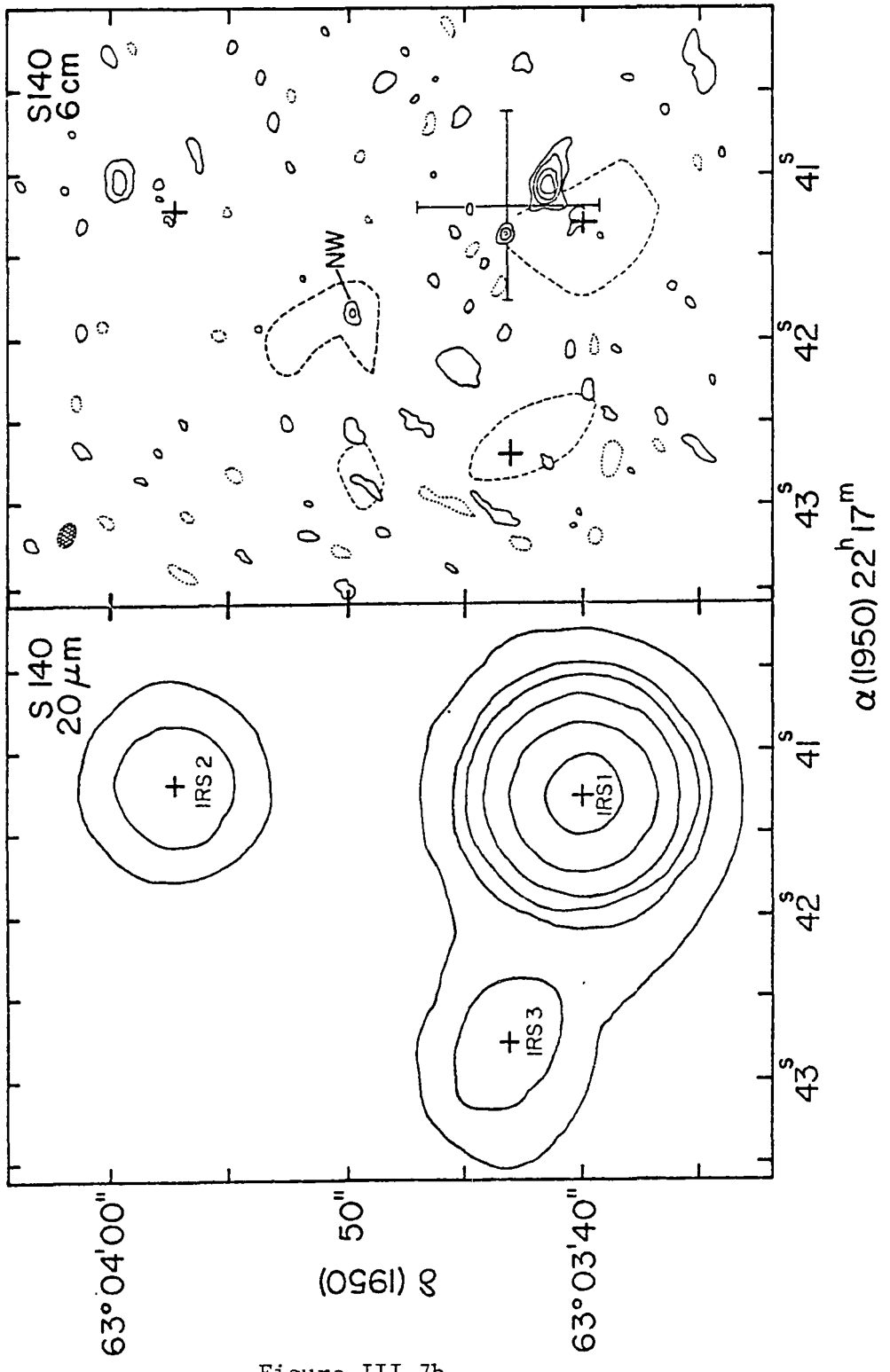

Figure III.7b.

some 20 × 50 pc. The densest region, which she designated Cep A, has a CO temperature of only 18 K, but shows self-reversed line profiles that have been interpreted by some authors as evidence for collapse (Snell and Loren 1977) and by others as evidence for expansion (Leung and Brown 1977). There is, however, an unambiguous association between self-reversed lines and embedded infrared objects (Snell and Loren 1977). At the densest part of the cloud Blitz and Lada (1979) and Lada et al. (1979) found very strong H_2O maser emission. Searches from MKO located a very cold, extended source of 20- m radiation (right at the position of the maser). With a $F_{25}/F_{12.8}$ flux ratio of 70 the object is one of the reddest ever found from a ground-based telescope. The 20-μm object was not mapped in detail, but four orth- outh scans were coadded to give the composite scan shown in Figure III.8 which indicates that the source has an extent of 7 to 9". B^2W^2 have found three weak H II regions located, within the errors, at the position of Cep A-IR (Figure III. 9).

21. Cep B

The second region examined by Sargent, Cep B is less dense than Cep A but has much hotter CO temperature, 29 K. Exhaustive searches at 10 and 20 μm at MKO and 10 μm by Sargent (1978, private communication) failed to reveal any point sources of radiation. The large beam AFGL survey did, however, find a strong source, #3000, in the vicinity, but this may be due to dust emission from the H II region S155 which abuts onto the Cep B cloud (Felli et al. 1978b).

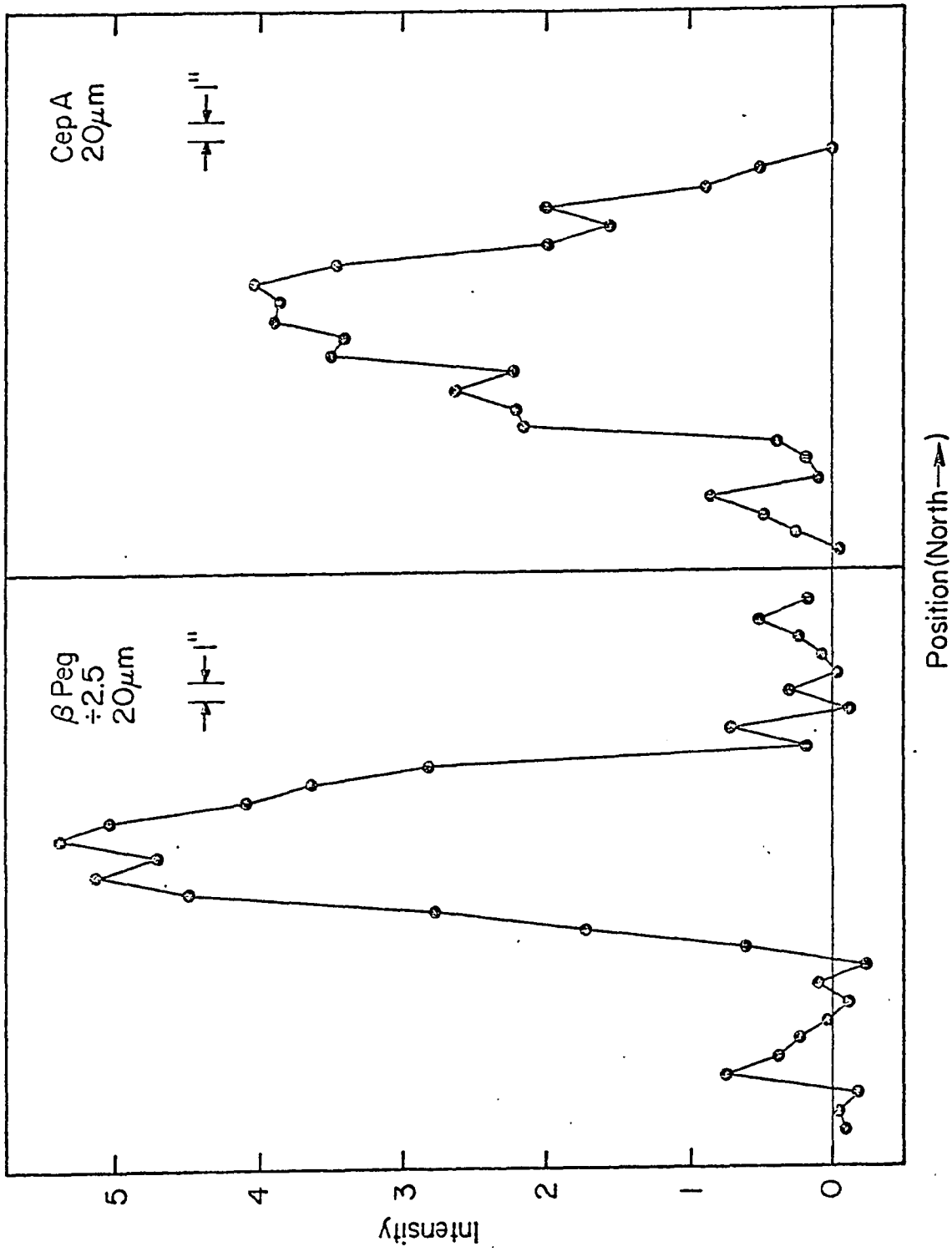

Figure III.8. Four line scans across the 20 μm source Cep A were co-added to show the extended nature of this object. A scan across the star βPeg taken immediately after is shown for reference.

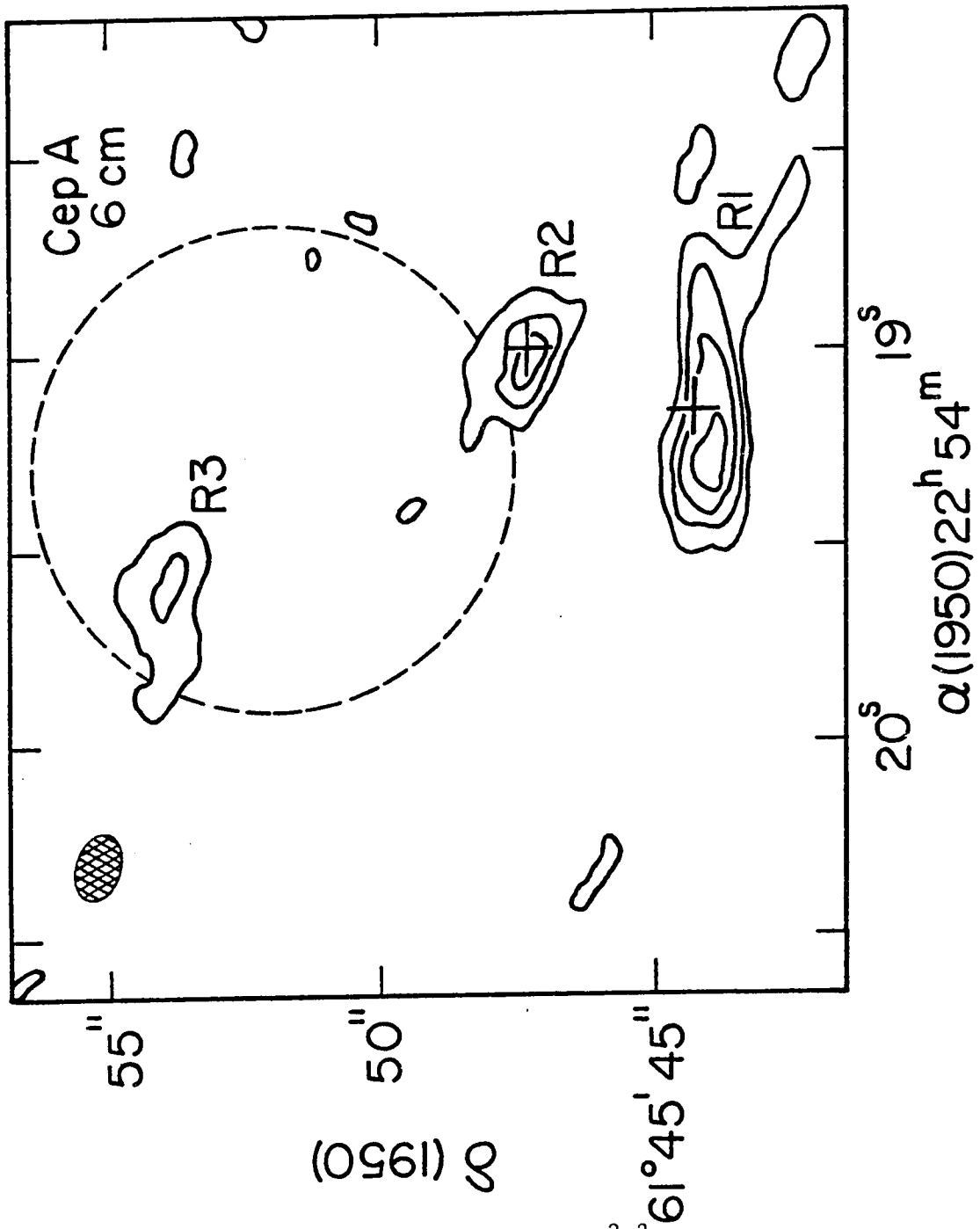

Figure III.9. 6cm map of the Cep A region (B^2W^2) with contours drawn at 20, 40, 60 and 80 percent of the peak flux of 3.5 mJy in a 1".2 by 0".7 beam. The dashed circle indicates approximate location of the 20 μm object. Crosses mark the position of H_2O masers.

III.2 Discussion of Searches

Searches of 24 molecular clouds at 2.2, 10 and 20 μm have led to observations of 41 discrete sources of radiation, of which 30 were found at 2.2 μm. Since normal field stars emit at near-infrared wavelengths (Johnson 1966), it is necessary to develop criteria to cull the garden-variety stars from the sample. The 1.2-2.2 μm photometry and the limited 3.4 μm data can be used for this purpose.

Purely stellar radiation arises in a photosphere hotter than 10^3K, whereas radiation from dust-enshrouded objects arises in grains heated to no more than 10^3K. On this basis one expects to find energy distributions that are flat or Rayleigh-Jeans for field stars, and distributions that rise sharply to longer wavelengths for embedded sources. Extreme interstellar reddening can modify a stellar spectrum to mimic that of a much cooler object. Distinguishing between low temperature and large amounts of reddening is difficult because at near infrared wavelengths the reddening vector lies in the same direction as the direction of decreasing blackbody temperature. From 1-2.2 μm data alone it is not easy to discriminate between extremely reddened stars and emission from dust. Data at 3.4 and 4.8 μm are valuable for this purpose, but relatively few of these data could be obtained with the 60-cm telescope.

In many cases, however, the available infrared colors are sufficient to identify as "stellar" any sources discovered in the course of a search. Allen et al. (1977) examined about 100 AFGL objects both photometrically and spectroscopically and found that those with J-H, H-K, or K-L colors less than 2^m could be identified positively as stars--primarily M, C, and emission line stars. Figure

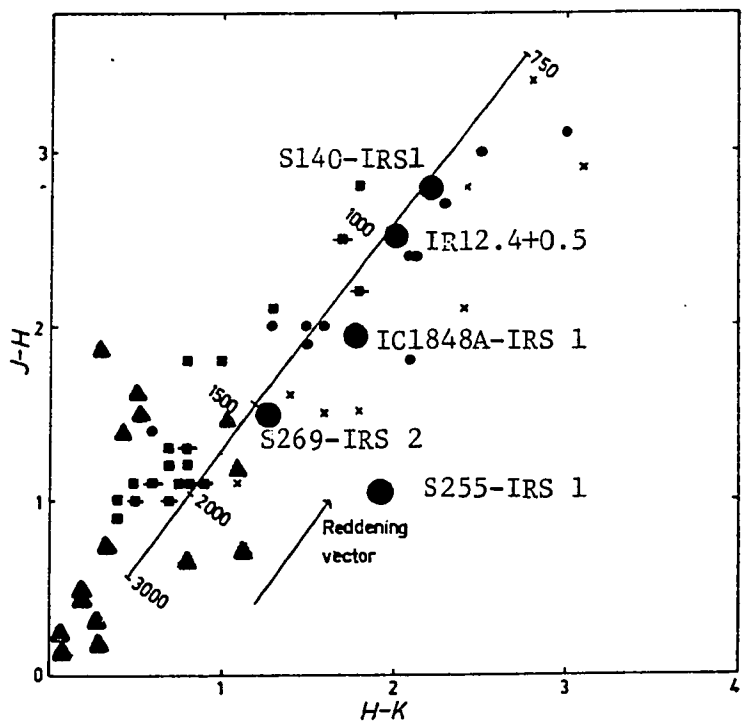

Figure III.10. Infrared color-color diagram from Allen et al. (1977). Filled squares, M stars; small filled circles, C stars; crosses, emission line stars; triangles, sources from Table III.2 which are probably stars; large circles, BN-like, dust embedded sources. The long line is the locus of blackbodies with the indicated temperatures. The reddening vector is indicated.

III.10 is a J-H/H-K color diagram which shows M and C stars as small squares and triangles, concentrated mostly in the lower left corner. The long line shows the locus of blackbodies of various temperatures (750 K - 3000 K). The short line shows the effect of increased reddening. The large triangles represent the sources discovered during the 2.2 μm searches (Table III.2). The location of these objects in the lower left part of the diagram suggests that these are cool or reddened stars. Embedded objects, such as S140-IRS 1, whose emission arises from hot dust (i.e., strong 10 μm sources), are shown for reference in the figure as large, filled circles.

Objects without complete J, H, and K photometry cannot be plotted in the figure, but are identified as stellar by having J-K $\lesssim 4$. With the possible exception of an object in VdB 45, the data suggest that the objects found in the 2.2 μm searches are all field stars. VdB 45-IR has K-L=2.2 suggesting the possibility of emission by heated dust (see Figure III.4), but the lack of a 10 μm source at this position shows that the embedded source, if any, is not a luminous one.

Sources discovered in the 10-20 μm searches are listed in Table III.3 and have the infrared properties expected of luminous objects embedded within a molecular cloud. The sources found in the long wavelength survey, and others already known from the literature, form the sample on which the discussion of subsequent sections will be based.

CHAPTER IV
DISCUSSION

IV.1 Summary of Searches and Numbers of Sources

Of the 24 molecular clouds examined for the survey reported here, 10 have been found to contain a total of 16 infrared objects that can be identified as luminous stars (or protostars) embedded within the cloud. 7 of the 16 infrared sources were discovered in the the course of this research: IC1848A-IRS 2, S235-IRS 4 (found independently by Evans, 1978, private communication), S255-IRS 2, S269-IRS 3, S140-IRS 2, S140-IRS 3 and Cep A. Observations were also made of IR 12.4+0.5 which was first found by Wright et al. (1979) at 69 μm. Subject to the limitations of sensitivity and spatial coverage discussed earlier, no new infrared sources were found in the vicinities of W3(OH), AFGL 2591, ρ Oph #29, OMC2-IRS 3 or in ten other candidate regions, S184, S187, VdB 19, 130, 132,136, and 155, NGC 1579, MC 12.8+0.5 and Cep B. One cloud, VdB 45, showed ambiguous evidence for emission from hot dust, but sensitive 10 μm observations are required for confirmation.

This survey is too limited in its spatial coverage and too biased in its selection of clouds to be of direct use to statistical investigations of the rate of star formation in the galaxy. An important conclusion to be drawn from this first-order attempt, however, is that stellar birth rates based solely on the frequency of BN like (T≃500K) objects are likely to be gross underestimates because they ignore the potentially large number of objects of low apparent color temperature

that are missed in typical 10 μm surveys. Four of the seven new objects discovered in this survey--IC1848A-IRS 2, S255-IRS 2, IR12.40+0.5 and Cep A-IR--have $20<F_{25}/F_{12.8}<70$ and were not found in searches at either 2.2 or 10 μm by other observers. IC1848A-IRS 2 was not found by Loren and Wooten (1978) at 2.2 μm; S255-IRS 2 was not found by either Pipher and Soifer (1976) at 10 μm or by EBB at 2.2μm; IR12.4+0.5 was not found by Wright et al. (1979) at 2.2 μm; and Cep A-IR was not found at 10 μm by Sargent (1978 private communication). These sources are obviously difficult to detect at wavelengths shorter than 20 μm with present-day sensitivities, yet they constitute more than 50% of the new sources found in a survey designed to be especially sensitive to objects of low color temperature. The limited number of sources like Cep A and IR 12.4+0.5 currently known makes it difficult to estimate their intrinsic frequency, but it is clear that if so limited a survey as this one could be so successful, then they must be quite numerous.

Bedejin et al. (1978) suggest that too small a number of BN/KL-like objects are known to be consistent with the rate of star formation derived from optical observations (Ostriker, Richstone, and Thuan 1974) and with theoretical estimates of the duration of the embedded, radio weak phase. Bedejin et al. (1978) predict that some 300 infrared sources with $L > 10^3 L_\odot$ should exist within 3 kpc of the Sun. Even including the results of this survey, only about 20 such sources are known.

A number of arguments suggest that this discrepancy is illusory. Most importantly, it is extremely unlikely that infrared surveys are complete down to $10^3 L_\odot$ (characteristic of an $8M_\odot$, B5V star) out to a

distance of 3 kpc. Examination of Figure II.2 shows that searches down to such level would have to be twice as snesitive at 10 μm and four times as sensitive at 20 μm as those conducted here. Further, the amount of sky covered down to even the present sensitivities is much smaller than the area over which, say, CO emission has been observed. An estimate of the completeness of this limited survey comes from the lowest bolometric luminosity listed in Table II.3, $6 \times 10^3 L_\odot$ for S235-IRS 4. All the rest exceed $10^3 L_\odot$. When one considers that there are about 100 times more B5 stars than B0 stars in the galaxy (Allen 1973), it is obvious that many more infrared objects with 10^3-$10^4 L_\odot$ remain to be discovered.

The effects of extinction within a molecular cloud may make even the sample of sources with $L > 10^4 L_\odot$ seriously imcomplete. The bias of CO and infrared surveys in favor of regions showing peculiar optical properties (e.g., the Sharpless HII regions and the Van den Bergh reflection nebulae) means that a cloud with activity on the side facing Earth is examined in preference to an apparently quiescent cloud. These optically dull clouds will be the last examined and may harbor embedded objects far from the sides facing Earth. The radiation from objects on the far side of a cloud, or embedded in the center can be attenuated by $A_V \geq 100^m$, corresponding to 2.2, 10, and 20 μm optical depths of 10, 8, and 5 (Becklin et al. 1978), respectively, and this means that far-side sources will be hard to detect shortward of 10 μm where cold, foreground grains are purely absorbing.

Cep A provides an excellent example of the type of deeply embedded object that may prove prevalent within dense clouds. Recent radio continuum measurements (B^2W^2) indicate the presence of three small

HII regions close to the position of the infrared source (Figure III.9). Infrared radiation from less obscured H II regions has a color temperature of 300-500 K (Gillett et al. 1975), but the observed color temperature of Cep A between 12.8 and 25 μm is less than 90K. The amount of 12.8 μm radiation actually received from Cep A is far less than expected from a $5 \times 10^4 L_\odot$ source with T≃500K. If cold, absorbing, foreground grains are responsible for the deficit, then it is straightforward to show that $\tau_{12.8} \simeq 8$ if the intrinsic spectrum of Cep A has a color temperature of 500K. With $\tau_{12.8}/\tau_{9.7} = 0.35$ (Gillett et al. 1975) and $A_V/\tau_{9.7} = 10\text{-}15$, the visual extinction to the weak HII region exceeds 200^m.

Cep A is situated in a typically dense molecular cloud core (as is discussed in the next section; see Table IV.1). The extreme redness of its spectrum is the result of a location deep within the cloud. Other clouds of comparable density may be shielding objects like Cep A from detection at short wavelengths. Future searches at long wavelengths are likely to find many objects resembling Cep A.

Although this study has attempted to avoid some of the selection effects that have marked earlier work, it too suffers from important biases. It must be remembered that the molecular clouds selected for examination have pathologically high temperatures and densities (>20K and $>10^4 cm^{-3}$) in comparison with more normal clouds (≃10K and $<10^3 cm^{-3}$). In many cases the clouds examined were already known to have at least one infrared source. The group of clouds cannot be considered as representative of 4000-some clouds thought to exist in the galaxy (Stark and Blitz 1979; Solomon, Scoville, and Sanders 1979); nor can the dense cores be considered as representative of a whole cloud.

While it is likely that the fraction of clouds containing infrared sources brighter than $10^4 L_o$ will prove to be less than the 50% found here, it is also probable that there exist many more embedded sources with 10^3-$10^4 L_o$ than the small number now known. The results presented here suggest that until a sensitive all-sky survey at $\lambda \geq 20$ μm is available, estimates of the current rate of star formation based on infrared source counts may be seriously in error.

IV.2 Location of Infrared Objects Within Molecular Clouds

The data presented here strongly confirm the tendency for finding embedded, compact infrared objects in the hottest, densest parts of molecular clouds (see Evans 1978 for a lucid summary). These cores, ≃1 pc across, are well defined by temperature enhancements of a factor of 1.5 to 3 and density enhancements of a factor of 10 to 100 (in a 1' beam) over the surrounding envelopes. Typical ^{13}CO column densities range from 5×10^{15} cm^{-2} in the envelopes up to 10^{17} cm^{-2} in the densest regions (Table IV.1). Millimeter observations of lines of molecules such as CS, H_2CO and HCN which require high densities for their collisional excitation imply core densities as high as $n_{H2} = 10^5$ cm^{-3} (Zuckerman and Palmer 1974). The eleven infrared objects discovered in this survey are all located within these regions of enhanced temperature and density, suggesting an intimate physical relationship between regions of high density and the presence of newly-forming stars. Table IV.1 lists ^{13}CO column densities in the vicinity of embedded infrared sources. Also given are the angular separations between the infrared positions and the positions of maximum gas temperature and density, inferred, respectively, from CO and ^{13}CO observations. In all sources except OMC 2 the infrared objects coincide with the densest parts of the clouds. Not all of the infrared objects, however, lie at the hottest part of their clouds.

The location of the S140 and S235 infrared sources at the positions of maximum density rather than maximum temperature (if the 1' offset is real) suggests that high density is the hallmark of a site of star formation and that gas temperature alone can be misleading. The cloud in which Cep A-IR is found does not have a particularly high T(CO), only

Table IV.1

Characteristics of Molecular Clouds near Infrared Sources

Cloud Name	$N(^{13}CO)$[1] 10^{16} cm^{-2}	Separation[2] bet. IR and T(CO) max.	Separation bet. IR and $N(^{13}CO)$ max.
S 184	1.4	no IR	no IR
IC 1848A	1.5	0'	?
OMC 1[3]	22	0'	0(2'?)
OMC 2[4]	-	0'	4'.5
S 235B[5]	4.8	1'	0'
Mon R2[6]	3.9	0'	0'
S 255	3.7	0'	0'
S269	1.1	0'	?
M17-KW[7]	10	0'	0'
IR 12.4+0.5[8]	3.2	1'	?
S 140	4.7	1'	0'
Cep A	5.8	0'	0'
Cep B	1.4	no IR	no IR

Notes:

1) ^{13}CO column densities are from the references listed in Table III.1 or from CO data combined with equation (2) of Evans et al. (1976).

2) Separations are entered as 0' if less than the 1' resolution of millimeter wavelength telescopes.

3) CO data from Liszt (1974). The location of the densest part of OMC 1 is uncertain. Ho and Barrett (1978) suggest the densest part lies 2' North of KL. The H_2CO data of Kutner, Evans and Tucker (1976) indicate the densest part is coincident with KL.

4) The infrared sources definitely are to the South of the ^{13}CO and H_2CO maxima (Kutner et al. 1976). The ^{13}CO column density is unknown.

5) Evans, 1979, private communication.

6) Loren 1977.

7) Lada 1976.

8) The location of the ^{13}CO peak is unknown. The ^{13}CO column density is for the position of the CO maximum. Wright et al. 1979.

18 K, but its ^{13}CO column density if 6×10^{16} cm^{-2} and strong H_2CO is observed (Sargent 1977). The negative outcome of the Cep B searches points out again that high CO temperature alone is not a sure indicator of an embedded infrared source. In Cep B the CO temperature is 29 K, but the density inferred from the weak ^{13}CO emission and the absence of H_2CO lines is low, $\leq 10^4$ cm^{-3} (Sargent 1977). Felli et al. (1978) have suggested that Cep B is heated from the outside by the visible O7 star HD 217086, 3.5 pc away. (Under this interpretation AFGL 3000 is the result of 150 K grains within and at the boundary of the S155 H II region. The failure to detect the source from the ground is due to its low surface brightness).

The idea of external heating could explain the negative results towards a number of other clouds. For example, the molecular cloud near S184 is only 3 pc away from an O5.5 star (Sharpless 1954) which could supply enough energy to heat the gas to the observed 15 K.

All the data presented here, however, suggest that CO temperatures in excess of 18 K, coupled with ^{13}CO column densities in excess of 2×10^{16} cm^{-2} (implying $n_{H2} \geq 10^4$ cm^{-3}), are indicative of a dense core within which one or more infrared objects are almost sure to be found.

It should not come as a surprise that the infrared sources discovered in the course of this survey are all located within the cores, for only these regions were examined at 10 and 20 μm--the wavelengths offering the greatest sensitivity to sources with $T_c \leq 500$ K. The limited spatial coverage of the long wavelength searches precludes making the definite statement that the most luminous young stellar objects are to be found only within a dense core, although there is evidence that this is the case.

First, the 2.2-μm searches conducted over a large fraction of a cloud's volume, not just around the core, failed to find additional sources of radiation that could not be identified as normal stars [see the results of Blair et al. (1978) for S140, of Evans et al. (1977) for S255 and of Wright et al. (1979) for IR 12.4 + 0.5]. Admittedly the 2.2-μm results set limits only on the existence of BN-like sources and it is possible that objects of low color temperature lurk undiscovered in the outer reaches of the clouds.

Second, there are hints that cool, but luminous objects are unlikely to be found outside the cores. In clouds with multiple sources the maximum separations between objects is less than 20", a factor of three less than a typical 10 to 20-μm raster dimension. The ratio of volume examined to the volume in which sources were found is at least 3^3, suggesting a concentration of infrared objects in a single center of activity. Finally, our whole understanding of the relationship of an embedded source to its surroundings requires that the gas and dust close to it be heated above the ambient temperature, producing some CO enhancement (Goldreich and Kwan 1974). The fact that the outlying portions of the clouds show no evidence for enhanced energy input, having temperatures ≃10 K, suggests the absence of luminous embedded objects. The complexities of cloud heating and of CO radiative transfer make it very difficult to set a lower limit to the luminosity of a source capable of producing an observable hot spot.

In summary, infrared objects brighter than, say, 10^4 $L_\odot$, characteristic of stars earlier than B1 are very likely to be found, perhaps exclusively, within the dense cores of molecular clouds. It remains possible that objects of lower luminosity and/or color temperature are

distributed more uniformly through the clouds, but have not yet been detected.

Location of Sources and Theories of Star Formation

The location of newly-forming stars is of relevance to understanding how and why interstellar clouds collapse. The simplest theoretical picture is of an isolated cloud that is unstable against contraction because its gravitational potential energy exceeds its thermal energy (e.g., Larson 1977). The theory of quiescent gravitational collapse suffers from the problem that it predicts that almost all of the observed molecular clouds should be collapsing into stars on a time scale of only a few million years, which is in direct conflict with the continued existence of clouds for the lifetime of the galaxy (10^{10} yr) and with the observed rate of star formation. If all the known clouds are producing stars, the predicted rate of formation is 30 to 100 times greater than that presently observed (Zuckerman and Palmer 1974; Evans 1978). Unless the present epoch has a very high rate of star formation, which does not appear to be the case (Lequeux 1979), something, usually thought to be magnetic fields (Mouschovias 1978), must inhibit collapse.

Stars are observed to form, however, implying that there must be mechanisms whereby the collapse of a rigid cloud can be initiated. Triggering mechanisms that have been proposed (see Lada *et al*. 1978 for review) include external pressures on clouds from H II regions (Oort 1954; Elmegreen and Lada 1977), from supernovae (Öpik 1953; Herbst and Assousa 1977) and shocks from the passage of spiral density waves (Woodward 1976).

One theory is that of "sequential star formation" (Elmegreen and Lada 1977). In this scenario OB stars form at one end of a giant molecular cloud, perhaps 20 × 60 pc in size, containing some 10^5 $M_\odot$ and elongated along the galactic equator. The creation of the first stars (triggered by some unspecified mechanism) leads to the formation of a giant H II region like the Trapezium or W3. The ionization from that forms at the interface between the H II region and the molecular cloud, and sends a shock wave into the otherwise stable cloud. The shock produces a thin, ≈0.1 pc, layer in which the density increases from about 10^3 cm^{-3} to greater than 10^5 cm^{-3}, making gravitational contraction possible (Figure IV.1). New OB stars form which are first observed as embedded infrared objects, OH and H_2O masers and compact H II regions. After ≈10^6 yr the stars emerge,forming another giant H II region which in turn shocks the remaining cloud. Another generation of OB stars forms and the process repeats until the whole cloud is consumed and dispersed.

"Sequential Star Formation" receives observational support from OB associations which show subgroups of different ages (Blaauw 1964) with young stars found close together and associated with more interstellar matter than the older stars. In some cases the line between subgroups lies in the galactic equator and points from old stars to young stars and on into the molecular cloud. Further support for the theory comes from the fact that some, <u>but not all</u>, H II regions form like blisters on the outer skin of massive molecular clouds (Israel 1978) and that some infrared objects,such as BN, are apparently located close to the surface of the molecular cloud, and hence close to the ionization front (Zuckerman and Palmer 1974).

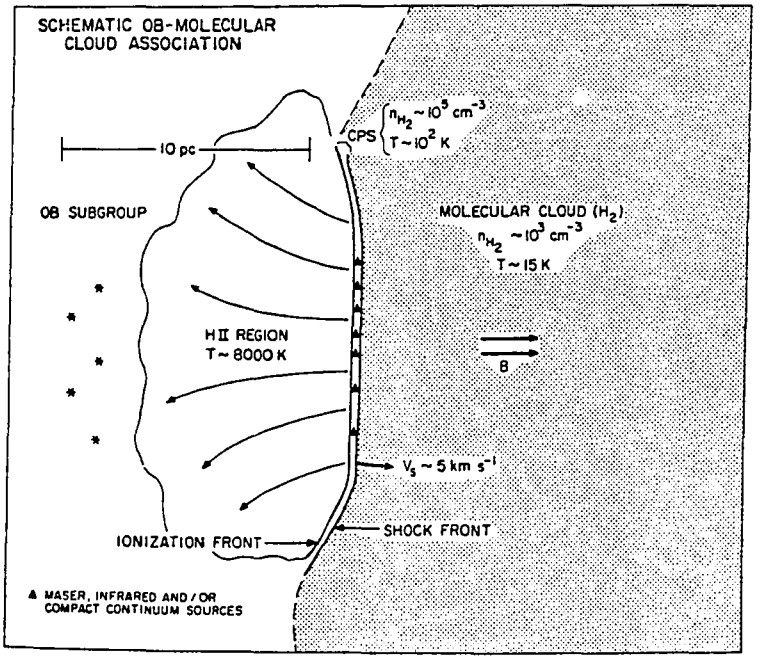

Figure IV.1. An idealized representation of the structure of a typical OB association. Sequential star formation suggests that new stars are found within a narrow shocked region adjacent to the "blister"-like HII region surrounding the youngest stars to have emerged from within the molecular cloud. The region denoted "CPS" (for cooled post-shock) is the layer described by Equation IV.1 in which the next round of stars are thought to form (Figure from Elmegreen and Lada 1977).

Although the theory of sequential star formation deals with distance scales much grander than the infrared observations presented in this dissertation, these data can be used to point out selection effects and to locate sites of star formation for comparison with the predictions of theory. As discussed earlier, previous searches have always been extremely biased toward looking close to H II regions, so that it is not surprising that most of the known infrared objects are found in proximity to ionization fronts. The existence of IR 12.4 + 0.5, found accidentally in a 69-μm survey and parsecs away from any known H II regions (Wright et al. 1979), and the existence of Cep A, found because of a large scale CO survey and located 3 pc away from the nearest H II region (Sargent 1977), suggest that stars can form far from other OB stars.

The selection effects due to searching at $\lambda \leq 10$ μm has lead to the discovery of infrared objects located preferentially at the near boundaries of molecular clouds where the intra-cloud extinction is low. The dearth of deeply embedded objects is an apparent one only and is not due to any inadequacies of star formation processes. Short wavelength searches at $\lambda \leq 10$ μm are insensitive to objects like Cep A to which the visual extinction may be as high as 200^m. For a typical $A_V/\tau_{9.7} = 10$ to 15, a mass absorption coefficient of 2500 g-cm^2 (Knacke 1978) and a gas-to-dust mass ratio of 100 $\tau_{9.7} \simeq 0.3\ n_3 \ell$ pc where n_3 is the constant H_2 number density in units of 10^3 cm^{-3} and ℓ is the absorption path length in parsec. With $n_3 = 50$ as an average density for Cep A (Sargent 1979) and an $A_V \simeq 200$ as derived earlier, $\ell \simeq 1$ pc and it is clear that Cep A is located deep within the cloud. Other objects could be hidden in the same way within other clouds. Radiative transfer

effects (Scoville and Kwan 1976; Leung 1976) and the real density distribution obviously play an important role in determing the exact position of infrared sources like Cep A; but the bias introduced by short wavelength searches has artifically created the need to explain the location of infrared objects only at the edges of clouds.

It is possible to show quantitatively that the infrared objects discovered here lie more deeply inside the cloud than the thickness of the shock layer predicted by Elmegreen and Lada (1977) and thus beyond the influence of the shock created by the external pressure of the H II region. The thickness of the shock layer, t, at the onset of gravitational instability is given by (see Equations 10, 13 and 18 or A17-22 of Elmegreen and Lada 1977)

$$t = 0.2\ N_0^{-1/5} n_3^{-1/5} T_2\ \text{pc} \qquad \text{IV.1}$$

where n_3 is the preshock cloud density in 10^3 cm^{-3}, T_2 is the temperature of material in 10^2 K and N_0 is a measure of the number of ionizing photons available in the external H II region. N_0 is the number of O stars, each emitting $N_L = 10^{49}$ Lyman continuum photons per second in a 10 pc^2 area. A single BOV star emitting $N_L = 10^{47.63}$ s^{-1} has N = 0.04 (Panagia 1973). Thus, t is the maximum distance inside a cloud in which a newly-formed star can be found. A value half as large as the prediction of Equation IV.1 is expected if stars form, on the average, in the middle of the layer.

For six of the seven clouds studied here, t is compared with the observed separation (projected onto the sky) between the infrared source(s) and the cloud boundary. The edge of a cloud is demarcated by

the lowest CO contour. IR 12.4 + 0.5 is not included as it does not lie near any H II regions. Columns 1-3 of Table IV.2 give the cloud name, the spectral type and N_0 for the exciting stars in the nearest H II region Column 4 gives the peak gas temperature within the cloud based on the observed T_A^* (CO), corrected for the breakdown of the Rayleigh-Jeans approximation at 2.6 mm (Zuckerman and Palmer 1974) with an antenna efficiency of 0.85 (Blair et al. 1978). Column 5 gives the thickness, t, of the shock layer. Column 6 gives the projected separation between the infrared source and the cloud edge along the line joining the exciting star and the infrared object. The lack of a CO map makes it impossible to estimate a separation for S269-IRS 3.

From the table it is obvious that the infrared sources are, in all cases, located further into the cloud than permitted by equation IV.1. although increasing T_2 to 1.0 would put S140 and S235-IRS 4 within the boundary of the shocked region. Large variations in n_3 and N_0 have little effect because of the 1/5 dependence. The location of the condensed core of the S140 cloud close to the H II region around HD 211880 (Blair et al. 1978) suggests there might be some physical interaction, but there is no evidence for any interaction between an external H II region and the molecular cloud in the cases of Cep A, S255, or IC1848A.

Assousa, Herbst and Turner (1977) have suggested that a supernova may have triggered star formation in the Cep OB3 Association. The youngest of the three pulsars in the region, PSR 2223 + 65 (Taylor and Manchester 1975) is only 1.1×10^6 yr old, comparable with the free-fall time of the Cep A cloud. However, the current location of the pulsar is 7 pc away from Cep A and its proper motion is unknown. An older, 1×10^7 yr, pulsar, PSR 2324 + 60, lies 45 pc away. The

Table IV.2
Location of Infrared Sources With Respect
To Edge of Molecular Cloud

Cloud	Sp	N_o	T_2	t(pc)	d_{obs}(pc)	References
IC 1848A	07&08V	1.11	0.32	0.06	0.67	Osterbrock 1957.
S 235	BOZAMS	0.002	0.34	0.15	0.33	Spectral type based on radio emission for S 235 Israel and Felli 1978.
S 255	~09V	0.21	0.39	0.11	0.73	Chopinet *et al*. 1974.
S 140	BOV	0.04	0.34	0.13	0.40	Blair *et al*. 1978
Cep A	08.5V	0.28	0.25	0.06	2.5	Garrison 1970.
S 269	BOZAMS	0.02	0.28	0.12	-	Israel 1976.

possibility of a physical association between the supernova blasts and the onset of collapse is intriguing, but at present highly speculative.

Selection effects of looking for infrared objects close to H II regions using wavelengths $\lambda \leq 10\ \mu m$ has created a sample of sources that is not representative of the true distribution of stars forming within molecular clouds. While new stars are found in close proximity to H II regions and their formation may, in some cases, have been initiated by shocks emanating from ionization fronts, it is by no means likely that is the sole, or even dominant mechanism by which stars can form out of molecular clouds. As presently formulated, the theory of shock induced collapse cannot account for the infrared objects located more deeply into a cloud than about 0.1 pc. Many objects are more deeply embedded than this. The existence of sources like Cep A and IRS 12.4 + 0.5 is strong evidence that stars can form without the agency of external H II regions and that other mechanisms, perhaps quiescent gravitational collapse, must play an important role.

IV. 3 The Formation of Multiple Stars

> "Such groups (as the Pleiades) are a necessary result of the condensation of nebulae with several nuclei, for it is plain that the nebulous matter being constantly attracted by these different nuclei must finally form a group of stars like the Pleiades. The condensation of nebulae with two nuclei will form stars in very close proximity, which will turn one around the other, similar to those double stars whose relative motions have already been determined."
>
> P. S. Laplace, Systeme du Monde, Note VII, 1796, quoted from Aitken, 1918, p. 284.

Approximately half of all stars earlier than spectral type B5 are members of binary systems or groups of higher multiplicity (Abt and Levy 1978). The separations between component stars and orbital periods range from 0.1 AU and 10 hr for the spectroscopic and eclipsing binaries, up to 0.1pc and 10^6 yr for the visual and common proper motion systems. Related to the latter are the compact clusters of five to twenty OB stars called "trapezia" by Ambartsumian (1956) after the group of seven Trapezium stars found at the center of the Orion Nebula. Typically trapezia contain an O5 star, an O7 star and ten B0-B8 stars for an average stellar mass of 10 M_o (Sharpless 1954). The groups have an overall extent of 0.1-1.0 pc with individual stars separated from one another by 0.02-0.2 pc, with three or more distances being roughly equal.

Accounting for the multiplicity of stars remains one of the outstanding problems in the theory of star formation. The question is just now being faced by theoreticians (Larson 1977), but has to date received little attention from infrared observers. The fact that many molecular clouds show multiple sources of infrared radiation bears directly on the problem.

The possible mechanisms for producing groups of stars have been known for many years and are summarized succinctly by Aitken (1918; p. 276):

> "(1) Two stars, hitherto independent, might approach each other under such conditions that each would be swerved from its original path and forced to revolve with the other in orbits about their common center of gravity (Capture Theory).
> (2) A single star, in its primal nebulous stage, or possibly even later, might divide into two, which would at first revolve in surface contact (Fission Theory).
> (3) The material in the primal nebula might condense about two nuclei separated by distances of the order of those now existing between the centers of the component stars (Independent Nuclei Theory)."

The infrared, optical and radio observations strongly suggest that the visual binaries and trapezia are created by the fragmentation of a single collapsing core into independent clumps of material, each capable of producing one (or more) star(s).

Separations Between Multiple Infrared Sources

Four and possibly five of the seven molecular clouds examined here have been found to contain more than one source of infrared radiation. S255 and IC1848 A each contain two objects. S140 contains three. The infrared source in Cep A is extended on a scale of 9" which is just the scale of distances between the three weak HII regions found by B^2W^2 (Figure III.9). The centroids of the radio and infrared emission coincide within the combined uncertainties and it seems likely that the infrared extent is the result of observing multiple sources with low spatial resolution. S235-IRS 3 is a compact HII region that lies within the same CO core as S235-IRS 4 (Israel 1976; Evans 1978 private communication), only 40" away.

Table IV.3 lists all of the clouds closer than 4kpc known to contain more than one infrared source. In making this compilation,objects showing weak radio continuum emission, but still clearly embedded within a cloud, were included to increase the size of the sample. In the table, Columns 1 - 3 give the name of the cloud, the distance to it in kpc, and the number of infrared sources. The average angular separation between objects, ρ, listed in Column 4, is the average, over all sources in the group, of the distances between one object and its two nearest neighbors. No separation is counted more than once. For a group of three sources ρ is just the average of the three unique distances between the three objects. For a group of many sources ρ is a measure of the separation between adjacent objects that is independent of the overall dimensions of the cluster. The physical separation, in pc, obtained from the angular separation using the distance to the cluster from Column 2, will be referred to as the nearest neighbor separation, r, and is tabulated in Column 5. Projection effects, to be discussed later, make r smaller than its true,three dimensional value. Notes and references are given in Column 6.

Separations Between Stars in Trapezia

Table IV.4 is a list of 31 trapezia with primary stars on the main sequence and of a spectral type earlier than B3 (maximum lifetime $\simeq 10^7$ yr). These multiple systems are taken from the lists of Sharpless (1954) and Salukvadze (1978). For each cluster the nearest neighbor separation was computed in the same manner as for the infrared objects above. Positions for the stars within each trapezium were taken from Sharpless (1954), the Aitken Double Star Catalogue (Aitken, 1932; hereafter ADS) and the Index Double Star Catalogue (Jeffers,

Table IV.3

Separations between Infrared Sources

Name	d(kpc)*	N	$\rho\pm\sigma$(")	r(pc)	Refs.
W3-IRS 3-7	3.0	5	29±21	0.42	1
IC 1848 A	2.0	2	23± 2	0.22	2
AFGL 437	3.0:	3	9± 3	0.14	3
OMC 1	0.5	6	11± 8	0.03	4
OMC 2	0.5	5	34±14	0.08	5
S235-IRS 3-4	1.8	2	48± 5	0.42	6
Mon R2-IRS 1-5	0.95	5	26±12	0.12	7
S255-IRS 1,2	2.5	2	16± 3	0.19	2,8
S106	2.3	2	23± 3	0.25	9
AFGL 2591	1.5:	2	5± 2	0.04	10
DR21/W75	1.5	3	32±13	0.23	11
S140-IRS 1-3	0.9	3	15± 4	0.06	2,8
Cep A	0.73	3	7± 3	0.02	2,8
NGC 7538-IRS 1-3	3.5	3	12± 3	0.21	11

Notes to Table IV.3

1) Wynn-Williams, Becklin and Neugebauer 1972.
2) This dissertation.
3) Kleinmann *et al*. 1977.
4) Rieke, Low and Kleinmann 1973.
5) Gatley *et al*. 1974.
6) Evans 1978, private communication.
7) Beckwith *et al*. 1976.
8) B^2W^2 1979.
9) Pipher *et al*. 1976.
10) Wynn-Williams *et al*. 1977.
11) Wynn-Wiliams, Becklin and Neugebauer 1974.

* A colon denotes an uncertain distance.

Table IV.4

Separations between Trapezium Stars

HD/BD #	Sp.	ADS/IDS #	d(kpc)	N	ρ±σ(")	r(pc)	Stars	Notes,Refs.
1810	B3:	307	1.70:	4	23± 9	0.19	A-D	1
5005	05.5f	719	2.10	11	15± 8	0.15	-	2
17179	B0.5	2135	1.02	4	24± 8	0.12	A-D	3
17505	06.5	2161	2.20:	16	17± 9	0.18	-	2,4
17520	08	2165	2.20	9	17± 8	0.18	-	2,4
18326	07	-	1.00	8	13± 4	0.06	-	2
20053	B3	2426	0.80:	5	25± 9	0.10	A-E	5
25638	09	2984	1.00	6	21±11	0.10	ABPQDE	6,7
32990	B2	3709	0.23	3	25± 9	0.03	A-C	7
35007	B3	3941	0.38	3	34± 3	0.06	A-C	7
37020	B0.5	4186	0.50	7	8± 3	0.02	A-G	4,8
37468	09.5	4241	0.50	5	20±12	0.05	A-E	4
41943	B1	4728	0.93	6	21±10	0.09	A-E,P	9,10
45546	B2	06230S0442	0.26	3	64±21	0.08	A-C	7
46150	05	5165	1.51	5	8± 4	0.06	A-E	4
46867	B0.5	06306N0523	1.20	3	35± 4	0.20	A-C	20
47732	B3	5316	0.72	3	20± 7	0.07	A-C	10,11
47839	07:	5322	0.71	9	33±23	0.11	A-G,K,S	4,11
73903	B1	08357S4552	1.82	12	41±28	0.36	A-L	4,12
76838	B3e	08535S4252	0.87	11	66±26	0.28	-	13
303308	03	10412S5910	2.63	15	8±14	0.11	A-H,P-S	4
153771	B3	16562S5056	0.72	6	28±13	0.10	A-F	14
159176	07:	17282S3231	1.06	3	9± 3	0.05	A-C	10,15
164536	B3:	17565S2415	1.70	4	26±12	0.21	A-D	16
22°3782	07	-	2.00	14	8± 2	0.07	-	2,4
202904	B2e	14831	0.20	3	17± 3	0.02	A-C	7,17
206267	B0	15184	0.83	4	13± 6	0.05	A-D	4
214167	B1.5	16095	0.45	7	27±13	0.06	A-E,R,S	7
221253	B3	16795	0.20	6	46±32	0.04	A-D,F,G	18
242935	07	-	3.20	5	16± 4	0.25	-	2,4
62°2093	08:	17171	2.50	5	11± 6	0.14	-	2,4,19

Notes to Table IV.4

1) Deutschmann, Davis and Schild 1976.

2) Sharpless 1954 .

3) Hill and Lynas-Gray 1977. Distance from colors and spectral type.

4) Humphries 1978.

5) Kennedy and Buscombe 1974. Distance from spectral type.

6) Murphey 1969.

7) Lesh 1968.

8) The Trapezium, θ^1 Ori. Includes an O6 star.

9) NGC 2169.

10) Becker and Fenkart 1971.

11) NGC 2264 .

12) Vela OB1.

13) Herbst 1975b. see discussion in text.

14) Herbst 1975a.

15) NGC 6383.

16) Whiteoak 1962.

17) υ Cyg. Snow, Peters and Mathiew 1979.

18) Eggen 1963. Star E is not a member.

19) Assume Cas OB2.

20) Hiltner 1956.

* A colon denotes an uncertain distance.

van den Bos and Greeby, 1963; hereafter IDS) using all stars in the group unless other data could be used to reject an interloping field star. Data for the trapezium around HD 76838 was taken from Herbst (1975b) using the stars numbered 25c-ℓ in addition to the ADS stars.

In the table, Columns 1-3 give the HD/BD number and spectral type of the primary star as well as the ADS/IDS number of the multiple system. All are main sequence stars except for a few, denoted by a colon in column 2, for which the luminosity class is unknown. Columns 4 and 5 give the distance to the trapezium and the number of stars therein. Columns 6 and 7 give the angular and physical nearest neighbor separations. Column 8 lists the stars used in making the average (in IDS notation). Column 9 lists references for distances and spectral types.

Comparison Between Infrared and Optical Results

Table IV.5 shows that the mean nearest neighbor separations for the infrared and optical samples are the same, ≃ 0.15 pc, within the combined standard deviations of the means. The similarity between the space distributions of the two samples can be seen in the histogram of Figure IV.2, which shows the relative frequency of a separation, log (d_{pc}) , for all distances between all sources (stars) within a cluster, not just for the nearest neighbors. The solid line gives the distribution for 739 intracluster separations for the 31 stellar trapezia. The dashed line gives the same information for 70 distances within 14 infrared groups. Each bin is 0.2 units wide in log(d_{pc}). The data used to make the figure are given in Table IV.6. The similarity between the two distributions is obvious and is reflected in the mean values given in Table IV.5. Studies of wide visual binaries

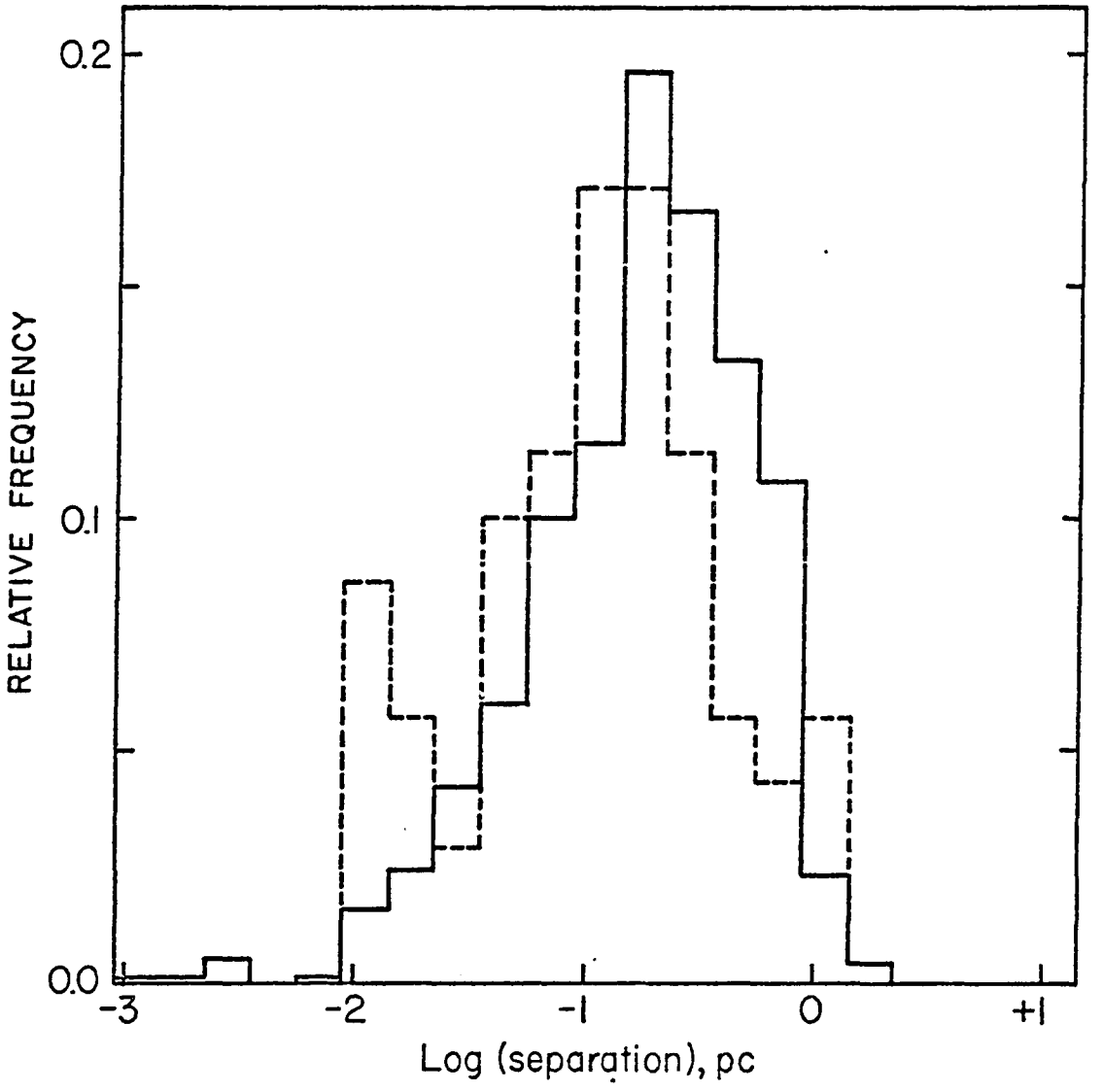

Figure IV.2. The separations between all objects within optical and infrared groups of sources (stars) is shown in this histogram. The solid lines represent the distances between all stars in the trapezium groups given in Table IV.4. The dashed lines give all the intra-cluster distances for the infrared groups given in Table IV.3. Each bin is 0.2 units wide in $\log(d_{pc})$.

Table IV.5

Mean Optical and Infrared Separations

	Optical			Infrared		
Value	Mean	σ	σ_{mean}	Mean	σ	σ_{mean}
Nearest Neighbor Distance, r	0.12 pc	0.08	0.01	0.17 pc	0.13	0.04
$\langle \log(d) \rangle^*$	-0.77	0.49	0.02	-0.95	0.53	0.06
$\langle 10^{\log(d)} \rangle^*$	0.27 pc	0.25	0.01	0.22 pc	0.27	0.03
Number of objects per group	6.6	3.8	0.7	3.3	1.4	0.4

*These values are averages over all distances between all sources (stars) within a group, as presented in Table IV.6 and Figure IV.2. These sizes reflect the overall dimensions of the clusters, while the nearest neighbor distances do not.

Table IV.6
Intracluster Separations

Distance $\log(d_{pc})$	Number with Given Separation $N_{optical}$	$N_{infrared}$
-2.95	1	0
-2.75	1	0
-2.55	4	0
-2.35	0	0
-2.15	1	0
-1.95	12	6
-1.75	18	4
-1.55	31	2
-1.35	44	7
-1.15	74	8
-0.95	86	12
-0.75	145	12
-0.55	123	8
-0.35	99	4
-0.15	80	3
+0.05	17	4
+0.25	3	0

(Van Albada, 1968; Tolbert, 1964) show separations of the same magnitude, or only slightly smaller, about 0.05 pc.

Whether the similarity between the infrared and optical space distributions is significant depends on the evolution of trapezia with time. Until recently it was thought that these small clusters were dynamically unstable, having net positive energy (Ambartsumian 1956); but recent work has shown that the trapezia are stable, gravitationally bound systems (Rybakov et al. 1971; Allen and Poveda 1974; Aarseth and Lecar 1975). Allen, Poveda, and Worley (1975) have examined the kinematics of 44 trapezia and found in the proper motions of the component stars no evidence for disintegration. The negative result is consistent with the N-body calculations of Allen and Poveda (1974, 1975) who find that trapezia endure for 10^6 yr, leading these authors to conclude that many OB stars more massive than 5 $M_\odot$ are to be found in the trapezia in which they were born.

The apparent dynamical stability of the trapezia coupled with the infrared observations of multiple sources distributed on the same distance scale provide strong evidence that trapezia and wide visual binaries form ab initio within collapsing molecular clouds. The creation of multiple systems by gravitational encounters well after the formation of these stars (Aitken's method #1) is not required.

Three major observational limitations can bias the infrared observations. First, the spatial resolution typical of infrared observations, 3-5", is significantly worse than that available routinely at optical wavelengths, ≃ 1". As hinted at by the radio observations of Cep A, there are multiple sources of infrared radiation separated by less than the usual infrared resolution. Evidence for multiplicity

on a 1" scale comes from the Very Long Baseline Interferometry of Genzel et al. (1978),who find that the H2O masers in W3-IRS 5 and OMC-1 are clustered into distinct "centers of activity," 10^{-3} pc across, and separated from one another by .02pc (figure IV.3). These authors attribute each "center of activity" to the presence of a single OB star. This is consistent with the observed optical distribution of stars.

While the lower limit of the infrared space distribution at $d=10^{-2}$ pc is certainly due to the effects of limited spatial resolution, the same is also true of the optical trapezia as well. Most of the optical separations used in compiling Table IV.4 are greater than 5". The mean nearest neighbor distance was recomputed for the optical sample neglecting all separations smaller than 5"; and the new value increased negligibly over the old one (from 0.12 pc to 0.13 pc). The effects of limited resolution do not invalidate the comparison between the optical and infrared samples.

A second effect concerns the size of the regions searched at infrared wavelengths, typically 1-2', compared with 3 - 5' at optical wavelengths. The infrared trapezia can be expected to have a smaller overall extent than the optical groups, simply because sources lying far from the brightest ones will not be found. The mean values in Table IV.5 reflect this effect.

Finally, the limited sensitivity of the infrared searches precludes finding the faintest members of the groups. In optical studies (e.g., Sharpless 1954) a magnitude range of 10^{m} between the brightest and faintest stars is found. In the infrared, the range is much more limited. For example, S140-IRS 2 has an integrated luminosity shortward of 25 μm that is about one-twentieth that

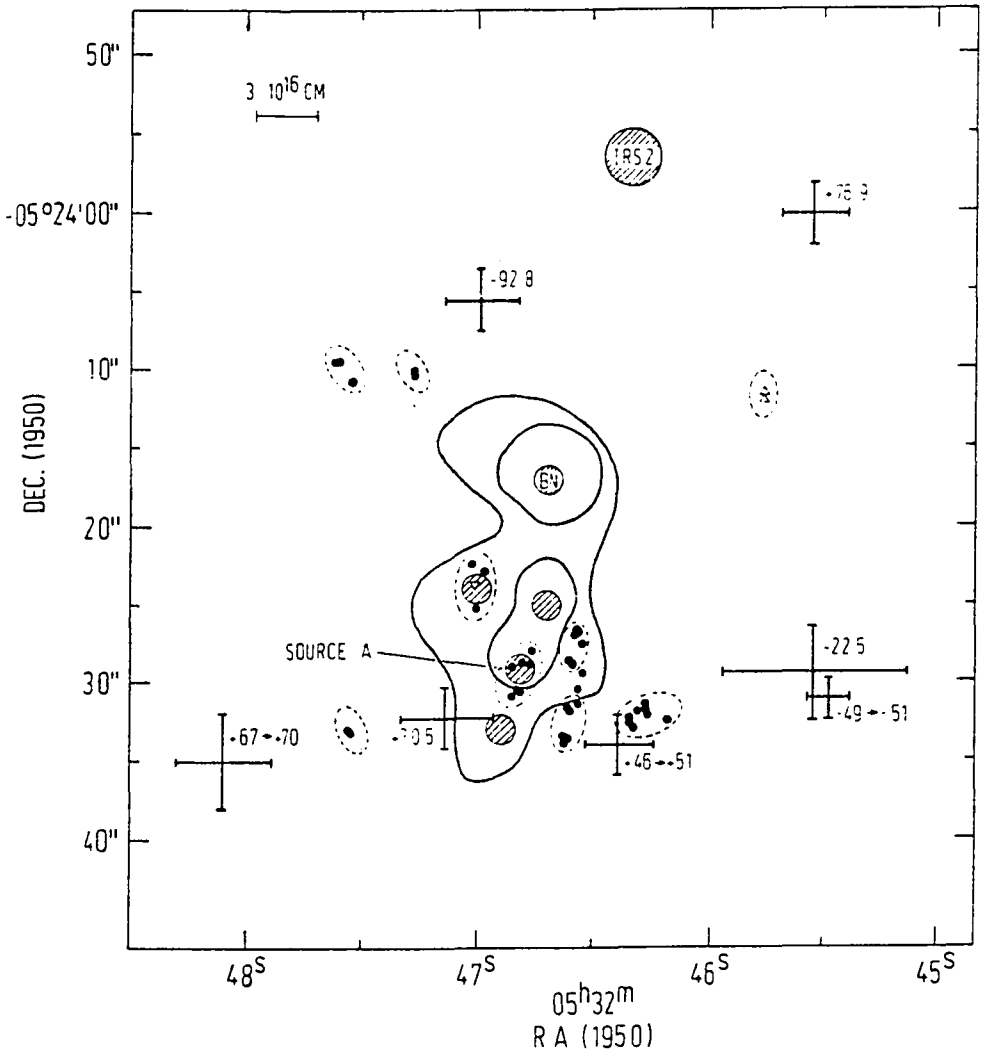

Figure IV.3a. Positions of H_2O masers in OMC 1 from VLBI observations (Genzel et al.1978) are superimposed on contours of 21 μm radiation (Rieke et al.1973). Dashed lines indicate boundaries of "centers of activity" that may correspond to individual stars. Shaded circles are compact infrared sources (Figure from Genzel et al. 1978).

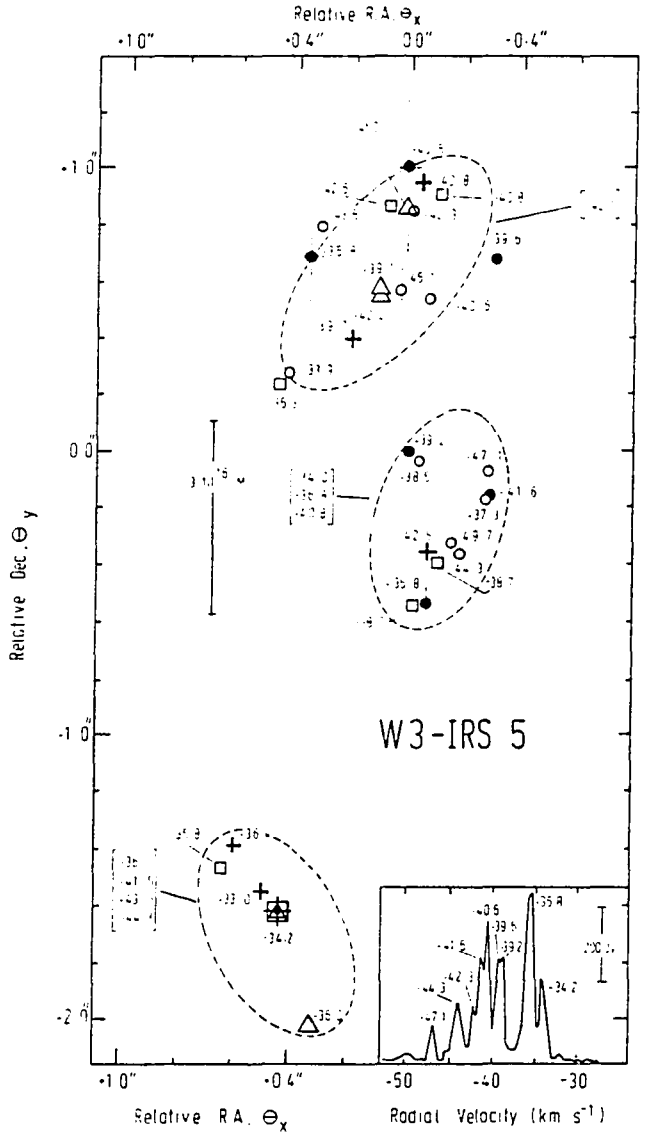

Figure IV.3b. Positions of H_2O masers around W3-IRS 5 from VLBI observations (Genzel et al. 1978). Dashed ellipses denote the approximate extent of "centers of activity" thought to correspond to individual, newly forming OB stars (Figure from Genzel et al. 1978).

of S140-IRS 1, corresponding to a bolometric magnitude difference of about $3\text{-}4^m$ (naively assuming equal bolometric corrections for the two objects). Search techniques such as those employed here cannot probe the less luminous end of the stellar distribution within these groups. It is not surprising that the infrared trapezia have apparently fewer members than the optical groups (Table IV.5)

Theoretical Considerations

The likliest mechanism by which multiple stars separated by the observed distances are formed is the fragmentation due to gravitational instabilities of a collapsing cloud core into individually evolving condensations (Laplace 1796; Aitken's method #3). A fragment will form when its size exceeds a critical dimension, called the Jeans length, R_J, above which its gravitational potential exceeds its thermal (and rotational) energies. Neglecting for the moment the effects of magnetic fields and rotation, a self-gravitating medium will be unstable against a perturbation of wavelength R_J larger than (see, e.g., Lang 1974, p. 306)

$$R_J = (\pi kT/\mu m_H G\rho)^{1/2} \quad , \qquad \text{(IV.2)}$$

where T is the gas temperature, ρ is its mass density (not to be confused with the intracluster separation defined above) and μ is mean molecular weight, 2.33 for molecular hydrogen plus cosmic abundances of helium and metals (Silk 1977). Other symbols have their usual meanings. The critical mass, M_J, contained within R_J is given by

$$M_J = \frac{\pi}{6}\,\rho R_J^3 \quad . \qquad \text{(IV.3)}$$

In practical units,

$$R_J = 6.75(T/n)^{1/2} \text{ pc} ,$$

$$M_J = 9.22(T^3/n)^{1/2} M_o , \qquad \text{(IV.4)}$$

$$R_J = 0.73M_J/T \text{ pc} ,$$

where n is the H_2 number density.

The observed separations between infrared sources can be compared with predictions after correction for projection effects. The simplest assumption is that the true separation vectors are inclined at random angles i to the line of sight. The mean nearest neighbor separation will then be reduced from its true value by the average value of sin(i) over the distribution. From Chandrashekar and Münch (1950) the reduction factor is $\pi/4$. From the mean infrared nearest separation listed in Table IIV.5 and a correction of 1.27, the best estimate of the mean distance between fragments is 0.22 ±0.05 pc.

Using quations (IV.4) the cloud conditions that lead to an average separation of 0.22 pc between stars of average mass (10 M_o) are a gas temperature of ≃ 30K and a density of 3×10^4 cm^{-3}. Although the temperature is slightly high, these are reasonable values for the physical conditions within a molecular cloud core before the formation of stars that can raise the gas temperature up to 80K (e.g., OMC-1).

These numbers are of course idealized, for in the real world the process by which gas is turned into stars has an efficiency of only 10 % -30% (Bertout and Yorke 1978) implying that production of a 10 $M_\odot$ star requires a 30-100 M_o fragment. On the other hand magnetic fields

and rotation stiffen the cloud against collapse with the result that significantly more mass is required to initiate a collapse within a given R_J (see, e.g., the virial theorem analysis of Chandrashekar and Fermi 1953). Realistic models including these and other effects are only now being attempted and definitive results are not yet known. But from the preliminary work that has been done, it does not appear that estimates based on the simple Jeans length analysis lead to wildly incorrect results. Larson (1977, p. 258) writes:

> "In summary, these crude 3-dimensional collapse calculations suggest that fragmentation is largely determined by the Jeans mass at the time when collapse begins. The condensations in a collapsing cloud are formed approximately satisfying the Jeans criterion, and depending in detail on how closely they satisfy it, they may form either single stars, binaries, or small multiple systems."

The detailed theory of fragmentation proposed by Silk (1977) also predicts clumpiness on the scale comparable to that observed here. "Detection of clumpiness on this scale (i.e., 0.1 pc) at densities of 10^4 cm^{-3} could provide a vital link between molecular clouds and the star formation process" (Silk 1978, p. 187). The infrared data give evidence for structure within the molecular clouds on a scale of about 0.1 pc.

An alternative to cloud fragmentation by gravitational instability is the fission (Aitken's method #2) of a rapidly rotating core that must convert its rotational angular momentum into orbital angular momentum before its collapse can continue. The core must fragment as its rotational energy approaches its gravitational energy. Calculations by Ostriker and Bodenheimer (1973) and by Gingold and Monaghan (1978) show that bifurcation occurs as $E_{rot} \simeq 0.25 \sim 0.4 E_{grav}$, or

$$\frac{1}{2} I \Omega^2 \geq 0.4 \frac{3}{5} G \frac{M^2}{R} \quad , \qquad \text{(IV.5)}$$

where $I = 2/5\ MR^2$ is the moment of inertia of a uniform spherical cloud of mass M and radius R, rotating at an angular velocity Ω. This condition becomes

$$\frac{1}{4\pi(0.4)G\mu m_H} > \frac{n}{\Omega^2} \quad , \qquad \text{(IV.6)}$$

or

$$77 > \frac{n}{\Omega_{14}^2} \quad ,$$

where Ω_{14} is the angular velocity measured in units of 10^{-14} rad s^{-1}. Observations of systematic velocity shifts in CO lines suggest, although not unambiguously, that clouds with $n \simeq 5 \times 10^3$ cm^{-3} have $\Omega_{14} \simeq 0.5$–2 (see, e.g., Schneps et al. 1978, for AFGL 437; Loren 1977 for Mon R2; and Field 1978, p. 243). A cloud collapsing with conservation of angular momentum will have $n/\Omega^2 \propto R$, so that bifurcation will occur when R drops below a value given by

$$\frac{77\ \Omega_{14,o}^2\ R_o}{n_o} \quad . \qquad \text{(IV.7)}$$

For a cloud of $n = 5 \times 10^3$ cm^{-3}, $R_o = 1.6$ pc, $\Omega_{14} \simeq 1$ (and $M=5\times10^3\ M_o$), the bifurcation distance is 0.02 pc, comparable to the smallest observed scales of fragmentation.

One might be tempted to attribute the existence of multiple sources to the effects of rotational, rather than gravitational, instabilities, as Schneps et al. (1978) suggest for AFGL 437.

Mouschavias (1979) has shown, however, that the assumption that angular momentum is conserved during a collapse is incorrect. Ω, and accordingly the bifurcation distance, will be much smaller than predicted on the basis of the above values of Ω and the conservation of angular momentum because of magnetic braking (Mestel 1965) whereby the cloud's angular momentum is deposited into the rest of the galaxy via the tension of twisting magnetic field lines. The process is so efficient in the case when the field is perpendicular to the rotation axis that "Consequently, a cloud with mass $10^3 M_\odot$ will lose at least 99 percent of its angular momentum in a time $\simeq 2 \times 10^6$ yr if its density is 10^2 cm^{-3}, and in a time $\simeq 1 \times 10^6$ yr if its density is 10^3 cm^{-3}" (Mouschovias 1979). For parallel field and rotation directions the characteristic damping time is longer, but in either case it is likely that the cloud will have its rotation damped efficiently.

As the cloud collapses its angular momentum will be removed by magnetic braking until the core density becomes large enough, around 10^6 cm^{-3} so that the magnetic field decouples from the gas becuase of the low level of ionization within the cloud. The exact density at which this occurs and the remnant angular momentum at this stage are unknown. Mouschavias (1977) suggests that the amount of angular momentum left is just comparable to that in binary stars of period less than 10 yr, and that close binaries are formed by the fission of the core at this time. Abt and Levy (1978) and Lucy and Ricco (1979) have proposed similar mechanisms.

The idea that gravitational fragmentation produces multiple systems and wide binaries, while rotational bifurcation produces close binaries receives support from an important physical difference in the properties of the two types of binary systems. Trimble (1974) and Abt and Levy (1978) have found that wide binary systems ($P > 10$-100 yr; $d \gtrsim 10^{-4}$ pc) are composed of stars whose masses are uncorrelated with one another. The individual primary and secondary stars separately follow the van Rhijn luminosity function (Abt 1978). Close binaries, on the other hand, tend to have primaries and secondaries of roughly equal mass. The lack of correlation for wide systems is consistent with the independent evolution of separate condensations into stars, while the strong correlation of the masses of close binaries is suggestive of the bifurcation of a rapidly rotating fragment into pieces of roughly equal size. (Lucy and Ricco, 1979) The calculations of Gingold and Monaghan (1978) show that the creation of fission fragments with mass ratios in the range $0.4 \sim 1$ is likely.

The fact that individual stars within wide binaries and trapezia are often themselves eclipsing or spectroscopic binaries (cf. the recent discovery that the Trapezium star θ^1A Ori is an eclipsing system; Lohsen 1975; Caton, Fallon, and Wilson, 1978) can be interpreted as evidence for the existence of two independent, but complementary, mechanisms for the production of multiple stars (Van Albada 1968b).

The scenario envisioned, then, is one wherein a single collapsing core within a $10^3 - 10^4$ $M_\odot$ cloud fragments into condensations separated by $10^{-2} \sim 10^{-1}$ pc as a density of 10^4 cm^{-3} is reached.

Individual fragments are weakly bound to one another gravitationally but collapse independently. Depending on the initial condiitons and in particular on the efficacy of magnetic braking, each condensation turns into one or more stars. A second round of gravitational fragmentation at higher densities and smaller separations to bridge the gap between 10^{-2} 10^{-4} pc cannot be ruled out, but Larson (1977) states that numerical models show no evidence for this hierarchical fragmentation that was first proposed by Hoyle (1953).

The infrared data provide observational support for existence of separate condensations within the cores of molecular clouds. Future observations at millimeter wavelengths with high spatial resolution $\leq$20" should find distinct enhancements in the gas density around each infrared object. Eventually infrared observations at high spectral resolution may be used to detect spectroscopic systems of stars and probe the conditions at which rotating cores bifurcate to produce close binary stars. Finally, more sensitive searches of molecular clouds over > 2' area should reveal the existence of more low mass members of the trapezium groups, rather than just the brightest two or three that can now be observed.

IV.4 Energy Distributions

The 2-25 μm energy distributions of the sources studied here resemble those of other objects such as BN, KL and W3-IRS 5 and, in general, conform to the characteristics of luminous embedded sources as modelled by various authors (Leung, 1976; Scoville and Kwan, 1976; Kwan and Scoville, 1976; Finn and Simon, 1977; Bedejin *et al*. 1978). It is beyond the scope of this dissertation to develop detailed models for each of the objects studied here, for these broad-band observations are ill-suited to the task. Measurements with fifty times the spectral resolution of these data are available for this purpose (Gillett *et al*, 1975; Willner 1976, 1977; Capps *et al*. 1978), and even their interpretation is ambiguous.

The contribution of this study is to point out the inadequacies of some of the assumptions upon which earlier work has been based. To date all rigorous radiative transfer models have assumed the existence of a single luminous source of energy located at the center of a spherically symmetric, homogeneous cloud of gas and dust. The data presented in this dissertation suggest that these assumptions are rarely satisfied.

By now the reader should be suspicious of the assumption that lone sources heat clouds. In S140 three discrete objects are observed and each much contribute to the emergent spectrum of the cloud as a whole. In S255 it is impossible to separate the individual contributions of the two sources to the far infrared fluxes. An attempt to attribute the 2-200 μm spectrum of S255 to a single object will be doomed to failure, because S255-IRS 1 dominates from 2-20μm, while S255-IRS 2 dominates from 20 μm up to some

unknown longer wavelength, where the contribution of each one becomes indistinguishable from the general background of warm grains.

A second example of the complexity of the real world comes from a comparison of S140-IRS 1 with Cep A-IR. Both objects emit a small amount of radio-continuum flux (B^2W^2), suggesting that each should show a spectrum characteristic of grains heated to 300K within a very compact HII region. The observed energy distributions could not, however, be more different from one another. S140-IRS 1, 2, and 3 emit strongly between 2-20 μm, and the bolometric correction to the luminosity observed shortward of 25 μm is only a factor of four. Cep-A IR on the other hand emits practically no radiation shortward of 20 μm and the bolometric correction to its luminosity is a factor of 400 (Koppenaal et al. 1979). If the intrinsic spectra of S140 and Cep A-IR are roughly the same, as the radio data suggest, then the differences in the emergent spectra must arise from the different locations of these sources within their respective molecular clouds. S140-IRS 1 must lie close to the near side of the cloud and suffer relatively little attenuation (A_V no larger than 10-30), while Cep A-IR must lie deep within its parent cloud ($A_V \geq 100$) and have almost all of its energy converted into photons longer than 20 μm.

Another suspect assumption is that these objects are surrounded by homogeneous envelopes of gas and dust. The 0.9-2.2 μm nebulosity observed around S255 (Evans et al, 1977), S269 (this work and Wynn-Williams et al. 1974), NGC 7538-IRS 9 (Werner et al. 1979) and S140-IRS 1 and 3 (Dinersten et al. 1979); B^2W^2) suggest that

there may be gaps in the cloud material through which radiation from hot interior regions can escape. The optical object MI-82 #1 (Minkowski 1946; Sibille et al. 1976) which lies within 3" of S235-IRS 4, shows strong Hα (Glushukov et al 1975) and Bα (Tokunaga and Thompson 1979b) and may be the result of radiation escaping from a compact, dense HII region related to the 20 μm source. The plasma must be optically thick at 6 cm, for no radio emission stronger than 5mJy is observed from this object (Harris, 1976; Israel and Felli, 1978). Optical nebulosity showing Hα and Hβ lines has also been observed close to IC1848A- IRS 1 and 2 (Cohen and Lewis 1978). The presence of 10 μm silicate absorption features toward these sources implies $A_V \simeq 20$ (for $A_V/\tau_{9.7} \simeq 10\text{-}15$) and precludes an identity between the optical and infrared objects. The leakage of optical and near infrared radiation is, however, possible. Harvey, Campbell and Hoffmann (1977) have invoked anisotropic dust distributions to explain the optical, near infrared and far infrared observations of NGC 2264.

The lack of symmetry and homogeneity complicates the analysis of the radiative transfer problem considerably, but may prove to be a blessing; for the radiation that emerges from a simple, homogeneous cloud reveals little about the nature of the underlying object. Leung (1976) has shown that the temperature of a nebular grain depends only weakly on the color temperature, T_*, of the exciting source, approximately $T_*^{-1/5}$. Objects with $T_* \simeq 10^3$K embedded within an optically thick cloud of dust will produce a temperature distributions that differs by less than a factor of

two from that produced by a $2x10^4$K object. Very similar energy distributions will result.

A sobering example of this insensitivity of 2-25 μm observations to the characteristics of the underlying object comes from the fact that extremely dust enshrouded Mira variable stars associated with OH masers such as OH 26.5 + 0.6 (Evans and Beckwith 1977) have 2-20 μm energy distributions that are indistinguishable from those of molecular cloud sources. Only observations at wavelengths longer than 30 μm or in radio molecular lines which show the existence of a giant cloud around the young stars differentiate between the two (Telesco and Kleinmann, 1979, private communication).

A simple analogy can be made. Consider infrared observations made of the outside of a great furnace. While the data allow an excellent determination of the total energy output of the furnace, they offer no clue as to whether the fuel being consumed inside is oil, coal or natural gas. The same is true of astrophysical sources. The 2-25 μm observations tell only that there is a luminous, object embedded with a coccoon of dust. Observations at other wavelengths---in the radio continuum, in the far infrared, in recombination or forbidden lines, in millimeter molecular lines, or in the leakage radiation escaping through chinks in the cloud walls---are required to probe more deeply into the nature of this object.

IV.5. The Nature of Objects in Molecular Clouds

A. Introduction

Earlier sections have dealt with the properties of the infrared objects embedded within molecular clouds without explicitly discussing their nature. The purpose of this section is to attempt to pinpoint the evolutionary status of these sources.

It is clear that these objects cannot be chance interlopers inside the clouds. Field stars of greater than $10^4 L_\odot$ are rare, and the odds against finding one in the densest part of practically every cloud examined are overwhelming. Because the time for a star to move out of the core of a cloud is short ($\lesssim 10^6$ yr) compared with the main sequence lifetime of a $10^4 L_\odot$ object ($\gtrsim 10^7$ yr), it is unlikely that these sources are post main sequence objects. Finally, theoretical calculations have shown that massive ($\gtrsim 5 M_\odot$) stars evolve toward the main sequence along tracks of roughly constant luminosity and every increasing temperature (Iben, 1965; see Yorke and Krügel 1977, for an alternative view) so that the total infrared luminosity of a developing star is close to that of the main sequence object it will eventually become. These considerations lead to the conclusion that the infrared objects found in molecular clouds, having luminosities of $6 \times 10^3 - 10^5 L_\odot$ are, or are in the process of becoming, late O and early B stars.

It is difficult to learn about the evolutionary stage of these objects. Placing a star in the HR diagram requires some "photospheric" temperature as well as a luminosity; but, as discussed in the previous section, the 7.8-25μm energy distribution reveals little

about the intrinsic temperature of the underlying object. Fortunately, observations in other spectral regions can be used to probe the conditions immediately surrounding the star.

Theoretical considerations suggest that newly forming massive stars will start to emit UV radiation capable of ionizing hydrogen ($\lambda < 912$ Å) while still embedded within the molecular cloud (Larson and Starrfield 1971; Kahn 1974). Recently B^2W^2 have found evidence for small amounts of ionized material around a number of molecular cloud sources.

The recombination of ionized hydrogen produces two types of radiation that can be detected under certain conditions. Free-free collisions between electrons and protons results in bremsstrahlung radiation at radio and infrared wavelengths. Although absorption and thermal emission by dust obscures this radiation at wavelengths less than 1mm, free-free emission can be detected at radio wavelengths. Free-bound collisions produce recombination lines that can be observed in embedded sources if the extinction in the surrounding molecular cloud is not too great. Lines in the Brackett series, Bα ($n=5\rightarrow4$; 4.05 μm) Bγ ($n=7\rightarrow4$; 2.10 μm) have been detected toward a number of BN-like objects (Gradsdalen, 1976; Hall et al., 1978; Simon, Simon and Joyce, 1979; Tokunaga and Thompson, 1979a, b).

In this section radio and Brackett-line observations will be used to estimate the number of Lyman continuum photons, N_L, emitted by the object responsible for the infrared emission. N_L will, in turn, be related to a quantity that can be used to place these objects on the HR diagram.

A few useful formulae are given here which can be used to obtain N_L and the physical conditions within the ionized region on the assumption that hydrogen is photo-ionized by UV radiation.

B. Conditions within the Ionized Regions

The number of ionizing photons emitted per second, N_L, can be obtained from recombination theory. For an optically thin plasma at 10^4K (Rubin 1968), N_L is given by

$$N_L = 7.5\text{x}10^{43}\ S_\nu\ \nu^{0.1} d_{kpc}^2\ T_4^{-0.45} \qquad (s^{-1}) \ , \qquad \text{(IV.8)}$$

where S_ν is the observed flux density measure in mJy at a frequency ν in GHz for a spherical HII region a distance d (in kpc) away. T_4 is the temperature in units of 10^4K. The electron density, n_e, within the HII region can be obtained if the diameter, ℓ, in pc, is known:

$$n_e = 4.71\ S_\nu^{1/2}\ \ell_{pc}^{-3/2}\ d_{kpc} \qquad (cm^{-3}) \ . \qquad \text{(IV.9)}$$

From Osterbrock (1974, eq. 9.5) it is possible to develop similar formulae for Brackett recombination lines.

$$B_\alpha: \qquad N_L = 3.22\text{x}10^{57} (\pi F_{B\alpha}) d_{kpc}^2 \qquad (s^{-1}), \qquad \text{(IV.10)}$$

$$B_\gamma: \qquad N_L = 9.10\text{x}10^{57} (\pi F_{B\gamma}) d_{kpc}^2 \qquad (s^{-1}), \qquad \text{(IV.11)}$$

where πF is the flux in the line (erg cm^{-2} s^{-1}) and the numerical coefficients are for a 10^4K plasma of density $10^4 cm^{-3}$ using Table 4.4 of Osterbrock (1974, p. 69) and the departure coefficients of Giles (1977). The numerical values in Equation IV.10-11 are practically independent of the electron density.

It is also possible to obtain the electron density from the recombination line data using Osterbrock's formalae:

$$B_\alpha: \qquad n_e = 2.84\text{x}10^7 \, (\pi F_{B\alpha})^{1/2} \, \ell_{pc}^{-3/2} \, d_{kpc}, \qquad \text{(IV.12)}$$

$$B_\gamma: \qquad n_e = 4.76\text{x}10^7 \, (\pi F_{B\gamma})^{1/2} \, \ell_{pc}^{-3/2} \, d_{kpc}. \qquad \text{(IV.13)}$$

From Equations IV.8-11 and the observations it is possible to estimate N_L and the conditions within the HII region. Two complications can cause a serious underestimation of N_L. If the plasma is optically thick to its own radiation, the resulting self-absorption will reduce the observed flux and lead to a low value of N_L. The optical depths at 6 cm and in the Brackett lines are given by (Osterbrock, 1974, p. 16, 79)

$$\tau_{6cm} = 1.12\text{x}10^{-8} n_e^2 \ell_{pc}, \qquad \text{(IV.14)}$$

$$\tau_{B\alpha} = 2.11\text{x}10^{-15} n_e^2 \ell pc , \qquad \text{(IV.15)}$$

$$\tau_{B\gamma} = 3.73\text{x}10^{-17} n_e^2 \ell pc. \qquad \text{(IV.16)}$$

Clearly self-absorption will become a serious problem at radio wavelengths long before it becomes one in the Brackett lines. Dense, very compact HII regions can be rendered undetectable by large 6 cm optical depths. The flux density from an optically thick source depends only on its angular size and temperature. The 6 cm flux from a 10^4K blackbody subtending a solid angle Ω, with an angular diameter, Θ("), is given by (Kraus 1966, p. 87)

$$S_\nu = 2kT\lambda^{-2}\Omega = 142\Theta^2 = 6.02\text{x}10^6 \ell_{pc}^2 d_{kpc}^{-2} \qquad \text{(mJy).} \qquad \text{(IV.17)}$$

In addition to self-absorption it is possible that dust within the ionized region will compete successfully with the gas for UV

photons. If this happens, N_L derived from observations of recombination radiation will be smaller than the true N_L by an amount that depends on the dust opacity, τ_{UV}. Petrosian, Silk and Field (1972) have presented an analytic expression for the fraction of the UV radiation actually absorbed by the gas, as a function of the dust opacity. This function is shown in Figure IV.4.

The dust optical depth has been estimated by Panagia and Smith (1978) from observations within a number of giant HII regions. These authors find

$$\tau_{UV} = 2.5\text{x}10^{-3} n_e \ell_{pc}. \qquad \text{(IV.18)}$$

Thronson and Harper (1979) have discussed the possible depletion of dust within compact HII regions by a factor of five to ten.

As shown in Figure IV.5 the above-mentioned effects all limit the values of n_e and ℓ for which it is possible to detect an ionized region. Line 1 is based on Equation IV.9 and 17 and shows a flux limit of 1 mJy (typical of 6 cm observations with the Very Large Array telescope) for an HII region 1 kpc away. Sources below or to the left of this line are undetectable with present-day techniques. Line 2 is based on Equation IV.14 and represents the values of (n_e, ℓ) that give $\tau_{6cm} = 10$, above which self absorption effects become severe. HII regions above and to the right of Line 2 will be undetectable unless their size exceeds a value determined Equation IV.17 and shown in the upper portion of Line 1.

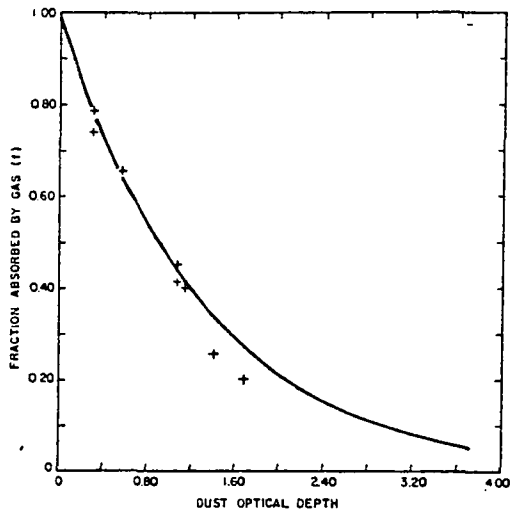

Figure IV.4. Fraction of ionizing radiation absorbed by gas plotted against the dust optical depth within the H II region. Crosses are numerical results (Figure from Petrosian et al. 1972).

The effect of dust internal to the ionized region is given in Line 3 using the UV opacity of Equation IV.18. Line 4 uses an opacity a factor of five smaller to account for the possible depletion of dust. For both lines τ_{UV} is equal to 8.2. This is the opacity at which the gas absorbs only 10^{-3} of the available UV radiation (Figure IV.4, Petrosian et al., 1972). Regions with (n_e, ℓ) above and to the Light of lines 3 or 4 will have little or no ionized gas because of quenching by dust.

A number of infrared sources are plotted in Figure IV.5 and Table IV.7. Radio data from B^2W^2 is used to locate Cep A-1 (the brightest of three radio sources), S140-IRS 1 and S255-IRS 2. It is assumed that S255-IRS 2 is related to the weak radio source found immediately to the north of the infrared position (Figure III.5b). Except for one of two radio sources coincident with S140-IRS 1, these HII regions are resolved and have sizes of 1-4". They must be optically thin, for, by Equation IV.17, the emission from an optically thick, 10^4K, plasma, greater than 1" across exceeds 140mJy, which is far larger than the limit of 25 mJy observed from these sources. W3(OH) is located in the (n_e, ℓ) plane using the data of Harten (1976). Brackett line observations were used to locate BN (Hall et al. 1978) and M17-KW (Tokunaga and Thompson, 1979a). A size of 1" was adopted for M17-KW and less than 0".5 for BN (Chelli et al., 1979). For smaller sizes the location of BN and KL move along the indicated lines.

The positions of these objects in the (n_e, ℓ) plane indicate that the objects powering S140-IRS 1, Cep A-1 and S255-IRS 2 are

Figure IV.5. Various mechanisms that limit the detection of compact HII regions are shown as solid lines. Ionized regions to the right of Line 1 (larger diameter, ℓ, and higher electron density, n_e) are detectable using the Very Large Array radio telescope. For regions in the (n_e,ℓ) plane above Line 2 , τ_{6cm}=10, self-absorption effects are important and may limit detectability. Lines 3 and 4 show the effect of different amounts of dust. Above and to the right of these lines, dust absorbs 99.9% of all UV photons (based on the model of Petrosian et al. 1972, Figure IV.4). Line 3 is based on the opacity given in Equation IV.18. Line 4 shows the effect of a factor of five less dust.

The positions in the (n_e,ℓ) plane are indicated for a number of infrared sources.

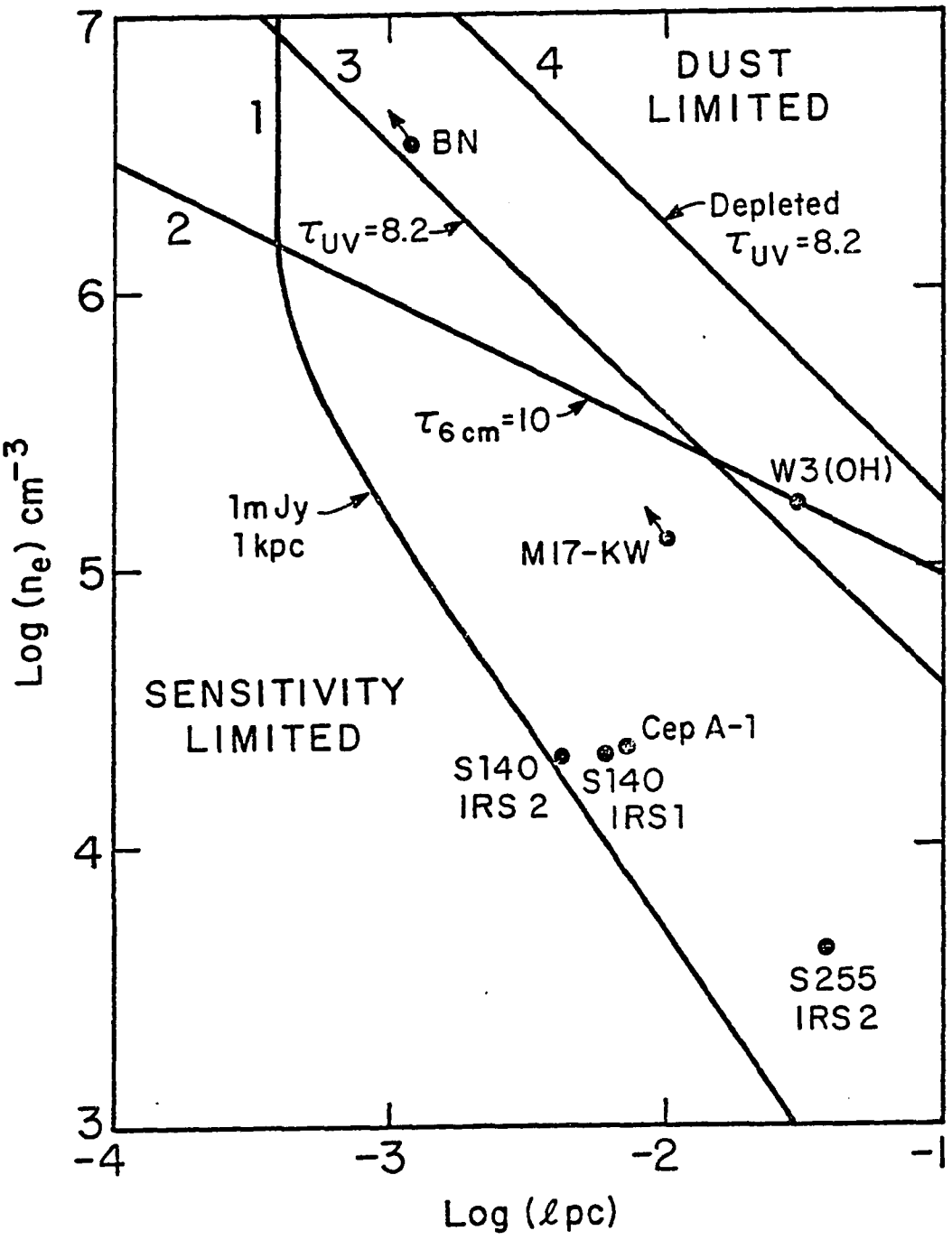
7
6
5
4
3
-4
-3
-2
-1
Log (n_e) cm^{-3}
Log (ℓpc)
1
2
3
4
DUST LIMITED
SENSITIVITY LIMITED
BN
Depleted
τ_{UV}=8.2
τ_{UV}=8.2
$\tau_{6\,cm}$=10
W3(OH)
1mJy
1kpc
M17-KW
Cep A-1
S140 IRS 2
S140 IRS1
S255 IRS2

Table IV.7

Physical Conditions Within Ionized Regions

Name	S_ν(6cm) mJy	diameter, (10^{-3} pc)	n_e (10^4 cm^{-3})	N_L ($10^{44}s^{-1}$)
AFGL 490[1]	<30	-	14	1.2×10^2
W3(OH)[2]	620	29	18	-
S235-IRS 4[3]	<5	20	6	2×10^3
BN[4]	<30	<1	>340	8×10^2
S255-IRS 2[5]	6	3.6	0.4	3×10^1
M17-KW[6]	<25[8]	<10	>12	5×10^2
S140-IRS 1[7]	6	6.2	2.2	4
S140-IRS 2[7]	2	4.4	2.1	1.5
Cep A-1[7]	15	7.1	2.2	7
Cep A-2[7]	6	5.0	2.4	3
Cep A-3[7]	4	5.0	2.0	2

Notes:

1) Thompson and Tokunaga 1979. Assumed distance 0.9 kpc. n_e and N_L from Brackett γ observation
2) Harten 1976.
3) Bγ measurement from Tokunaga and Thompson 1979b.
4) Bγ measurement from Hall et al. 1978.
5) B^2W^2. Assumes radio and infrared objects are related.
6) Tokunaga and Thompson 1979a.
7) B^2W^2
8) Matthews, Harten and Goss 1979.

surrounded by small, weak HII regions of moderate density, $n_e \simeq 2x10^4 cm^{-3}$.

Location of Infrared Objects in the HR diagram

The ratio of the total luminosity, L_*, to the UV luminosity, L_α, is based on N_L and can be compared with theoretical model atmospheres. L_α is defined as the number of Lyman continuum photons, N_L, times the energy in a single Lyman-α photon (λ=1215Å). The ratio of total to UV luminosity is

$$L_*/L = L_*/(h \nu_\alpha N_L) \qquad \text{(IV.19)}$$

L_*/L_α is very sensitive to photospheric temperature and ranges from 4 to 10^4 for 50,000K (05) to 18,000K (B3). Subtle radiative transfer effects can also produce relatively large variations in the predicted value of L_*/L_α for stars cooler than 25,000K as shown in Figure IV.6. Plotted in the figure is log L_* vs. log(L_*/L_α). The critical dependence of L_*/L_α on temperature makes this diagram similar to an HR diagram for OB stars. The three curves in the figure show the range of values for L_*/L_α as a function of spectral type for various stellar atmosphere models. To construct the curves (see Table IV.8) the temperature and luminosity of a particular ZAMS star were taken from Panagia's (1973) tabulation. The bottom curve (1) gives Panagia's (1973) values of L_*/L_α. The middle line (2) gives values from Kurucz's (1979) line blanketed, LTE model atmospheres. The top curve (3) displays values from Mihalas' (1972) non-LTE calcuations. In these latter two cases ,values were calcuated from

Table IV.8

Ratio of Total to UV Luminosity

Spectral Type	$\log L_*$ ($L_\odot$)	Panagia(1973) T (10^3K)	Panagia(1973) L_*/L_α	Mihalas(1972) T (10^3K)	Mihalas(1972) L_*/L_α	Kurucz(1979) T (10^3K)	Kurucz(1979) L_*/L_α
O4	6.11	50.0	3.5	50.0	4.1	50.0	4.0
O5	5.83	47.0	3.9	-	-	-	-
O5.5	5.60	44.5	4.2	45.0	4.2	45.0	4.5
O6	5.40	42.0	5.0	-	-	-	-
O6.5	5.17	40.0	5.4	40.0	5.5	40.0	5.3
O7	5.00	38.5	5.7	-	-	-	-
O7.5	4.92	37.5	6.1	37.5	6.9	-	-
O8	4.81	36.5	6.9	-	-	-	-
O8.5	4.73	35.5	7.9	35.0	9.8	35.0	10.0
O9	4.66	34.5	9.2	-	-	-	-
O9.5	4.58	33.0	13.2	32.5	19.5	-	-
B0	4.40	30.9	26.0	30.0	88.1	30.0	56.1
B0.5	4.04	26.2	1.5×10^2	25.0	2.3×10^3	25.0	5.1×10^2
B1	3.72	22.6	6.3×10^2	22.5	8.8×10^3	22.5	1.6×10^3
B2	3.46	20.5	1.5×10^3	20.0	2.7×10^4	20.0	5.5×10^3
B3	3.02	17.9	5.0×10^3	17.5	7.7×10^4	18.0	1.9×10^4

the tabulated models for stars of the appropriate temperature and log g=4. For the cooler stars there is a range in log L_*/L_α of almost a factor of 10, which is a measure of uncertainty in the parameter.

Observational data are plotted on Figure IV.6 in the following manner. Open circles denote infrared sources of known total luminosity with detectable radio emission. N_L and L_*/L_α were calculated using Equation IV.8 with no correction for possible absorption by dust. Because of the low spatial resolution at far infrared wavelengths, it is necessary to apportion the total luminosity between the members of multiple systems in a somewhat arbitrary fashion. Thus 60% of the total luminosity of the Cep A region is assigned to Cep A-1 (the brightest radio source); 100% of the luminosity of the S140 region was assigned to S140-IRS 1 (which is a factor of 10 more luminous than S140-IRS 2 or 3 shortward of 25 μm); and 50% of the luminosity of the S255 region was assigned to S255-IRS 2.

Filled triangles represent sources of known total luminosity for which only radio upper limits are available. The location of these sources in the HR diagram is very uncertain, as the lack of detectable radio emission could be due <u>either</u> to very small N_L (moving the objects to the right in the diagram) <u>or</u> to a large N_L hidden by dust or self absorption (moving the objects to the left).

Filled circles show well-studied compact HII regions from Thronson and Harper (1979). Open diamonds show sources whose L_*/L_α is known from Brackett line measurements. The location of BN follows the discussion of

Figure IV.6. An "HR" diagram for infrared objects embedded within molecular clouds. The total luminosity of each object, from airborne observations, is plotted on the ordinate. The ratio of the total luminosity to the Lyman continuum luminosity is plotted on the abscissa. This latter quantity is a sensitive function of temperature.

The three solid lines are from model atmosphere calculations from (1) Panagia (1973), (2) Kurucz (1979) and (3) Mihalas (1972). The positions of various spectral types along the Zero Age Main Sequence are shown to the left of Line 1.

Various infrared objects are located in the diagram using available infrared and radio data. Filled squares represent sources of known total luminosity and a Lyman continuum luminosity inferred from 6 cm data. Filled triangles represent sources with only an upper limit to the 6 cm radiation. Filled circles are known compact HII regions from Thronson and Harper (1979). Open diamonds have their Lyman continuum luminosity estimated from measurements of Brackett recombination lines.

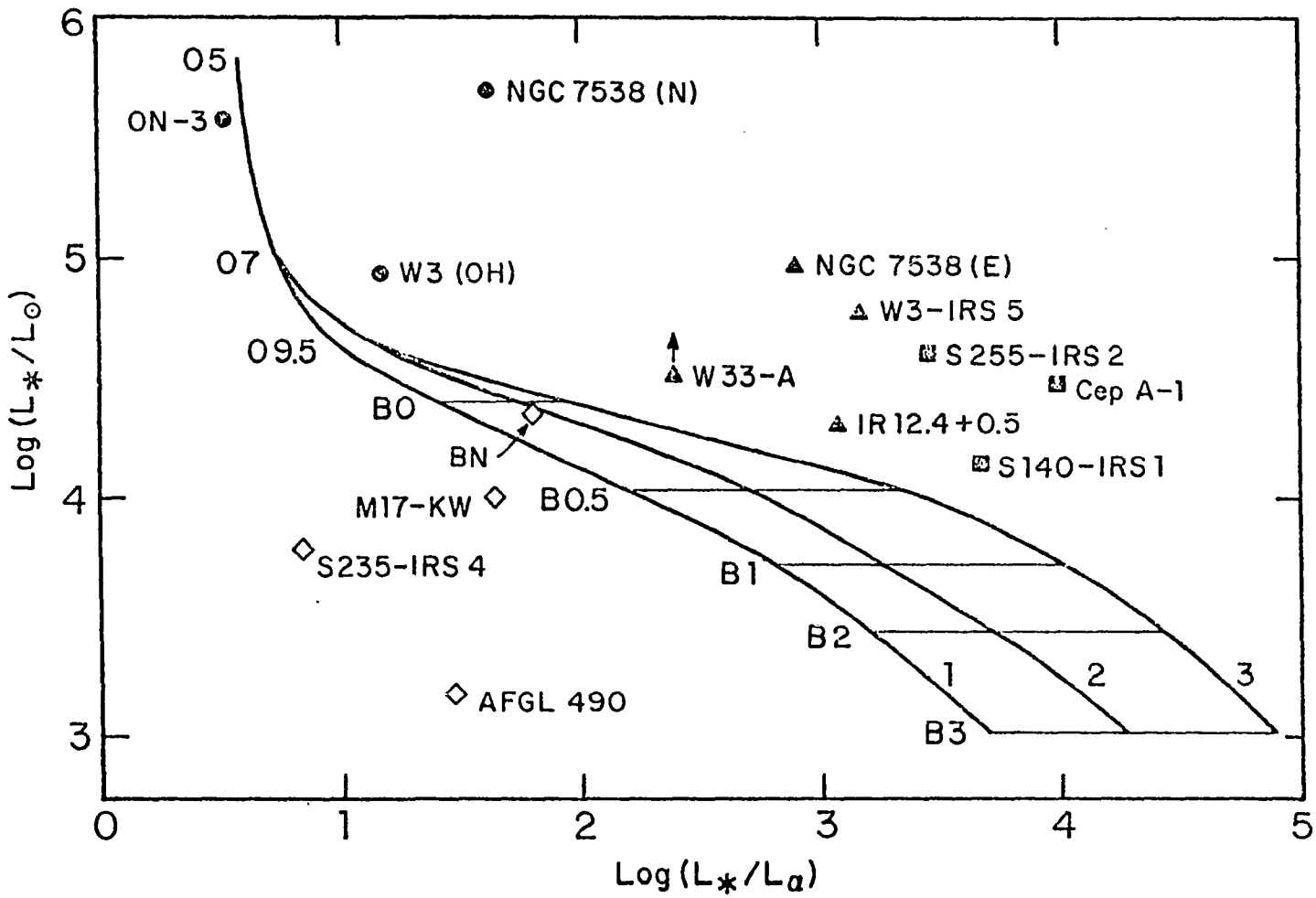
6
5
4
3
0
1
2
3
4
5
Log (L*/L⊙)
Log (L*/La)
O5
ON-3
O7
O9.5
B0
BN
M17-KW
B0.5
S235-IRS 4
B1
B2
B3
1
2
3
AFGL 490
NGC 7538 (N)
W3 (OH)
NGC 7538 (E)
W3-IRS 5
S 255-IRS 2
Cep A-1
W33-A
IR 12.4+0.5
S140-IRS 1

Figure IV.6

Joyce, Simon and Simon (1978). The total luminosity of M17-KW is unknown, but probably exceeds $10^4 L_\odot$ (Werner et al., 1979; Tokunaga and Thompson, 1979a). The positions of AFGL 490 and S235-IRS 4 in the figure are from Bγ line measurements as well.

Examination of the figure leads to the conclusion that S140-IRS-1, BN and M17-KW are probably main sequence B0∿B1 stars. Uncertainties in true total luminosity and in the effects of dust are enough to permit a shift of S140-IRS 1 down and/or to the left in the diagram, putting it close to the main sequence.

On the other hand objects such as Cep A, and S255-IRS 2 (on the assumption that the weak radio emission really is associated with the infrared object) are so far above and to the right of the main sequence that it is unlikely that any reasonable combination of overestimated luminosity and dust absorption can be invoked to bring these objects onto the main sequence. For example, the density and size of Cep A-1 ($2\times10^4 cm^{-3}$, 7×10^{-3}pc) are such that the dust opacity τ_{UV} is less than 0.4, by Equation IV.18. From Figure IV.4 the correction factor to the observed N_L is only about 1.4. The relatively small change in L_*/L_α is inadequate to bring the star responsible for the ionization within Cep A-1 close to the main sequence. Only an error of a factor of ten in the total luminosity of this object, which seems unlikely, could account for the displacement from the main sequence. Far infrared observations at high spatial resolution can remedy the uncertainty.

Little can be said about those sources without detectable radio emission. Sensitive VLA measurements may help to determine their location in the HR diagram.

The Brackett line observations toward a number of sources call into question the assumptions which Figure IV.6 is based. AFGL 490 (Simon et al. 1979; Thompson and Tokunaga 1979) and S235-IRS 4 (Tokunaga and Thompson 1979b) both emit more recombination line radiation than expected for the observed total luminosity (Harvey et al. 1979). If the ionization is radiative, then the observed line flux means that the ratio L_*/L_α is small and that these objects lie well below the main sequence of Figure IV.6. This peculiar location in the "HR" diagram may be due to a number of possible effects:

(1) The correction to be observed Brackett line flux for extinction within the molecular cloud is both large and uncertain (2≃8). If the reddening correction is much smaller than assumed, the positions of S235-IRS 4 and AFGL 490 shift to the right in Figure IV.6, close to the main sequence.

(2) The vertical location of each source in the figure depends on the square of its distance from the sun, so that moving an object further away moves it closer to the main sequence. For S235, however, the uncertainty in the distance is apparently no larger than 50 percent (Georgelin 1978, private communication). The distance to AFGL 490 is a kinematic one based on molecular lines (Harvey et al. 1979) and should be reliable for the Perseus Arm (Kraus 1966, p. 347).

(3) The assumption of radiative ionization by photospheric UV photons may be incorrect. Thompson and Tokunaga (1978) have invoked ionization due to the release of kinetic energy by infalling material to explain the anomalously strong Bγ line emission seen toward NGC 2264. A similar mechanism may be operating in AFGL 490

and S235-IRS 4. Alternatively a stellar wind mechanism, such as that proposed by Schwartz (1975) to explain the ionization observed in T Tau, may be operating. In S235-IRS 4 Glushukov et al. (1975) have found evidence for supersonic gas velocities in the H_α lines, and it is of relevance to note that Genzel et al. (1979) invoke the existence of a supersonic stellar wind to explain the kinematics of H_2O masers around W 51 (Main). It is possible that the role of shock ionization has been neglected in some sources.

(4) The unreddened fluxes and the application of standard recombination theory may be correct, in which case young objects like AFGL 490 and S235-IRS 4 are passing through an evolutionary phase during which they emit unusually large amounts of UV radiation.

The solution to this problem is not yet known, but it may be significant that the anomalously high recombination line radiation arises in objects with the smallest total luminosities, 10^3-$10^4 L_\odot$. The luminous objects such as, S140-IRS 1 and Cep A can, it appears, be explained as being precursors to late O and early B stars surrounded by small amounts of ionized material. The amount of ionization is consistent with these objects being on a radiative track to the main sequence.

CHAPTER V

SUMMARY AND CONCLUSIONS

The observational results and discussions presented in the preceding chapters are summarized briefly here.

(1) Of the 24 molecular clouds examined at 20, 10 and 2.2 μm, about 50 percent have been found to contain embedded sources of infrared radiation more luminous than $6 \times 10^3 L_\odot$. Searches at 20 μm were particularly fruitful, yielding discoveries of four objects that had been missed in earlier searches at 10 μm. Searches at 2.2 μm, on the other hand, only led to the discovery of sources that could, in most cases, be identified with field stars on the basis of their 1.2-3.4 μm colors.

The molecular clouds associated with nearby H II regions and OB associations tend to contain luminous embedded objects, while those associated with reflection nebulae do not. It should be remembered reflection nebulae are a manifestation of low mass, low luminosity stars ($<5M_\odot$, $<10^3 L_\odot$) and it is possible that the clouds near these nebulae harbor embedded objects too faint to have been detected in this survey.

(2) Elevated gas temperature and density are the hallmarks of the site of an embedded infrared source, although high gas temperature alone is not. The combination of a CO temperature >18K and a ^{13}CO column density $>2 \times 10^{16} cm^{-3}$ is indicative of a dense cloud core almost sure to contain an infrared object. The failure to find a compact infrared source in Cep B demonstrates that a "hotspot" can be created in the absence of an internal source of energy by external heating due to a nearby O star (Felli _et al_. 1978).

(3) The fact that the searches at 20 μm revealed the existence of sources that escaped detection at 2.2 and 10 μm points out an important bias in short wavelength studies. Extinction within a dense cloud ($A_V > 100^m$) can obscure an object like Cep A of luminosity $5 \times 10^4 L_\odot$ at wavelengths as long as 10 μm. The selection effect inherent in searches at 2.2 and 10 μm can result in a serious underestimate of the number of embedded sources. The fact that objects discovered at 2.2 and 10 μm lie close to the near surface of the cloud, where the intra-cloud extinction is low, has created an artificial need to explain a preferential location for star formation at the edges of clouds. The results of the 20 μm observations suggest that embedded sources can be located more deeply within a cloud than can be explained by the triggering of gravitational collapse due to shocks from external H II regions (Elmegreen and Lada 1977).

(4) A definitive understanding of where stars form within molecular clouds and of the current rate of star formation must await the results of a more complete survey than this one. The Infrared Astronomical Satellite (IRAS) will cover the whole sky at wavelengths inaccessible from the ground and with far more sensitivity at 10-20 μm than the work presented here. Such a survey will yield a census of the population of sources embedded within molecular clouds and permit an unbiased statistical investigation of the problem of star formation in the Galaxy.

(5) The infrared sources found in molecular clouds tend to be found in clusters whose characteristic size is very similar to that of the trapezium-like groups of OB stars. A possible explanation for

the formation of these multiple systems is that the molecular cloud core breaks up due to a Jeans instability at $n_{H2} \simeq 10^4 cm^{-3}$ into independently condensing nuclei each capable of producing one (or more) star(s).

(6) The 2-25 μm energy distributions of the embedded sources present a confusing welter of characteristics. Simple models with a single source of radiant energy located at the center of a homogeneous cloud of gas and dust are probably inadequate to explain the data. The location and number of sources appears to be critical in the formation of the observed spectrum. The existence of faint optical and 2.2 μm nebulosity suggests, in some cases, that there may be holes in the surrounding clouds through which radiation from the underlying object may escape.

(7) Infrared sources within molecular clouds may be associated with a very small amount of ionized matter (B^2W^2). Luminous objects such as Cep A and S140-IRS 1 ($L>10^4 L_\odot$) are surrounded by weak, resolved H II regions detectable at radio wavelengths. The strength of the radio emission is consistent with photo-ionization by the UV radiation emitted from the photospheres of pre-main sequence OB stars. On the other hand, applying the same model to the recombination line observations of lower luminosity sources such as S235-IRS 4 and AFGL 490 ($<6x10^3 L_\odot$) leads to an UV radiation field much <u>greater</u> than expected for a star of the appropriate luminosity. Either these objects pass through hitherto unrecognized evoluitonary phase of very high temperature or the application of standard H II region theory is in error. In this case other ionization mechanisms, as discussed by Tokunaga and Thompson (1979b) may be operating.

REFERENCES

Aarseth, S. J., and Lecar, M. 1975, Ann. Rev. Astr. Ap., 13, 1.

Abt, H. A. 1978, Protostars and Planets, Ed. T. Gehrels (Tucson: Univ. Ariz. Press), p. 323.

Abt, H. A., and Levy, S. G. 1978, Ap. J. (Suppl.), 36, 241.

Aitken, R. G. 1918, The Binary Stars (New York: Univ. of Calif. Press.

Aitken, R. G. 1932, New General Catalog of Double Stars (Washington, DC: Carnegie Institution).

Allen, C., and Poveda, A. 1974, IAU Symposium, 62, 239.

Allen, C., and Poveda, A. 1975, Publ. A. S. P., 87, 499.

Allen, C., Poveda, A., Worley, C. E. 1974, Rev. Mex. Astron. Astrof., 1, 101.

Allen, C. W. 1973, Astrophysical Quantities (London: Athlone Press).

Allen, D. A. 1972, Ap. J (Letters), 172, L55.

Allen, D. A., Hyland, A. R., Longmore, A. J., Caswell, J. L., Goss, W. M., and Haynes, R. F. 1977, Ap. J., 217, 108.

Ambartsumian, V. A. 1956, Vistas in Astronomy, ed. A. Beer, (New York: Pergamon Press) 2, 1708.

Assousa, G. E., Herbst, W., and Turner, K. C. 1977, Ap. J (Letters), 218, L13.

Barnea, D. I., and Silverman, H. F. 1972, I.E.E.E. Trans., C21, 179.

Becker, W., and Fenkart, R. 1971, Astr. Ap. (Suppl.), 4, 241.

Becklin, E. E., and Neugebauer, G. 1967, Ap. J., 147, 799.

Becklin, E. E., Matthews, K., Neugebauer, G., and Willner, S. P. 1978, Ap. J., 220, 831.

Beckwith, S., Evans II, N. J., Becklin, E. E. and Neugebauer, G. 1976, Ap. J., 208, 390.

Bedejin, P. J., Habing, H. J., and de Jong, T. 1978, Astr. Ap., 69, 73.

Beichman, C. A., Becklin, E. E., and Wynn-Williams, C. G. 1979, Ap. J. (Letters), in press.

Bertout, C., and Yorke, H. W. 1978, Protostars and Planets, Ed. T. Gehrels, (Tucson: Univ. Ariz. Press), p. 648.

Blaauw,A. 1964, Ann. Rev. Astr. Ap., 2, 213.

Blair, G. N., Evans II, N. J., Van den Bout, P. A., Peters III, W. L. 1978, Ap. J., 219, 896.

Blair, G. N., Peters III, W. J., Van den Bout, P. A. 1975, Ap. J. (Letters), 200, L161.

Blitz, L., and Lada, C. J. 1979, Ap. J., 227, 152.

Bodenheimer, P. 1972, Contrib. Lick Obs., #358.
1978, Ap. J., 224, 488.

Bracewell, R. 1965, The Fourier Transform and its Applications, (New York: McGraw-Hill)

Burton, W. B., Gordon, M. A., Bania, T. M., and Lockman, F. J., 1975, Ap. J. (Letters), 202, 30.

Capps, R. W., Gillett, F. C. Kanacke, R. F. 1978, Ap. J., 226, 863.

Caton, D. B., Fallon, F. W., and Wilson, R. E. 1977, Publ. A. S. P., 89, 530.

Chandrashekar, S. and Fermi, E. 1953, Ap. J., 118, 116.

Chandrashekar, S., and Munch, G. 1950, Ap. J., 111, 142.

Chelli, A., Lena, P. and Sibille, F. 1979, Nature 278, 143.

Chopinet, M., Deharveng-Baudel, L., Lortet-Zuckermann, M. C. 1974, Astr. Ap. 30, 233.

Cohen, M., and Lewis, R. R. 1978, preprint.

Cohen, M., and Woolf, N. J. 1971, Ap. J., 169, 543.

Crampton, D., and Fisher, W. A. 1974, Publ. Dom. Astron Obs., XIV, 12.

Davidson, K., and Harwit, M. 1967, Ap. J., 148, 443.

de Jong, T., Maeder, A., Eds. 1977, IAU Symposium 75, Star Formation (Dordrecht-Holland: D. Reidel)

Deutschman, W. A. ,Davis, R. J., and Schild, R. E. 1976, Ap. J. (Suppl.), 30, 97.

Dinerstein, H. L., Lester, D. F., and Rank, D. M. 1979, Ap. J., 227, L39.

Dyck, H. M., and Simon, T. 1977, Ap. J., 211, 421.

Eggen, O. 1963, A. J., 68, 483.

Elias, J. 1978, Ap. J. 224, 453.

Elmegreen, B. G. 1977, preprint, submitted to Massive Molec. Cloud Workshop Gregynog, Wales.

Elmegreen, B. G. and Lada, C. J. 1977, Ap. J., 214, 725.

Elmegreen, B. G. and Lada, C. J. 1978, Ap. J., 219, 467.

Encrenaz, P. J. Falgarone, E., and Lucas, R. 1975, Astr. Ap., 44, 73.

Evans II, N. J., 1978, Protostars and Planets, Ed. T. Gehrels, (Tucson: Univ. Ariz. Press), p. 158.

Evans II, N. J., and Beckwith, S. 1977, Ap. J., 217, 729.

Evans II, N. J., Blair, G. N., and Beckwith, S. 1977, Ap. J., 217, 448.

Felli, M., Harten, R. H., Habing, H. J., and Israel, F. P. 1978a, Astr. Ap. (Suppl.), 32, 423.

Felli, M., Tofani, G., Fanti, C., and Tomasi, P. 1977, Astr. Ap. (Suppl.), 27, 181.

Felli, M. Tofani, G. Harten, R. H., and Panagia, N., 1978b, Astr. Ap. 69, 199.

Field, G. B. 1978, Protostars and Planets, Ed. T. Gehrels, (Tucson: Univ. Ariz. Press), p. 243.

Field, G. B., Sommerville, W. B., Dressler, K. 1966, Ann. Rev. Astr. Ap., 4, 207.

Finn, G. D., and Simon, T. 1977, Ap. J., 212, 472.

Garmany, C. D. 1973, A. J., 78, 185.

Garrison, R. F. 1970, A. J., 75, 1001.

Gatley, I., Becklin, E. E., Matthews, K. , Neugebauer, G., Penston, M. V., Scoville, N. 1974, Ap. J. (Letters), 191, L121.

Gatley, I., Becklin, E. E., Werner, W. M., Wynn-Williams, C. G. 1977, Ap. J., 216, 277.

Gatley, I., Werner, W. W., Sellgren, K., Becklin, E. E. 1978, preprint.

Genzel, R., and Downes, D. 1977, Astr. Ap. (Suppl.), 30, 145.

Genzel, R., and Downes, D. 1979, Astr. Ap., 72, 234.

Genzel, R., Downes, D., Moran, J. M., Johnston, K. J., Spencer, J. H., Walker, R. C., Haschick, A., Matveyenko, L. I., Kogan, L. R., Kostenko, V. I., Ronnang, B., Rydbeck, O. E. H., Moiseev, I. G. 1978, Astr. Ap., 66, 13.

Genzel, R., Downes, D., Moran, J. M., Johnston, K. J., Spencer, J. H., Matveyenko, L. I., Kogan, L. R., Kostenko, V. I., Ronnang, B., Haschick, A. N., Reid, M. J., Walker, R. C., Giuffrida, T. S., Burke, B. F., Moiseev, I. G. 1979, submitted to Astr. Ap.

Georgelin, Y. M., Lortet-Zuckermann, M. C., and Monnet, G. 1975, Astr. Ap., 42, 273.

Giles, K. 1977, M. N. R. A. S., 180, 57p.

Gillett, F. C., Forrest, W. F., Merrill, K. M., Capps, R. W., Soifer, B. T. 1975, Ap. J., 200, 609.

Gingold, R. A. Monaghan, J. J. 1978, M. N. R. A. S., 184, 481.

Glushkov, Yu., I., Denisyuk, E. K., Karyagina, Z. V. 1975, Astr. Ap., 39, 481.

Goldreich, P., and Kwan, J. 1974, Ap. J., 189, 441.

Grasdalen, G. L. 1974, Ap. J., 193, 373.

Grasdalen, G. L. 1976, Ap. J. (Letters), 205, L83.

Habing, H. J., Goss, W. M., Matthews, H. E., Winnberg, A. 1974, Astr. Ap., 35, 1.

Habing, H. J., Israel, F. P. 1979, preprint.

Hall, D. N. B., Aikens, R. S., Joyce. R., and McCurnin, T. W. 1975, Appl. Opt., 14, 450.

Hall, D. N. B., Kleinmann, S. G., Ridgway, S. T., Gillett, F. C. 1978, Ap. J. (Letters), 223, L47.

Harris, D. L., Morgan, W. M., Roman, N. G. 1954, Ap. J., 119, 622.

Harris, S. 1976, M. N. R. A. S., 174, 601.

Harris, S. 1976, M. N. R. A. S., 177, 1.

Harris, S., and Wynn-Williams, C. G. 1976, M. N. R. A. S., 174, 649.

Harten, R. H. 1976, Astr. Ap., 46, 109.

Harvey, P. M. ,Campbell, M. F., Hoffmann, W. F. 1977, Ap. J., 215, 151.

Harvey, P. M. ,Campbell, M. F., Hoffmann, W. F. 1978, Ap. J., 219, 891.

Harvey, P. M., Campbell, M. F., Hoffmann, W. F. 1979, Ap. J., 228, 445.

Harvey, P. M., Campbell, M. F., Hoffmann, W. F., Thronson, H. A., Gatley, I. 1979, Ap. J., 229, 990.

Herbig, G. H. 1960, Ap. J. (Suppl.), 4, 337.

Herbig, G. H. 1971, Ap. J., 169, 537.

Herbig, G. H., and Rao, N. K., 1972, Ap. J., 174, 401.

Herbst, W. 1975a, A. J., 80, 212.

Herbst, W. 1975b, A. J. 80, 683.

Herbst, W., Assousa, G.E. 1977, Ap. J., 217, 473.

Hill, P. W. and Lynas-Gray, A. E. 1977, M. N. R. A. S., 180, 691.

Hiltner, W. A. 1956, Ap. J. (Suppl.), 2, 389.

Ho, P. T. P., and Barrett, A. H. 1978, Ap. J. (Letters), 224, L23.

Hollenbach, D. J., Werner, M. W., and Salpeter, E. E. 1971, Ap. J., 163, 165.

Hoyle, F. 1953, Ap. J., 118, 513.

Hoyle, F., and Wickramasinghe, N. C. 1977, M. N. R. A. S., 181, 51p.

Humphreys, R. M. 1978, Ap. J. (Suppl.), 38, 309.

Iben, I. 1965, Ap. J., 141, 993.

Israel, F. P. 1976, Astr. Ap., 52, 175.

Israel, F. P. 1977, Astr. Ap. 60, 233.

Israel, F. P. 1977, Astr. Ap., 61, 377.

Israel, F. P. 1978, Astr. Ap., 70, 769.

Israel, F. P. and Felli, M. 1978, Astr. Ap., 63, 325.

Jeffers, H. M., van den Bos, W. H., Greeby, F. M. 1963, Index Catalogue of Visual Double Stars, Publ. Lick Obs., XXI (IDS).

Johnson, H. L. 1966, Ann. Rev. Astr. Ap., 4, 193.

Joyce, R. R., Simon, M., and Simon, T. 1978, Ap. J., 220, 156.

Kahn, F. D. 1974, Astr. Ap., 37, 149.

Kennedy, P. M. and Buscombe, W. 1970, MK Spectral Classification.

Kleinmann, D. E., and Low, F. J. 1967, Ap. J. (Letters), 149, L1.

Kleinmann, S. G., Sargent, D. G., Gillett, F. C. Grasdalen, G. L., Joyce, R. R. 1977, Ap. J. (Letters), 215, L79.

Knacke, R. 1978, Protostars and Planets, Ed. T. Gehrels, (Tucson: Univ. Ariz. Press), p. 112.

Knacke, R., and Thomson, R. 1973, Publ. A. S. P., 85, 341.

Knapp, G. R., Kuiper, T. B. H., Knapp, S. L., Brown, R. L. 1976, Ap. J., 206, 443.

Knapp, G. R., Kuiper, T. B. H., Knapp, S. L., Brown, R. L 1977, Ap. J., 214, 78.

Koppenaal, K., Sargent, A. I., Nordh, H. L., Van Duinen, R. J., Aalders, W. 1979, submitted to Astr. Ap.

Krassner, J., Pipher, J.L., and Sharpless, S. 1979, submited to Astr. Ap.

Kraus, J. D., 1966, Radio Astronomy, (New York: McGraw Hill)

Kurucz, R. 1979, Ap. J. (Suppl.), 40, 1.

Kutner, M. L., and Dickman, R. L. 1978, private communication.

Kutner, M. L., Evans II, N. J., Tucker, K. D. 1976, Ap. J., 209, 452.

Kutner, M. L. Tucker, K. D., Chin, G., and Thaddeus, P. 1977, Ap. J. 215, 521.

Kwan, J., and Scoville, N. 1976, Ap. J., 209, 102.

Lada, C. J. 1976, Ap. J. (Suppl.), 32, 603.

Lada, C. J. Blitz, L., and Elmegreen, B. G. 1978, Protostars and Planets, Ed. T. Gehrels, (Tucson: Univ. Ariz. Press), p. 341.

Lada, C. J., Elmegreen, B. G., Cong, H., Thaddeus, P. 1978, Ap. J. (Letters), 226, L39.

Lada, C. J., Reid, M., Blitz, L., Moran, J. 1979, in preparation.

Lang, K. R. 1974, Astrophysical Formulae, (New York: Springer-Verlag)

Larson, R. B. 1970, M. N. R. A. S. , 150, 93

Larson, R. B. 1977, IAU Symposium 75, Star Formation, Eds. de Jong, T., and Maeder, A. (Boston: D. Reidel), p.

Larson, R. B., and Starrfield, S. 1971, Astr. Ap. 13, 190.

Lequeux, J. 1979, Astr. Ap., 71, 1.

Lesh, J. 1968, Ap. J. (Suppl.), 17, 371.

Leung, C. M. 1976, Ap. J. 209, 75.

Leung, C. M., and Brown, R. L. 1977, Ap. J. (Letters), 214, L73.

Liszt, H. S. Wilson, R. W., Penzia, A. A., Jefferts, K. B. Wannier, P. G., Solomon, P. M. 1974, Ap. J., 190, 557.

Lo, K. Y., and Burke, B. F. 1973, Astr. Ap., 26, 487.

Lohsen, E. 1975, Inf. Bull. Var. Stars, #988.

Loren, R. B., 1976, Ph.D. dissertation, Univ. of Texas, Austin.

Loren, R. B. 1977, Ap. J., 215, 129.

Loren, R. B., Wooten, H. A. 1978, Ap. J. (Letters), 225, L81.

Low, F. J., and Hoffmann, W. F. 1963, Appl. Opt., 2, 649.

Low, F. J., and Rieke, G. H. 1974, Methods of Experimental Physics Ed. N. Carleton, (New York: Academic Press), 12, 415.

Lucy, L. B., and Ricco, E. 1979, A. J., 84, 401.

Lynds, B. T. 1962, Ap. J. (Suppl.), 7, 1.

Martin, A. H. M., Gull, F. 1976, M. N. R. A. S., 175, 235.

Matthews, H. E., Goss, W. M., Winnberg, A., and Habing, H. J. 1977, Astr. Ap., 61, 261.

Matthews, H. E. Harten, R. H., and Goss, W. M. 1979, Astr. Ap., 72, 224.

Mestel, L. 1965, Quat. J. Roy. Astr. Soc., 6:161, 265.

Mihalas, D. 1972, Non-LTE Model Atmospheres for B and O Stars, NCAR-TN/ STR-76.

Minkowski, R. 1946, Publ. A. S. P., 58, 305.

Morrison, D. 1973, Icarus, 19, 1.

Morrison, D., and Simon, T. 1973, Ap. J., 186, 193.

Mouschovias, Th. 1976, Ap. J., 206, 753.

Mouschovias, Th. 1977, Ap. J., 211, 147.

Mouschovias, Th. 1978, Protostars and Planets, Ed. T. Gehrels, (Tucson: Univ. Ariz. Press), p. 209.

Mouschovias, Th. , Paleologou, E. V. 1979, Ap. J. 230, 204.

Murphy, R. E. 1969, A. J., 74, 1082

Myers, P. C. 1977, Ap. J., 211, 737.

Oort, J. H. 1954, Bull. Astron. Neth., 12, 177.

Opik, E. 1953, Irish Astron. J. 2, 219.

Osterbrock, D. E. 1957, Ap. J., 125, 622.

Osterbrock, D. E. 1974, Astrophysics of Gaseous Nebulae, (San Francisco: W. H. Freeman)

Ostriker, J. P., and Bondenheimer, P. 1973, Ap. J., 180, 171.

Ostriker, J. P., Richstone, O., Thuan, T. X. 1974, Ap. J. (Letters) , 188, L87.

Panagia, N. 1973, A. J., 78, 929.

Panagia, N., and Smith, L. F. 1978, Astr. Ap., 62, 277.

Petrosian, V., Silk, J., Field, G. B., 1972, Ap. J. (Letters), 177, L69.

Pipher, J. L., Sharpless, S., Savendoff, M. P., Kerridge, S. J., Krassner, J., Schurmann, S., Soifer, B. T., Merrill, K. M. 1976, Astr. Ap., 51, 255.

Pipher, J. L., and Soifer, B. T. 1976, Astr. Ap., 46, 153.

Pottasch, S. 1956, Bull. Astron. Neth., 13, 77.

Price, S. D. and Walker, R. G., 1976, AFGL 4 Color Sky Survey, AFGL-TG-76-0208.

Racine, R. 1968, A. J., 73, 233.

Reifenstein III, E. C., Wilson, T. L., Burke, B. F., Mezger, P. G., Altenhoff, W. J. 1970, Astr. Ap., 4, 357.

Rieke, G. H., Low, F. J., Kleinmann, D. E. 1973, Ap. J. (Letters), 186, L7.

Rouan, D., Lena, P. J., Puget, J. L., de Boer, K. S., Wijnbergen, J. J. 197 Ap. J. (Letters), 213, L35.

Rubin, R. H. 1968, Ap. J., 154, 391.

Rybakov, A. I., Kalinina, E. P., Kholopov, P. N., Duboshin, G. N. 1971, Soviet AJ., 15, 406.

Salukvadze, G. N. 1978, Astrophysica, 14, 78.

Sargent, A. I. 1977, Ap. J., 218, 736.

Sargent, A. I. 1979, preprint

Schneps, M. H., Martin, R. N., Ho, P. T. P., Barrett, A. H. 1978, Ap. J., 221, 124.

Schwartz, R. D. 1975, Ap. J., 195, 631.

Scoville, N. Z., and Kwan, J. 1976, Ap. J., 206, 718.

Sharpless, S. 1954, Ap. J., 119, 334.

Sharpless, S. 1959, Ap. J. (Suppl.), 4, 257.

Silk, J. 1977a, Ap. J., 214, 152.

Silk, J. 1977b, Ap. J., 214, 718.

Silk, J. 1978, Protostars and Planets, Ed. T. Gehrels, (Tucson: Univ. of Ariz. Press), p. 000.

Simon, T. 1976, A. J., 81, 135.

Simon, T., Simon, M., Joyce, R. R. 1979, Ap. J. 230, 127.

Snell, R. L., and Loren, R. B. 1977, Ap. J., 211, 122.

Snow, T. P., Peters, G. J., and Mathieu, R. D. 1979, Ap. J. (Suppl.), 39, 359.

Solomon, P. M., Scoville, N. Z., and Sanders, D. 1979, preprint. quoted in Stark and Blitz 1979.

Stark, A. A., and Blitz, L. 1978, Ap. J. (Letters), 225, L15.

Taylor, J. H., and Manchester, R. N. 1975, A. J., 80, 794.

Thaddeus, P. 1977, IAU Symposium 75, Star Formation, Eds. de Jong, T., and Maeder, A. (Boston: D. Reidel), p. 37.

Thompson, R. I., and Tokunaga, A. T. 1978, Ap. J. 226, 119.

Thompson, R. I., and Tokunaga, A. T. 1979, preprint.

Thronson, H. A., and Harper, D. A. 1979, Ap. J., 230, 133.

Tokunaga, A. T., Erickson, E. F., Caroff, L. J., Dana, R. A., 1978, Ap. J., 224, L19.

Tokunaga, A. T., and Thompson, R. I. 1979a, Ap. J., 229, 583.

Tokunaga, A. T., and Thompson, R. I., 1979b, preprint.

Tolbert, C. R. 1964, Ap. J., 139, 1105.

Traub, W. A., Stier, M. T. 1976, Appl. Opt., 15, 364.

Trimble, V. 1974, A. J., 79, 967.

Underhill, A. B. 1968, The Early Type Stars, (Dordrecht, Holland: D. Reidel)

Van Albada, T. S. 1968a, Bull. Astr. Inst. Neth., 20, 47.

Van Albada, T. S. 1968b, Bull. Astr. Inst. Neth., 20, 57.

Van den Bergh, S. 1966, A. J., 71, 990.

Werner, M. W., Becklin, E. E., Gatley, I., Matthews, K., Neugebauer, G., Wynn-Williams, C. G. 1979, submitted to M. N. R. A. S.

Werner, M. W., Becklin, E. E., and Neugebauer, G. 1977, Science, 197, 723 (WBN).

Westerhout, G. 1958, Bull. Astr. Inst Neth., 14, 215.

Whiteoak, J. B. 196^2, M. N. R. A S., 125, 105.

Willner, S. P. 1976, Ap. J., 206, 728.

Willner, S. P. 1977, Ap. J., 214, 706.

Wilson, R. W., Jefferts, K. B., Penzias, A. A. 1970, Ap. J. (Letters), 161, L43.

Woodward, P. R. 1976, Ap. J. 207, 484.

Wright, E. L., deCampli, W., Fazio, G. G., Kleinmann, D. E., Lada, C. J., Low, F. J. 1979, Ap. J., 228, 439.

Wynn-Williams, C. G. 1971, M. N. R. A. S., 151, 397.

Wynn-Williams, C. G., Becklin, E. E., Forster, J. R., Matthews, K., Neugebauer, G., Welch, W. J., Wright, M. C. A. 1977, Ap. J. (Letters), 211, L89.

Wynn-Williams, C. G., Becklin, E. E., Neugebauer, G. 1972, M. N. R. A. S., 160. 1.

Wynn-Williams, C. G., Becklin, E. E., Neugebauer, G. 1974, Ap. J., 187, 473.

Yorke, H. W., and Krugel, E. 1977, Astr. Ap., 54, 183.

Zuckerman, B., and Palmer, P. 1974, Ann. Rev. Astr. Ap. 12, 279.